

**GEOMECHANICAL BEHAVIOUR OF FIBRE-REINFORCED
CEMENTED PASTE BACKFILL UNDER CYCLIC LOADING
CONDITIONS**

by

Javaughn Romario McLean

A thesis

submitted to the Faculty of Graduate Studies
in partial fulfilment of the requirements for the
Degree of Master of Science

in

Civil Engineering

Supervisor

Dr. Liang Cui

Associate Professor – Dept. of Civil Engineering

Lakehead University

Thunder Bay, Ontario

August 2022

© Javaughn McLean, 2022

Author's Declaration Page

I hereby declare that I am the sole author of this thesis. This is a true copy of the thesis, including any required final revisions, as accepted by my examiners. I understand that my thesis may be made electronically available to the public.

Abstract

Cemented paste backfill (CPB) is considering a promising mine backfilling technology with several technical, environmental, and economic benefits for the underground mining operation. After placed into underground voids (termed stopes), the hardened CPB mass is required to provide reliable ground support to control ground pressure and limit surface subsidence. However, due to the complex field loading conditions, CPB mass may experience dynamic loadings induced by mining activities (such as drilling, blasting, and mechanical excavation) and seismic events. However, as a soft cementitious material, aged CPB is highly brittle in nature and also featured with poor strain-hardening capabilities, the low tensile strength, and weak post-peak resistance. As a result, the in-situ CPB mass may undergo catastrophic failure under complex field dynamic loading condition. This highlights the complexity of loading conditions in-situ and the need to improve the mechanical stability and performance of CPB. Consequently, fiber reinforcement has recently attracted increasing attention in the improvement of the geomechanical behavior and performance of CPB. The benefits of small fiber inclusions on the mechanical performance of cementitious composites under quasi-static loading conditions and fiber reinforced cementitious composites (FRCCs) under cyclic loading conditions have been fairly established by previous researchers. However, there are no studies that have systematically studied the application of fiber reinforcement in CPB technology under cyclic loading conditions. The purpose of this thesis research is to study the geomechanical behavior of fiber-reinforced cemented paste backfill (FR-CPB) under cyclic loading conditions. This body of work studies the effects of fiber inclusion on the evolutive cyclic compressive and tensile behaviors and mechanical properties of FR-CPB. Curing time, fiber length and fiber content were used to study the evolution of FR-CPB's mechanical properties, including hysteretic energy dissipation, secant modulus, degraded stress, and damping index. Cyclic stress-strain data reveals that the geomechanical behavior of FR-CPB is highly influenced by curing time. Aging of FR-CPB results in a strengthened fiber-bridging effect leading to improvement in composite strength and, thus, load carrying capacity through full realization of the cement hydration process. Furthermore, different cyclic behavior and damage mechanisms are observed for FR-CPB. Additionally, the hysteretic energy dissipation capacity, secant modulus, degraded stress, and damping index of FR-CPB all show positive evolutionary trends. It is also found that fiber reinforcement plays a pivotal role in the pre-peak response of FR-CPB. Furthermore, there exist

a critical fiber length of 13 mm and a critical fiber content of 0.5wt% (0.5% of total weight of cement, water, and tailings). When these parameters are employed, FR-CPB demonstrates the most consistent enhancement to strength development and mechanical properties under cyclic loadings. The findings herein seek to promote further understanding of fiber reinforcement techniques and the safe design and implementation of FR-CPB in the mining industry.

Acknowledgements

First and foremost, I would like to thank God the gift, for God the giver. Through him I had the strength and determination to persist and accomplish the completion of this thesis.

Second, thank you, Dr. Liang Cui, for the faith you showed in selecting me to carry out this body of work. There were times of doubt and apprehension on my part. However, your words of encouragement were pivotal in my overcoming difficulties. Further, your diligence and devotion to your work are unmatched, and for that, I am grateful for your supervision and expertise throughout this process.

Third, I would like to show special appreciation and thanks to the lab technicians Morgan Ellis and Cory Hubbard for their assistance and support during my studies; the members of my research team (Brett Holmberg, Sami Hassan, Aaron McAdie, and Suman Poudel) who provided their friendship and support during an unprecedented time of a global pandemic.

Finally, to my parents – Michelle and Manley, thank you for your unconditional love and support throughout the duration of my studies. To my partner and future wife, Michka, you have been a tremendous force and a point of inspiration in my life and studies; thank you for loving me and supporting me throughout this phase of our lives. And to my siblings, Kimoy, Kanice, and Rahiem, take my sacrifices and accomplishments as an example to always work hard and strive for excellence.

Table of Contents

Author's Declaration Page	ii
Abstract iii	
Acknowledgements	v
List of Tables	ix
List of Figures	x
Nomenclature	xiii
Roman	xiii
Greek	xiv
Chapter 1 Introduction	1
1.1 Background	1
1.2 Problem statement	3
1.3 Research methodologies.....	4
1.4 Thesis organization	6
Chapter 2 Literature review	8
2.1 Introduction	8
2.2 Cyclic Tensile Behavior of Fiber-reinforced Cementitious Materials	9
2.2 Cyclic Shear Behavior of Fiber-reinforced Cementitious Materials.....	14
2.3 Cyclic Compressive Behavior of Fiber-reinforced Cementitious Materials.....	19
Summary	25
Chapter 3 Experimental testing program	27
3.1 Materials.....	27

3.1.1 Tailings	27
3.1.2 Binder and Water	27
3.1.3 Polypropylene microfibers	28
3.2 Mix recipe and curing method	29
3.3 Mechanical testing program	31
3.3.1 Cyclic compressive tests.....	32
3.3.2 Cyclic tensile tests	34
3.4 Scanning electron microscope (SEM) analysis.....	35
3.5 Determination methods of mechanical properties of FR-CPB.....	35
3.5.1 Cumulative dissipation energy	35
3.5.2 Secant modulus.....	36
3.5.3 Degraded stress.....	36
3.5.4 Damping index	37
Chapter 4 Chapter 4 Experimental results.....	39
4.1 Compressive behavior and properties of FR-CPB under cyclic loadings.....	39
4.1.1 Effect of fiber length on the time-dependent cyclic compressive behavior of FR-CPB	39
4.1.2 Effect of fiber content on the time-dependent cyclic compressive behavior of FR-CPB	41
4.1.3 Effect of fiber inclusion on the hysteretic energy dissipation	44

4.1.4 Effect of fiber inclusion on the secant modulus	47
4.1.5 Effect of fiber inclusion on the degraded stress	49
4.1.6 Effect of fiber inclusion on the damping index	52
4.2 Tensile behavior and properties of FR-CPB under cyclic loadings	55
4.2.1 Effect of fiber length on the time-dependent cyclic tensile behavior of FR-CPB.....	55
4.2.2 Effect of fiber content on the time-dependent cyclic tensile behavior of FR-CPB.....	57
4.2.3 Effect of fiber inclusion on the hysteretic energy dissipation	60
4.2.4 Effect of fiber inclusion on the secant modulus	62
4.2.5 Effect of fiber inclusion on the degraded stress	64
4.2.6 Effect of fiber inclusion on the damping index	67
Chapter 5 Conclusions and recommendations	69
5.1 Conclusions	69
5.2 Recommendations for future work.....	72
Chapter 6 References	74

List of Tables

Table 3.1 Chemical composition of quartz tailings.....	27
Table 3.2 Physical properties of the adopted tailings.....	27
Table 3.3 Physical and mechanical characteristics of polypropylene fibers.....	28
Table 3.4. Summary of mix recipe and curing times adopted for cyclic tensile tests.....	30
Table 3.5. Summary of mix recipe and curing times adopted for cyclic compressive tests.	30

List of Figures

Figure 1.1 Research methodologies applied in this thesis research.	6
Figure 2.1 Schematic of an ideal cyclic stress-strain curve.	10
Figure 2.2 Type of cracks generated in the cementitious material under cyclic tensile loading: (A) without fiber reinforcement, and (B) with fiber reinforcement [47].	12
Figure 2.3 Comparison of pullout lengths of fibers embedded in the cementitious materials under (A) monotonic loading, and (B) cyclic loading [56].	13
Figure 2.4 Typical crack surfaces of FRCC under cyclic tensile loading [57].	13
Figure 2.5 Pinched hysteresis loops of FRCC under cyclic loading [60].	15
Figure 2.6 Evolution of excess pore water pressure and effective stress in cemented paste backfill under cyclic shear loading: (A) with fiber reinforcement, and (B) without fiber reinforcement [11].	16
Figure 2.7 SEM images of (A) ITZ between fiber and matrix [70] and (B) crack isolator role played by fiber [71].	17
Figure 2.8 Typical stress-strain curves of cementitious material under cyclic compressive loading: (A) without fiber reinforcement, (B) with fiber reinforcement [88].	21
Figure 2.9 Effect of fiber volume fraction on stiffness degradation [88].	23
Figure 2.10 Effect of fiber volume fraction on stiffness degradation [100].	24
Figure 2.11 CT images of cracking process in FRCC under cyclic compressive loading: (A) 0 cycles, (B) 20,000 cycles, and (C) 2,000,000 cycles [107].	25
Figure 3.1 Particle size distribution of studied tailings compared with the average of nine Canadian hard-rock mine tailings [23].	28
Figure 3.2 Adopted polypropylene fibers - from left to right: 6 mm, 13 mm, and 19 mm.	29
Figure 3.3 Cylindrical samples cured in the laboratory.	31

Figure 3.4. Experimental setup of MTS system controller and loading frame.....	32
Figure 3.5. Schematic diagram of cyclic compressive loading procedure (adopted in part from [47]).....	33
Figure 3.6 Schematic diagram of cyclic tensile loading procedures (adopted in part from [47]).	34
Figure 3.7 Definition of mechanical properties of FR-CPB: (a) hysteretic dissipation energy, (b) secant modulus, (c) degraded stress, and (d) damping index.	38
Figure 4.1 Effect of fiber length (6mm, 13mm, and 19mm) on the cyclic compressive stress-strain behavior of FR-CPB with a fixed fiber content of 0.5wt% at 7 days (a, b, and c), 28 days (d, e, and f), and 90 days (g, h, and i).	41
Figure 4.2 Evolution of cementitious microstructure in FR-CPB (A) 3 days, (B) 28 days, (C) 56 days.	43
Figure 4.3 Effect of fiber content (0.25wt%, 0.5wt%, and 0.75wt%) on the cyclic compressive stress-strain behavior of FR-CPB with a fixed fiber length of 13mm at 7 days (a, b, and c), 28 days (d, e, and f), and 90 days (g, h, and i).	44
Figure 4.4 Effect of fiber inclusion on the hysteretic dissipation energy of FR-CPB at 7 days (a and b), 28 days (c and d), and 90 days (e and f).	46
Figure 4.5 Effect of fiber inclusion on the secant modulus of FR-CPB at 7 days (a and b), 28 days (c and d), and 90 days (e and f).	48
Figure 4.6 Effect of fiber inclusion on the degraded stress of FR-CPB at 7 days (a and b), 28 days (c and d), and 90 days (e and f).	50
Figure 4.7 Effect of fiber length (a, b, and c) and fiber content (c, d, and e) on the post-peak failure patterns of 90-day FR-CPB.	51

Figure 4.8 Effect of fiber inclusion on the damping index of FR-CPB at 7 days (a and b), 28 days (c and d), and 90 days (e and f).	54
Figure 4.9 Effect of fiber length (6mm, 13mm, and 19mm) on the cyclic tensile stress-strain behavior of FR-CPB with a fixed fiber content of 0.5wt% at 7 days (a, b, and c), 28 days (d, e, and f), and 90 days (g, h, and i).	57
Figure 4.10 Effect of fiber content (0.25wt%, 0.5wt%, and 0.75wt%) on the cyclic tensile stress-strain behavior of FR-CPB with a fixed fiber length of 13mm at 7 days (a, b, and c), 28 days (d, e, and f), and 90 days (g, h, and i).....	60
Figure 4.11 Effect of fiber inclusion on the hysteretic dissipation energy of FR-CPB at 7 days (a and b), 28 days (c and d), and 90 days (e and f).	62
Figure 4.12 Effect of fiber inclusion on the secant modulus of FR-CPB at 7 days (a and b), 28 days (c and d), and 90 days (e and f).	64
Figure 4.13 Effect of fiber inclusion on the degraded stress of FR-CPB at 7 days (a and b), 28 days (c and d), and 90 days (e and f).	66
Figure 4.14 Effect of fiber inclusion on the damping index of FR-CPB at 7 days (a and b), 28 days (c and d), and 90 days (e and f).	68

Nomenclature

Roman

AE	Acoustic emission
AF	Average frequency
C _C	Coefficient of curvature
C _m	Cement content
CPB	Cemented paste backfill
CT	Computed tomography technology
C _U	Uniformity coefficient
D _i	Damping index
D _e	Dissipated energy
D _{e, cum}	Cumulative dissipated energy
FBZ	fiber bridging zone
F _C	Fiber content
F _L	Fiber length
FM-ITZ	Fiber matrix interfacial transition zone
FPZ	Fracture process zone
FRCC	Fiber reinforced cementitious composites
FR-CPB	Fiber reinforced cemented paste backfill
FRS	Fiber reinforced shotcrete
F _s	Factor of safety
GDP	Gross domestic product
G _s	Specific gravity

ITT	Indirect tensile tests
ITZ	Interfacial transition zone
MTS	MultiPurpose TestWare Software
PPF	Polypropylene fiber
PWP	Pore water pressure
RA	Rise angle
RL_{area}	Area under reloading curve
$S_{e, plastic}$	Plastic strain energy
SEM	Scanning electron microscopy
S.M _i	Secant modulus of i th loop
UCS	Unconfined compression strength
UL_{area}	Area under unloading curve
W/C	Water-cement ratio

Greek

Δu	Pore pressure increment
$\sigma_{1,2}$	N th pair of cyclic stresses
σ_{peak}	Peak stress
σ_{min}	Minimum stress
$\epsilon_{1,2}$	N th pair of cyclic strains
$\epsilon_{\sigma, peak}$	Strain corresponding to the peak stress
$\epsilon_{\sigma, plastic}$	Plastic strain at the end of unloading phase
g	Gravitational constant

γ_{CPB} Dry density of synthetic tailings

V_{mold} Volume of plastic mold

Chapter 1 Introduction

1.1 Background

The contribution of minerals extraction to the world economy through the provision of raw materials cannot be underestimated. The extraction of precious minerals contributes to the evolution of societies around the world by boosting economies and employment markets [1]. In 2020, the minerals sector was responsible for providing 692 000 jobs and generated \$107 billion to Canada's nominal gross domestic product (GDP), and accounted for \$102 billion of Canada's total domestic exports [2]. Furthermore, it has been found that more than 1 150 million tons of heavy metals have been produced since the Stone Age, with a waste-to-product ratio of 100:1 in volume; that is approximately [3]. Further, production of this waste material termed mine tailings is estimated between 5 and 7 billion tonnes per year worldwide [4]. Subsequently, this level of mining activity and significant generation of waste material requires new and improved storage methods as opposed to conventional methods such as tailings ponds. Conventional storage methods not only contradict urban development and environmental initiatives but also pose significant threats to the environment due to catastrophic failures. Over a 58-year period, there were 117 total tailings pond failures due to a host of intrinsic and extrinsic factors [3,5].

To rectify the environmental issues and provide a safe disposal method for mine tailings, cemented paste backfill (CPB) technology has received significant attention due to the technical, environmental, and economic benefits it offers. Furthermore, the implementation of CPB may reduce surface subsidence, decrease rehabilitation costs, and provide ground support to the surrounding rock mass [3]. Typically, cemented paste backfill is a cementitious material formed by mixing hydraulic binders (e.g., Portland cement, fly ash, and blast furnace slag), dewatered mine tailings, and mixing water. Compared to other disposal methods, CPB has several advantages, namely (1) it provides higher tailings use which reduces the need for surface disposal and its environmental impacts, (2) it significantly reduces mine operating and maintenance costs (for example, less damage to roads), and (3) it offers versatility as a part of tailings can be used for sprayed applications such as shotcrete [5]. CPB is commonly designed using a strength-based design approach, i.e., the factor of safety, $F_s = \frac{strength}{stress}$, to account for the unknown nature of in-service loads [6]. Moreover, CPB may be used as pillar structures in

underground stopes or act as a concrete beam in underhand cut and fill mining method to provide adequate ground support to surrounding rock mass.

Due to this requirement, mechanical behavior plays an important role in the stability analysis of CPB mass under quasi-static loading conditions. Correspondingly, previous studies have been conducted to investigate the mechanical behaviors of CPB materials experimentally and numerically under monotonic loading conditions. Under compressive loading, Jafari et al. [7] found that CPB behaves linearly in the pre-yield compression section. Further, Chen et al. [8] found that the CPB matrix displayed brittle failure with a low strain, which was significantly alleviated when fibers were added to the matrix. Furthermore, similar findings were obtained by Yi et al. [9], where CPB failed suddenly after the peak stress and exhibited limited post-peak softening. Moreover, unreinforced specimens showed distinct spalling/splitting with no signs of strain-hardening behavior. Under tensile loading, Libos and Cui [10] found that the slope of the force-displacement curve in the pre-peak zone increases with time, indicating improved material stiffness. Furthermore, there is evidence of pseudo-strain hardening behavior as crack bridging forces develop due to fiber inclusion. As for shear loading, Festugato et al. [11] found that CPB demonstrates a pronounced hardening effect which leads to higher shear deformation and higher strength. It is worth noting that CPB develops greater strength by experiencing a higher level of deformation, however, the cementitious matrix suffers greater damage. Similarly, numerical modeling and simulations [12,13] have been conducted to investigate the strain response and failure patterns of CPB as well as simulate the application of CPB in strip mining methods.

Cemented paste backfill may be described as a slurry when freshly placed and becomes brittle in nature as the mass ages. In this research, late-aged CPB is of concern to study the effects of fiber inclusion on the geomechanical behavior under cyclic loading conditions. Specifically, it has been established previously that CPB becomes resistant to liquefaction when the unconfined compressive strength (UCS) reaches a minimum value of 100 kPa [14] and Alainachi [1] found that 4 hours-CPB sample was resistant to shaking-induced liquefaction. Soft cementitious materials such as CPB are commonly highlighted by their limited strain-hardening behavior and weak tensile capacity. Due to the complex nature of loadings existing in underground stopes, there is a need to improve the mechanical behavior and properties of cementitious composites, short – randomly distributed fibers may be added to the matrix as reinforcements [15]. The

emergence of fiber reinforcement as a promising technique is owing to the ability of fibers to provide bridging forces across cracks in the cementitious matrix, thereby restricting crack growth [16]. Correspondingly, the cementitious matrix, in conjunction with fiber reinforcement, has the capacity to withstand deformation to a higher degree resulting in more ductile material behavior. It is widely accepted that the role of fibers is only initiated once the composite matrix has undergone cracking or exceeded the first-crack stress [17]. Specifically, after the matrix cracks, the fibers' tensile strength is mobilized, and the tensile forces are transferred back into the matrix [18]. This transference of stress to the matrix causes subsequent cracks to develop and further fibers to be involved in the cracking process; this defines the multiple cracking characteristics afforded to cementitious composites by fiber reinforcement. Furthermore, this improved cracking behavior provides a significant enhancement to energy dissipation and the degradation rate of stress and material stiffness [19].

For example, previous studies [9,20,21] showed that fiber reinforcement complements the cementitious matrix in the strength development of FR-CPB. Moreover, the fiber-matrix network acts in unison by providing resistance to the applied loads through an enhanced grain-fiber interaction and thus improving the crack resistance of FR-CPB. Furthermore, the introduction of fiber reinforcement creates new damage mechanisms such as fiber sliding, fiber pullout, fiber-matrix debonding, and fiber rupture, which contribute to the mechanical response of FR-CPB as well as the damping characteristics [16,22].

1.2 Problem statement

The cyclic geomechanical behaviors of FR-CPB is of great significance in the safe implementation of CPB as a backfill method as the cyclic stress-strain relationship may be evaluated to provide insight into the pre- and post-peak behavior and the evolution of mechanical properties. Previous studies [10,23,24] focused on the conventional geomechanical behaviors including compressive, tensile, and shear behaviors of CPB and/or FR-CPB materials under monotonic loading. However, there exists complex dynamic loadings in underground stopes due to seismic loadings and dynamic loadings induced by mining operations such as drilling and blasting [25]. This dynamic loading causes a progressive degradation in load carrying capacity due to damage accumulation in the cementitious matrix; this significantly affects the engineering

performance. Consequently, a thorough understanding of the cyclic geomechanical behaviors of FR-CPB is needed to prevent surface subsidence and to ensure safety to mine workers during operation. However, no studies have been designed and conducted to systematically investigate the cyclic geomechanical behavior of FR-CPB under cyclic loadings, which significantly affects the thorough understanding of mechanical behaviors of FR-CPB under complex field loading conditions and thus the safe design of FR-CPB technology [16].

To address this research gap, a comprehensive experimental testing program is developed through this thesis study to investigate the effect of fiber length and fiber content on the cyclic compressive and tensile behaviors and properties of FR-CPB at various curing times. To study the effects of fiber length on the cyclic compressive and tensile behaviors of FR-CPB, three fiber lengths are selected namely 6 mm, 13 mm, and 19 mm while the fiber content is held constant at 0.5wt%. On the other hand, to study the effects of fiber content, fiber length is fixed at 13 mm and three fiber contents are selected namely 0.25wt%, 0.5wt%, and 0.75wt%. Furthermore, an extensive period of trial testing is forecasted to create a custom cyclic sequence that verifies the ability of the testing system to employ the established loading rate and displacement increment to produce the known cyclic hysteretic behaviors of FR-CPB. Moreover, the stress-strain data is recorded to analyze the evolution of the mechanical properties of FR-CPB under the test conditions.

To further the understanding of the cyclic geomechanical behaviors of FR-CPB, the recorded data is used to study the hysteretic energy dissipation capacity, secant modulus, degraded stress, and the damping index. Subsequently, the obtained results may significantly improve the understanding of engineering behavior of FR-CPB materials, and thus promotes its successful application in underground mine backfill operation.

1.3 Research methodologies

The methodologies adopted in this thesis research are illustrated in the schematic flowchart in Figure 1.1. To better understand the geomechanical behavior of fiber reinforced cemented paste backfill under cyclic loading conditions, this study was conducted in 5 steps:

- **Step 1** – In this step the research problem is identified, studied, and the research objectives are outlined.
- **Step 2** – In this step extensive review of the current literature regarding (1) the constitutive behavior of FRCC, (2) factors affecting the mechanical properties of FRCC, and (3) failure patterns of FRCC under cyclic loading conditions. After establishing a baseline, the research gap is established – there have been no previous works that systematically studied the geomechanical behavior of FR-CPB under cyclic loading conditions.
- **Step 3** – In this step, an extensive testing program and test schedule is designed to address the research gap. Several trial tests are proposed using a custom cyclic sequence to confirm cyclic loading rate and strain increment to ensure an accurate representation of the damage process in FR-CPB through stress-strain data.
- **Step 4** – Over a six-month period, the cyclic compressive and tensile responses of FR-CPB samples are tested for curing periods of 7, 28, 90 days and the mechanical properties are calculated. The effect of fiber length and fiber content are studied.
- **Step 5** – Involves processing and analyzing the experimental results through cyclic stress-strain data to assess the geomechanical behavior of FR-CPB with regards to the test conditions.

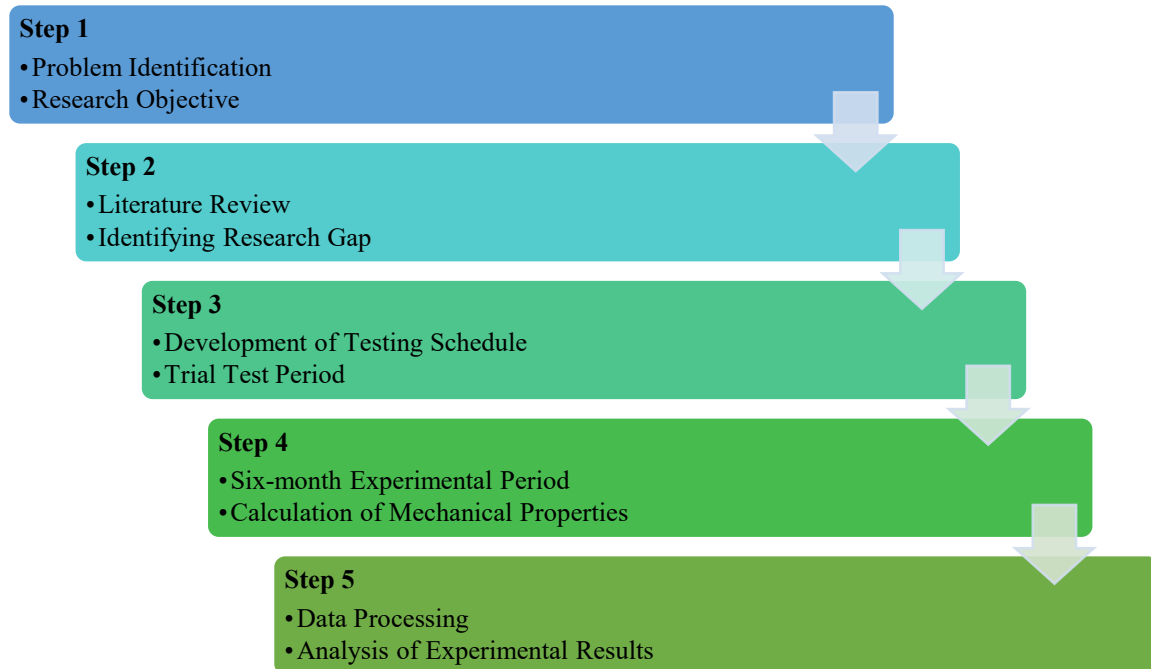


Figure 1.1 Research methodologies applied in this thesis research.

1.4 Thesis organization

The organization of this thesis is a paper-based thesis consisting of technical papers formatted in five total chapters as seen below:

Chapter 1: entails the introduction to the body of work. It contains background information on the area of study, the research problem, research objectives, research methodology, and organization of the thesis.

Chapter 2: provides a literature review detailing the current literature regarding the multiscale geomechanical behavior of fiber reinforced cementitious materials (FRCC) under cyclic loading conditions – Technical Paper #1.

Chapter 3: presents the experimental testing program utilized in the completion of the 2nd and 3rd technical papers which studies the evolutive cyclic compressive and cyclic tensile responses of fiber reinforced cemented paste backfill (FR-CPB)

Chapter 4: details the experimental results obtained from employing the experimental program detailed in chapter 3.

Chapter 5: provides the summary and conclusions that can be drawn from the body of work presented. Furthermore, recommendations for future work are also provided in this section.

Chapter 2 Literature review

2.1 Introduction

As a type of construction material, cementitious composites are commonly subjected to complex field loading conditions during their service life [26–28]. As a result, the external loadings may cause the development of compressive, tensile and/or shear stresses in the porous mixture and thus dominate the failure behaviors at the macroscale [10,29,30]. However, irrespective of the external loading conditions, the crack initiation is commonly associated with the local stress concentration near defects at the microscale [31]. Since mechanical stability is one of the most important design criteria, cementitious composites are required to offer adequate stress resistance and sufficient tolerance for permanent deformation in engineering applications. However, as a type of brittle material, cementitious composites such as cemented paste backfill (CPB), cemented soil, and concrete are commonly featured by the far limited strain-hardening behavior and weak post-failure performance [32]. To improve the mechanical behavior and properties of cementitious composites, it has been found that reinforcement through the addition of short fibers is a promising technique [33–36]. This is because fibers in cementitious materials are able to produce the bridging forces across cracks in the porous matrix [20,34,37,38], thus, acting as crack arresters at the microscale. Correspondingly, the fiber-reinforced cementitious composites (FRCC) can withstand larger plastic deformation and improve material ductility [32,38]. Subsequently, the macroscale stress-strain behavior, especially post-failure behavior, can be considerably improved and becomes more favorable for engineering applications in practice. Therefore, understanding of multiscale geomechanical behaviors of fiber-reinforced cementitious composites (FRCC) plays a key role in the safe and optimum design of FRCC.

The performance of FRCC is dependent on the in-service and environmental loading conditions. Previous studies show that FRCC can demonstrate distinctive mechanical behaviors under monotonic and cyclic loadings [33,39]. For example, cyclic loading can cause a progressively decrease in the load-carrying capacity of FRCC. Such degradation of load-carrying capacity can be partially attributed to cyclic loading-induced damage accumulation in the porous matrix [40]. Therefore, the resultant material degradation causes a poor engineering performance of FRCC relative to that under quasi-static loading conditions. Furthermore, the fibers embedded into the matrix can suffer severe extrusion or even rupture during the cyclic loading process, which

causes a reduction in the crack bridging capacity [41,42]. Consequently, FRCC could show different failure patterns, material properties, and constitutive behaviors under cyclic loading conditions. Accordingly, the obtained findings about the quasi-static behavior may be invalid for FRCC under cyclic loading conditions.

Additionally, FRCC may be subjected to various types of dynamic loadings in the field and thus cause different stresses inside the FRCC. For example, as one of the most critical components of a building structure, fiber-reinforced concrete columns such as bridge piers are designed to withstand large axial and shear forces, especially in seismic regions [43]. Correspondingly, the resultant dynamic compressive and shear stresses govern the stability of FRCC. Furthermore, fiber-reinforced shotcrete (FRS) linings have been widely used in underground mines and civil tunnels to prevent the occurrence of many disasters such as caving, slabbing, and rockburst as a result of complex field loadings [44,45]. As a result, FRS is commonly exposed to high tensile and compressive stresses due to vibrations from blasting operations, which may cause various dynamic failures such as the cracking of the shotcrete lining, failure along the shotcrete-rock interface, and flexural failure of the shotcrete [46]. Therefore, to improve the understanding of the multiscale geomechanical behaviors of FRCC under dynamic loadings, this study aims to provide a critical review of (1) the cyclic compressive, tensile, and shear behaviors, (2) the failure patterns, and (3) the mechanical properties of FRCC under cyclic loadings, which can benefit the safe and optimal design of FRCC under cyclic loading conditions [41]. Future work related to cyclic geomechanical behaviors is also suggested through the identification of the research gap in this field of knowledge.

2.2 Cyclic Tensile Behavior of Fiber-reinforced Cementitious Materials

Due to the effects of fiber reinforcement, the constitutive tensile behavior of FRCC under cyclic loading is featured by an ascending branch akin to the plain cementitious material and an enhanced post-peak branch [47]. Figure 2.1 represents a typical stress-strain curve that can be used to explain the damage process of FRCC under cyclic loading conditions. For the pre-peak behavior (path 0B), the material exhibits high elasticity making it difficult to spot the hysteretic loops [48]. This is because the crack bridging capacity of the fibers is not realized until the first crack appears; at first-crack stress, the first crack occurs. However, the carrying capacity of fibers bridging this crack enables the load to be increased, and further causes the propagation of

microcracks. Moreover, point A signals a transition point on the stress-strain curve from linear to non-linear regimes due to the multi-cracking characteristic afforded by the fibers. When the fibers in the weakest crack have failed, the crack localizes and the material exhibits a softening behavior [17]. Correspondingly, the peak point is followed by a noticeable stress drop with distinguished unloading and reloading paths that highlights the hysteretic behavior of FRCC under cyclic tensile loading [39]. However, in the post-peak region (paths CD and DE in Figure 2.1), fiber sliding, and pull-out mechanisms are the main contributors to energy dissipation which causes more defined hysteretic loops with increasing load cycles [19]. Conversely, the sudden drop after the peak stress is caused by fracturing of the cementitious matrix. The cracks begin to propagate and coalesce into a main crack causing severe deformation of fibers, fracturing of fibers, and debonding of fibers with the continuously increasing displacement and loading cycles [19]. Therefore, it has been widely accepted that fiber reinforcement in cementitious composites mainly affects the post-peak performance, specifically to transform the brittle nature of cementitious matrix to a more ductile one with improved mechanical properties [49]. In particular, previous studies [50,51] have successfully demonstrated the benefits of incorporating fibers into the cementitious matrix to improve the cyclic tensile behavior of FRCC. The results indicate that the integration of fibers significantly improves peak stress, peak strain, ductility, and toughness. Furthermore, the rate at which a composite's stiffness degrade is significantly alleviated by the inclusion of high modulus fibers with increasing volume fraction or aspect ratio [52].

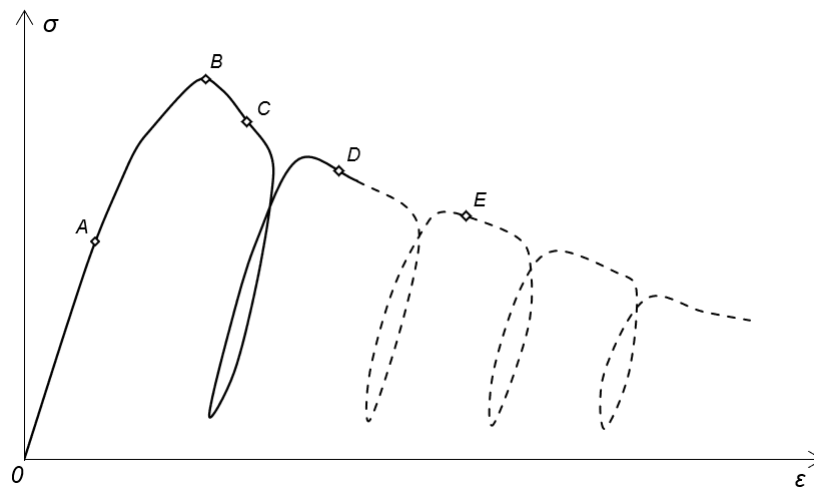
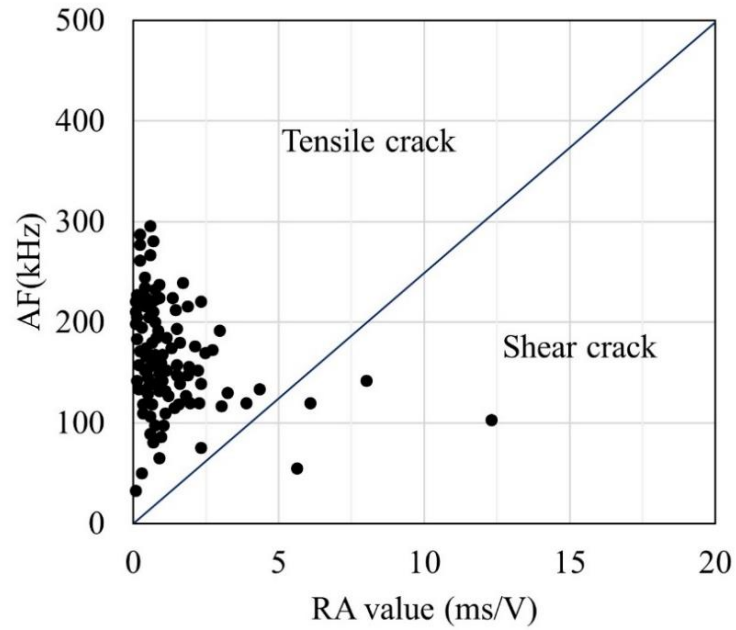
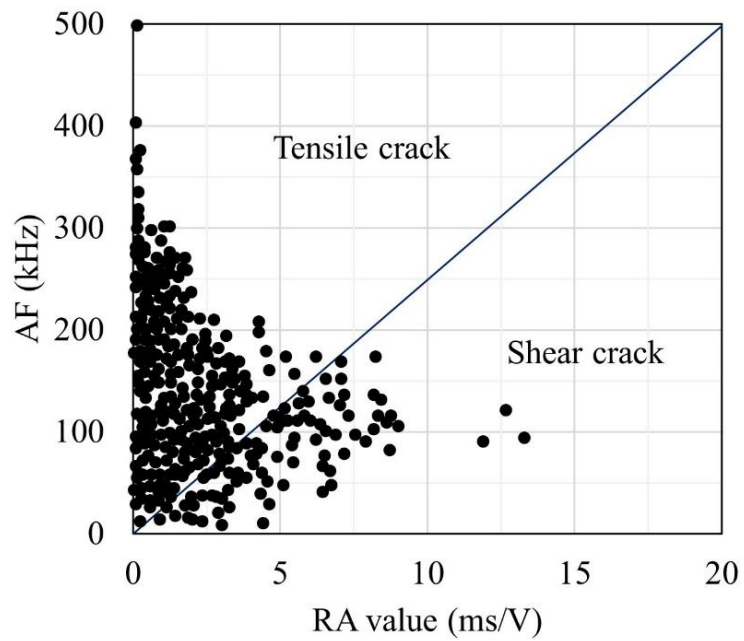


Figure 2.1 Schematic of an ideal cyclic stress-strain curve.

In addition to the constitutive behavior of FRCC, understanding the bridging behavior and any synergy between these bridging mechanisms in FRCC is vital to determining its crack-restraining capabilities. The acoustic emission (AE) technique, as a non-destructive testing approach, has been widely adopted for the investigation of local damage in cementitious materials. This is because AE indices such as the average frequency and rise angle can be used to characterize the mode of cracking and quantify the damage level in FRCC [53]. For example, Li et al. [48] and Aggelis [54] utilized the AE technique to investigate cracking modes of FRCC under cyclic tensile loadings. As shown in Figure 2.2, it has been found that compared with plain concrete FRCCs produce far more AE events and show clear signs of crack propagation due to the fiber effects. Moreover, it has also been found that a cementitious composite subjected to complex loadings experiences tensile cracks in the initial stage of the damage process while shear cracks dominate in the later stages [55]. In addition, Soulioti et al. [56] described each fiber pull-out incident as a potential AE event and these events increase with the fiber volume content, which clearly indicates the development of multiple cracking in the FRCCs. Furthermore, the failure patterns of FRCCs under cyclic tensile loading can be further qualitatively analyzed by examining the pull-out length of fibers and the fracture surfaces through SEM observation as seen in Figure 2.3 and Figure 2.4. In comparison to quasi-static experiments, fibers that are pulled out due to dynamic loading are approximately 91.6% longer with distinct wave-shaped textures in the axial direction; indicative of pronounced plastic deformation [57]. This pronounced plastic deformation is a result of higher strain rates and higher crack opening velocities resulting in fiber-matrix debonding, destroyed fibers, and ultimately loosening of the microstructure due to pronounced micro-crack development [58]. Moreover, several factors such as the bond strength between the fiber and the cementitious matrix, fiber aspect ratio, and matrix strength can contribute to the multiscale behavior of FRCC [59]. There exist a research lag and further investigations are necessary to fully understand the mechanical behavior of FRCC under cyclic tensile loading.

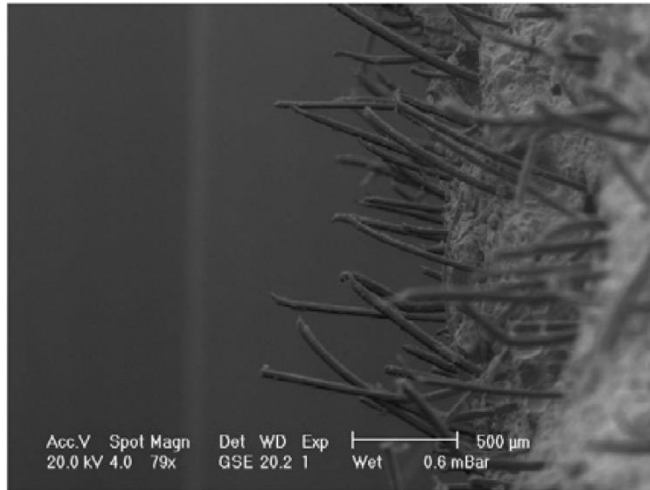


(A)

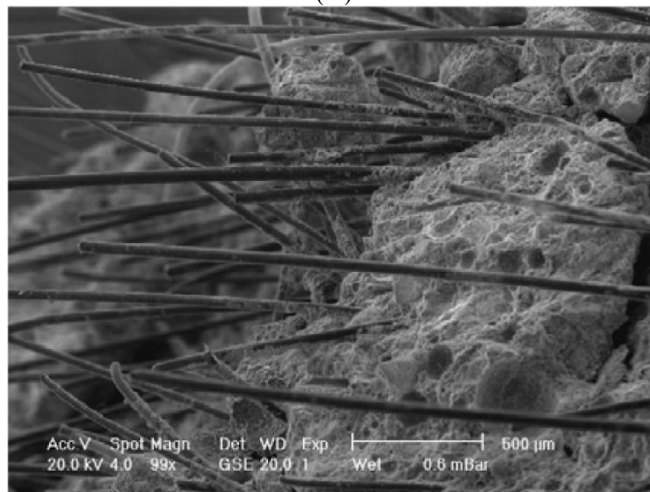


(B)

Figure 2.2 Type of cracks generated in the cementitious material under cyclic tensile loading: (A) without fiber reinforcement, and (B) with fiber reinforcement [47].



(A)



(B)

Figure 2.3 Comparison of pullout lengths of fibers embedded in the cementitious materials under (A) monotonic loading, and (B) cyclic loading [56].

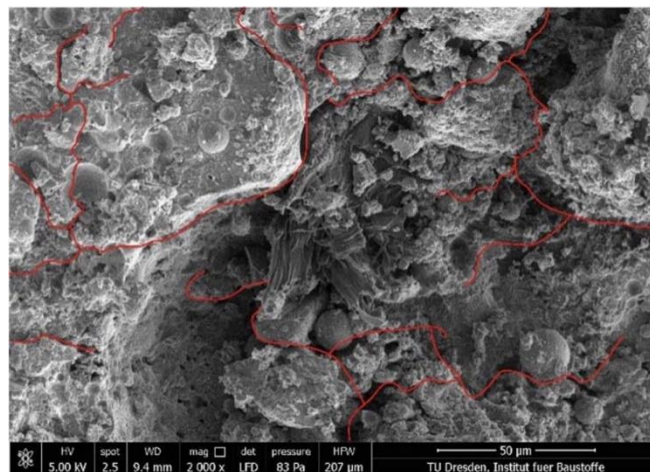


Figure 2.4 Typical crack surfaces of FRCC under cyclic tensile loading [57].

2.2 Cyclic Shear Behavior of Fiber-reinforced Cementitious Materials

Due to the incompatible material properties and the interfacial transition zone (ITZ) between fibers and cementitious matrix, the reinforcing effect mainly occurs in the post-cracking stages indicating that the pre-cracking response of FRCC is dominated by the cementitious matrix [60]. Therefore, to identify the characteristics of the cyclic shear behavior of FRCC, the focus of this review is placed on its post-cracking response. In the post-cracking stages, the cyclic shear response is highlighted by distinct constitutive behaviors, namely, pinched hysteresis loops and accumulated volumetric plastic strain. The pinching of the strain curve (see Figure 2.5) is attributed to the combined effects of frictional resistance and stiffness degradation, respectively [61,62]. This is because the inclusion of fibers not only increases the shear resistance through their dowel action and axial fiber stress [63] but also causes the multi-cracking behavior of the FRCC matrix. Although the multi-cracked matrix implies a stronger energy-dissipation ability and thus a higher load-carrying capacity, the generated multiple cracks inevitably cause a considerable reduction in the stiffness during the unloading process. Therefore, the stiffness degradation under cyclic shear loading contributes to a more pinched hysteresis loop [11,64]. However, the multiple cracks can offer a higher friction resistance for a given shear displacement, which indicates a higher energy dissipation capacity. In other words, the improved friction resistance by multiple cracks intends to increase the area of hysteresis loops and thus result in a more complex unloading/reloading behavior. It should be noted that the effectiveness of friction resistance along crack surfaces depends on the degree of crack closeness during the unloading/reloading process. For example, when stiff fibers such as steel fibers are adopted, the reinforcing fibers may prevent the cracks from closing and weakens the interface shear resistance [65].

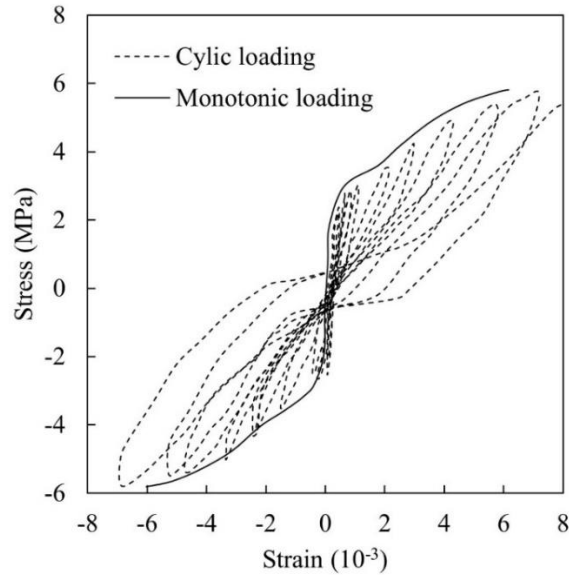
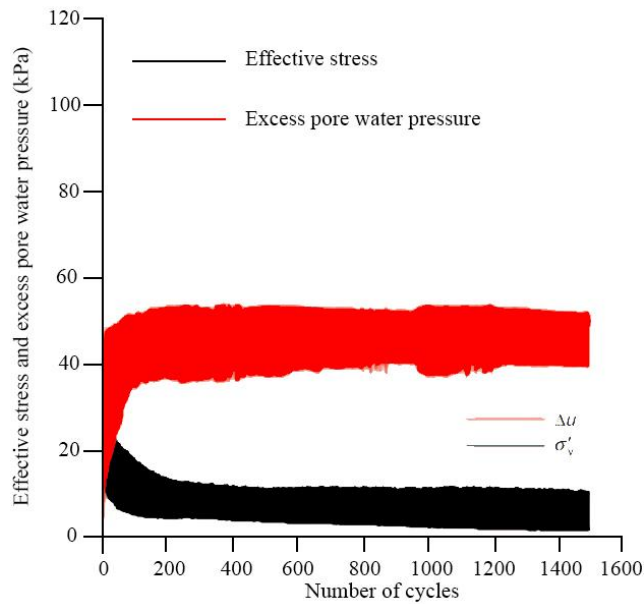


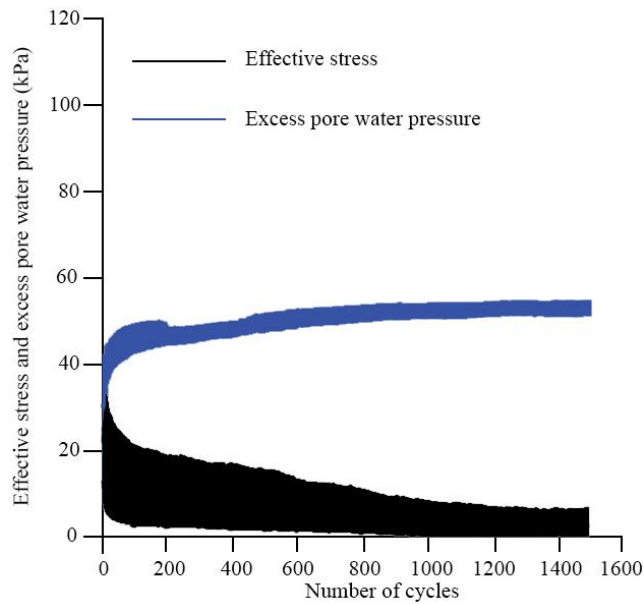
Figure 2.5 Pinched hysteresis loops of FRCC under cyclic loading [60].

Another important characteristic of the cyclic shear response is the accumulation of volumetric plastic strain. For soft cementitious materials such as CPB, shear deformation causes volume changes (especially volume contraction) and increases pore water pressure, which may contribute to material liquefaction [66,67]. Under cyclic shear loading, the accumulation of volumetric plastic strain occurs in the matrix, and this strain is irrecoverable. Due to the irrecoverable nature of this deformation, the matrix retains this volume change during the unloading process. Correspondingly, the accumulation of plastic strain under cyclic loading will result in the continuous development of excess PWP. This excess PWP causes a reduction in effective stress and material strength. In engineering applications, it is imperative to have a material with rapid dissipation of this excess PWP. In this regard, it has been found that the incorporation of fibers can speed up PWP dissipation [11]. This is because (1) the inclusion of fibers induces multiple cracking responses. The resultant macro- and micro-cracks directly form the preferential seepage channels inside the matrix and thus increase the nominal hydraulic conductivity. (2) The ITZ formed between fibers and matrix possesses a larger pore size compared to those inside the matrix [68]. Such larger pores can further enhance the hydraulic conductivity of FRCCs. As a result, rapid dissipation of excess PWP can be obtained in soft fiber-reinforced cementitious materials under cyclic shear loadings, especially during the post-cracking stages. Festugato et al. [11] studied the cyclic shear response of fiber-reinforced cemented paste backfill (FR-CPB). Cyclic shear tests were performed on FR-CPB specimens

under 50 kPa of initial effective vertical stress and $\pm 2.5\%$ of controlled shear strain. After 1500 cycles, the FR-CPB specimens (see Figure 2.6 (A)) had a pore pressure increment (Δu) of approximately 40 kPa and showed a 27% reduction in Δu compared to that (approximately 55 kPa) of the non-reinforced specimens (see Figure 2.6 (B)). Moreover, the confirmed rapid dissipation of excess PWP by the inclusion of fibers directly increases the effective stress.



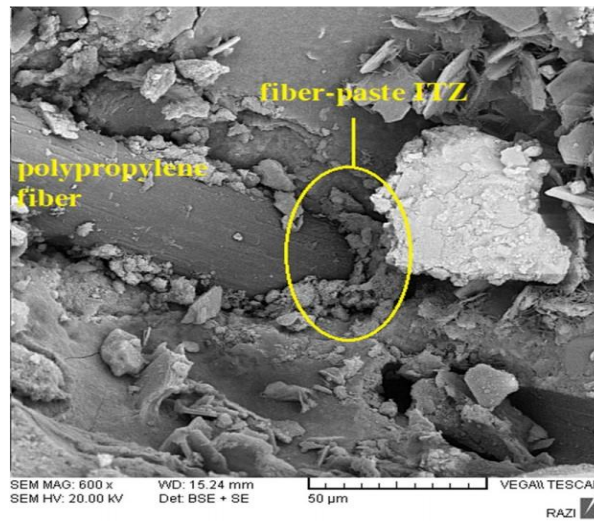
(A)



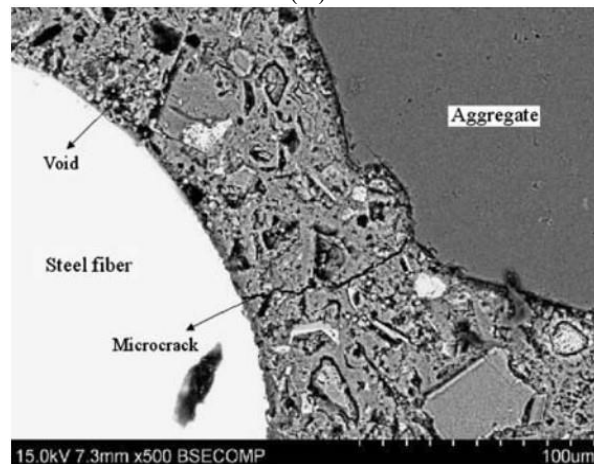
(B)

Figure 2.6 Evolution of excess pore water pressure and effective stress in cemented paste backfill under cyclic shear loading: (A) with fiber reinforcement, and (B) without fiber reinforcement [11].

For the failure patterns under cyclic shear loading, cementitious materials can exhibit significant quasi-ductile behavior when compared to the behavior of their individual components [69]. Such macro-scale mechanical behavior can be attributed to the development of multiple micro-cracks primarily in the ITZ between cement paste and aggregate, which is often considered the weak link in cementitious materials. When fibers are introduced into the porous matrix, a series of new ITZ between fibers and solid particles in the cementitious matrix can be generated (see Figure 2.7). Similarly, the ITZ associated with the inclusion of fibers possesses strong heterogeneity and weaker fracture toughness compared with the cementitious matrix [70].



(A)



(B)

Figure 2.7 SEM images of (A) ITZ between fiber and matrix [70] and (B) crack isolator role played by fiber [71].

Consequently, when micro-cracks propagate into this the new ITZ, the composite may experience crack deflection and/or branching parallel to the fibers. Furthermore, as shown in

Figure 2.7 (B), fibers can serve as a crack isolator in conjunction with the ITZ and prevent the coalescence of micro-cracks [71,72]. Together with the stress transfer mechanism of fiber reinforcement, this crack isolator role played by the ITZ can further contribute to (1) the improvement of post-cracking stiffness and maintenance of matrix integrity [73] and (2) multiple cracking behaviors of FRCC [74,75]. Under shear loading conditions, the resultant multiple cracks cause more crack surfaces to exist in the cementitious matrix, and subsequently, more energy can be dissipated. Moreover, the inherent crack deflection and branching indicate that shear cracks can transform into tensile cracks [76]. As the cracks propagate further into the cementitious matrix, we may discuss a relatively larger-scale fracture process zone (FPZ) formed ahead of the crack tip to better understand the particularly complex nature of the cracking process in cementitious materials. The FPZ is defined as a damage region between the intact material and the fully developed macro-crack [77]. Previous studies [78,79] confirm that the formation of FPZ has the ability to delay crack growth and results in non-linear fracture behaviors. The FPZ of cementitious materials without fibers consists of two zones (1) zone of micro-cracks and (2) aggregate bridging zone. When fibers are introduced to the matrix, the fibers can form the additional fiber bridging zone [80], which not only extends the net bridging zone, but also enlarges the zone of micro-cracks through fiber-induced multiple cracking processes. As a result, the reinforced FPZ improves the fracture toughness of the FRCC. Then, under cyclic shear loading, more energy can be dissipated by this enhanced FPZ, which also confirms the role of fiber reinforcement in the post-cracking stages. In addition, the FPZ will become a crushed zone under cyclic shear loading [81]. This crushed zone with loose particles and dust has two interesting implications: (1) the separation of solid particles from its original matrix requires more energy dissipation, and (2) the existence of particles and dust in the crack space prevents the closure of cracks, thus, affecting the macro-scale volume change. Hence, the crack propagation in the ITZ and FPZ eventually affects the crack coalescence and, thus the failure patterns at the macroscale. More specifically, the low tensile strength of plain cementitious materials implies that flexural failure plays a crucial role in the failure patterns [47]. However, when fibers are introduced, the stress transfer mechanism causes a more important role played by the combined flexural and shear failure patterns. For instance, through an experimental study on the axial cyclic compression behavior of FRCC, Li et al. [82] found that the hybrid-fiber reinforced shear keys experienced concrete crushing and spalling from the specimens

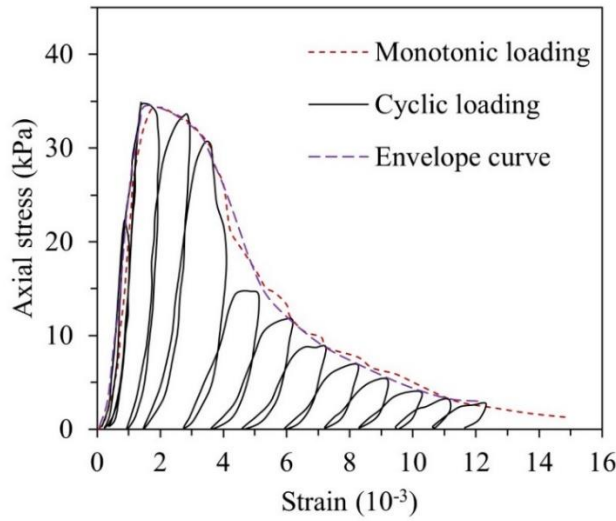
during tests and were accompanied by shear tension failure mode under cyclic loading. This is because the opening of flexural cracks was delayed by the fiber bridging effect, which leads to crack inclination and the subsequent “flexure-shear failure”. Similar findings were also realized in recent publications [83,84], which further highlights the effect of fiber addition on the failure patterns of FRCC under cyclic shear loading.

2.3 Cyclic Compressive Behavior of Fiber-reinforced Cementitious Materials

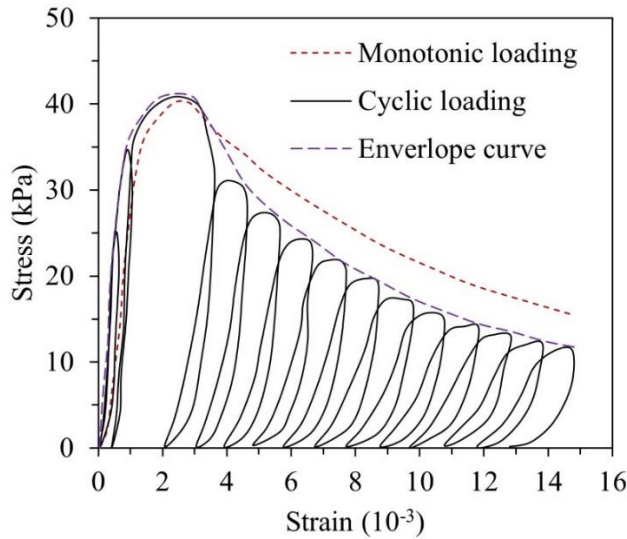
The envelope curve, usually referenced as the upper boundary of the cyclic response, can be used to analyze the mechanical behavior of FRCC under cyclic compressive loading [46].

Specifically, the deviation of the stress-strain curve from the monotonic envelope could be an important characteristic to aid in understanding FRCC’s post-peak behavior in this loading regime. Li et al. [84] found that the envelope curve consists of the ascending and the descending branches. As shown in Figure 2.8, the ascending branch prior to the peak stress closely traces the monotonic envelope curve. The minimal pre-peak deviation between cyclic and monotonic envelope curves was also observed from the synthetic FRCCs [60], which further confirms the weak effect of fiber reinforcement on the pre-peak behavior under compressive loading conditions. Contrastingly, the post-peak discrepancy between cyclic and monotonic envelope curves appears when the fibers are introduced into the cementitious materials (see Figure 2.8(A) & (B)). The inconsistent cyclic and monotonic envelop curves in the post-peak stage can be attributed to the strengthened multiple-cracking characteristic of FRCC under cyclic compressive loading [85,86]. Specifically, this multiple cracking process results in significant microscale damage accumulation and macroscale stress deterioration [19,87]. Consequently, fiber reinforcement is able to yield different damage and post-peak (softening or hardening) mechanisms responsible for the macroscale mechanical response under monotonic and/or cyclic loadings [86]. Secondly, it has also been found that the increased loading cycles result in a more defined hysteresis loop in FRCC, which indicates an improved hysteretic energy dissipation capability. In contrast, plain cementitious composites are featured with narrow hysteresis loops under cyclic compressive loading [88] and several major cracks from the beginning of loading till specimen failure [89]. This is because the formation of fiber bridging zone in the vicinity of crack front extends FPZ and the resultant stress transfer causes multiple cracking in the matrix [87,89]. More precisely, the prerequisite for the effectiveness of fiber reinforcement is the

development of locally matched stress levels between fibers and adjacent cementitious matrix [90,91]. However, distinct mechanical properties between fiber and granular materials may cause unmatched stress levels when the deformation of fiber drops to a certain value and thus fade the local fiber reinforcement effect [92]. In other words, the cyclic loading and unloading processes will repeatedly reactivate and deactivate the fiber reinforcement at the cost of damage accumulation in the cementitious matrix. Consequently, strengthened stress transfer through combined fiber and aggregate bridging zones into the cementitious matrix is able to endow the materials with significantly improved mechanical performance, including the higher hysteretic energy dissipation capacity.



(A)



(B)

Figure 2.8 Typical stress-strain curves of cementitious material under cyclic compressive loading: (A) without fiber reinforcement, (B) with fiber reinforcement [88].

In addition to the stress-strain response, the macroscale volume change of FRCC can also demonstrate different characteristics when subjected to cyclic compressive loading. The macroscale volume change is intimately related to the crack opening and closing during the loading and unloading processes [93]. As previously discussed, fibers embedded into the matrix may act as crack arresters and cause crack branching and deflection. Consequently, both tensile and shear cracks are able to propagate inside the cementitious composite and promote multiple cracking behaviors. The effect of tensile cracks on volume change is straightforward, i.e., the opening and closing of tensile cracks can directly cause the local volume expansion and contraction. However, the volume change associated with shear cracks is dependent on cementation extent [94]. To maintain the shear crack growth, the debonding process accompanied by the particle sliding and rotation along the rough crack surfaces are required [95]. Therefore, similar to the over-consolidated soils, a larger local volume expansion can be expected along the shear cracks when FRCCs are prepared with higher cement content [96]. Conversely, soft cementitious materials with lower cement content, such as FR-CPB, possess weak bond strength. As a result, the shearing process along crack surfaces can cause the debonding processes to a larger regime in the vicinity of crack surfaces and promote particle re-packing to a greater extent, which in turn weakens the sliding and rotation of particles along the crack surfaces. Consequently, the locally depressed volume expansion can be expected in soft cementitious materials [97]. Additionally, the introduction of fibers indirectly contributes to the confinement of the cementitious composite [98]. This is because fiber bridging capacity is able to provide passive confinement to the damaged matrix [99] and thus further limit the volume change at a given stress level.

In terms of mechanical properties of FRCCs under cyclic compressive loading, the elastic modulus, compressive strength, energy dissipation capacity, and Poisson's ratio can be extracted from the macroscale stress-strain behaviors and used to evaluate the engineering performance of FRCCs. Specifically, the evolution of elastic modulus can be used as a valuable indicator for the damage accumulation inside cementitious materials. When materials are cyclically loaded, the material stiffness degrades due to crack propagation. However, it has been confirmed that the addition of fibers into the cementitious matrix is able to effectively alleviate the degradation rate

of elastic stiffness (see Figure 2.9) [89] and improve the ductile response of cementitious material at the macroscale [100]. With regards to composite strength, the effect of fibers is less significant, and some studies [101,102] even found a negative effect of fibers on the compressive strength of FRCCs. As previously discussed, fibers are most effective when their tensile strength is mobilized through their bridging capacity across tensile cracks. However, under compressive loading, fibers may initiate matrix crushing through local stress concentration and induce defects in the cementitious matrix as a result of inadequate compactness [103,104], which may adversely affect the compressive strength of FRCC. However, the fiber reinforcement technique is able to act as a positive contributor to the compressive strength when a multiscale reinforcement approach is adopted. Furthermore, the hysteresis loops in Figure 2.8 suggest the inclusion of fibers significantly improves the hysteretic energy dissipation in FRCCs [19,87]. When FRCCs are cyclically loaded, the reinforcement mechanisms, including fiber bridging, fiber sliding, fiber pull-out, and fiber-matrix debonding, are responsible for the formation of energy dissipation capacity [105]. Correspondingly, the absence of these mechanisms in plain cementitious materials inevitably results in smaller hysteretic loops and subsequent low energy dissipation capacity, because the coalescence of microcracks into macrocracks is the only avenue for energy dissipation in plain cementitious materials. Lastly, Zhou, et al. [99] have identified that the cracking process significantly influences the evolution of Poisson's ratio. As illustrated in Figure 2.10, Poisson's ratio of plain cementitious materials increases exponentially with axial strain due to progressive micro-cracking in the cementitious matrix. However, when the fiber reinforcement is introduced into the cementitious materials, the Poisson's ratio shows a logarithmic relationship to the axial strain and such observation clearly confirms the fiber's crack-bridging capacity is also able to restrict further crack opening in the lateral direction and thus affects the macroscale volume change.

For the failure patterns of FRCCs under compressive loading, the plain cementitious composites are dominated by tensile cracks parallel to the loading direction [19]. With the introduction of fibers into the matrix, the failure mode is transformed into a more ductile shear failure [89]. For instance, through CT scan technology, Minguez et al. [106] reconstruct crack propagation inside the cementitious matrix under cyclic compressive loadings. The obtained CT images (Figure 2.11) clearly show the crack branching and deflection inside the FRCCs. Such cracking process inside the matrix can be attributed to multiple mechanisms, including (1) exceedance of the

tensile strength of the matrix, (2) debonding between fibers and matrix, and (3) debonding between aggregates and matrix [87]. More specifically, due to the relatively weak tensile strength, the tensile microcracks can be developed in the matrix under cyclic compressive loadings. However, due to the development of FPZ in the vicinity of crack surfaces, the initial tensile microcracks are restrained and/or deflected by the fibers, limiting crack growth and thus restricting volume changes in the cementitious matrix [19,87,100]. In other words, these fibers act as crack barriers, resulting in a more curved and inclined cracking path as the load increases [18,87]. The microscale crack deflection and possible branching in vulnerable regions such as ITZ can further complicate the local stress state, including shear stress concentration and associated shear crack propagation [107]. Consequently, FRCCs may exhibit both macroscale tensile and shear cracks under cyclic compressive loadings.

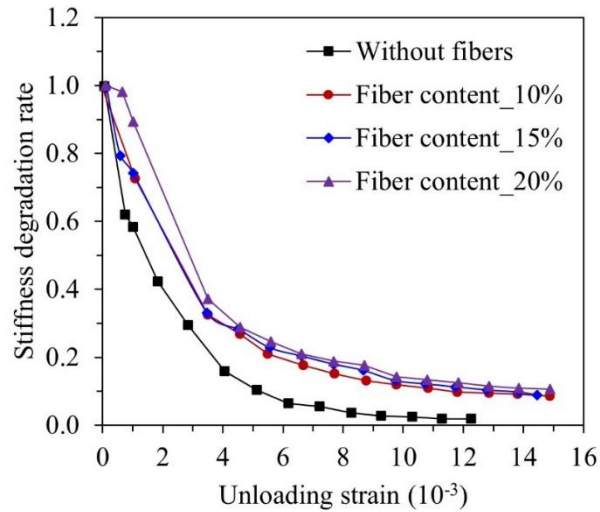


Figure 2.9 Effect of fiber volume fraction on stiffness degradation [88].

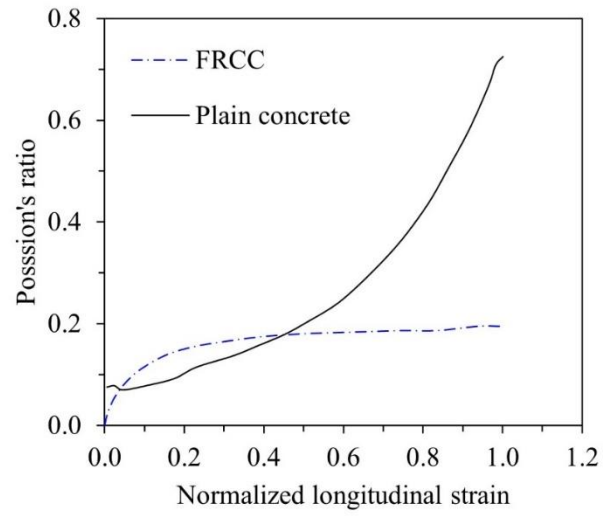
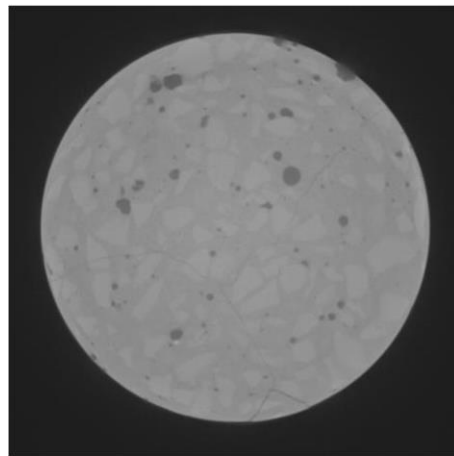
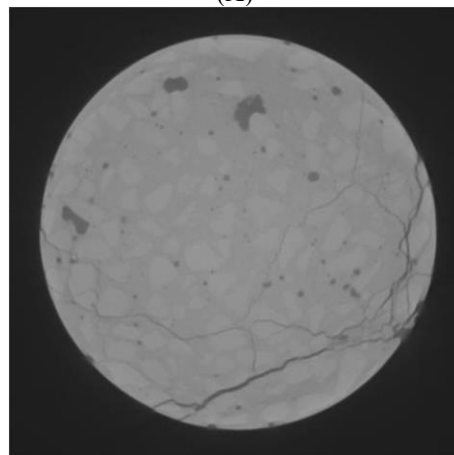


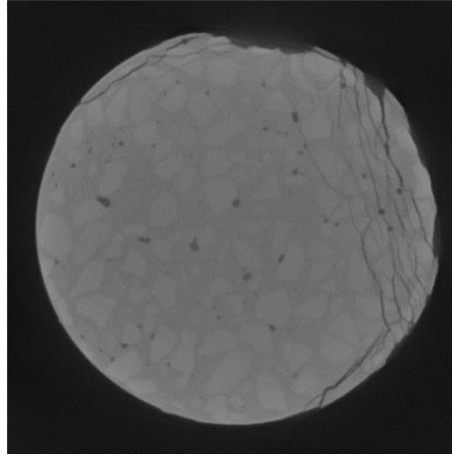
Figure 2.10 Effect of fiber volume fraction on stiffness degradation [100].



(A)



(B)



(C)

Figure 2.11 CT images of cracking process in FRCC under cyclic compressive loading: (A) 0 cycles, (B) 20,000 cycles, and (C) 2,000,000 cycles [108].

Summary

This literature review presents a comprehensive overview of start-of-the-art research on the FRCC under cyclic loading conditions. The macroscale constitutive behavior and the associated mechanical properties and microscale cracking processes under cyclic tensile, shear, and compressive loading conditions are summarized in-depth. Based on the study findings in the present literature, the following conclusions can be drawn:

- (1) For the macroscale constitutive behavior, the fiber reinforcement mainly improves the post-cracking behavior, especially in the post-peak stage. Correspondingly, the enhancement of material stiffness, hysteretic energy dissipation capacity, and ductility has been observed from FRCC under cyclic tensile, shear, and compressive loadings.
- (2) The crack opening and closing at the microscale govern the macroscale volume change under cyclic shear loadings. In contrast, the shear-induced volume change is dominated by the particle repackaging along the shear cracks.
- (3) The inclusion of fibers is able to enlarge the pore size of ITZ and thus accelerates dissipation of the excess PWP under cyclic loading, which can significantly improve the mechanical performance of soft cementitious materials such as CPB.
- (4) For the microscale crack propagation under cyclic loadings, introducing fibers into the cementitious matrix extends the FPZ and causes complex cracking processes such as

crack deflection and branching. Consequently, the FRCC commonly demonstrates both tensile and shear cracks under cyclic loadings.

Based on the multiscale geomechanical behavior of FRCC, the multiscale reinforcement technique can be considered a promising approach to restrict cracking at different length scales inside the cementitious matrix under cyclic loadings.

This literature review highlights a gap in previous research works as the cyclic response of fiber reinforced cemented paste backfill has not been thoroughly studied. Compared to conventional FRCCs, CPB possesses a lower cement content (typically 1/3 that of conventional FRCC), finer tailings particle size, no coarse aggregate, and are placed in massive in-situ structures in underground stopes. Moreover, CPB must provide ground support to the surrounding rock mass while experiencing extreme dynamic loadings. In practice, CPB technology experiences compressive loads when used in open stope mining and tensile loads when utilized in underhand cut-and-fill mining. These factors highlight the importance of the current body of work as it aims to further advance CPB technology and the implementation of fiber reinforcement techniques.

Chapter 3 Experimental testing program

3.1 Materials

The materials used for the fiber reinforced cemented paste backfill (FR-CPB) specimen preparation include tailings, general use Portland cement as a binder, water, and polypropylene microfibers.

3.1.1 Tailings

Natural mine tailings possess various chemical constituents, such as sulfide minerals which interact with cement and may introduce significant uncertainties to the interpretation of the experimental results [109]. To negate the introduction and effects of these uncertainties, quartz (silica) tailings that contain 99.7% SiO₂ were employed in this experiment. Table 3.1 and Table 3.2 present the chemical composition and physical properties of the selected tailings. Figure 3.1 illustrates that the particle sizes are distributed over a wide range with a uniformity coefficient C_U of 14.2 and a coefficient of curvature C_C of 1.5 which signals a well-graded material and is comparable to the tailings of nine Canadian hard-rock mines [24].

Table 3.1 Chemical composition of quartz tailings.

Composition	SiO ₂	C _a O	Al ₂ O ₃	Fe ₂ O ₃	FeO	K ₂ O	TiO ₂
Weight percentage (%)	99.7	0.02	0.17	0.03	0.024	0.02	0.02

Table 3.2 Physical properties of the adopted tailings.

Element unit	G _s	D ₁₀	D ₃₀	D ₆₀	C _u	C _c
	-	μm	μm	μm	-	-
Silica	2.65	1.80	8.3	25.5	14.2	1.5

3.1.2 Binder and Water

Ordinary Portland cement was adopted as the binding agent, tap water was used for mixing tailings, binder, and fibers into finished FR-CPB specimens.

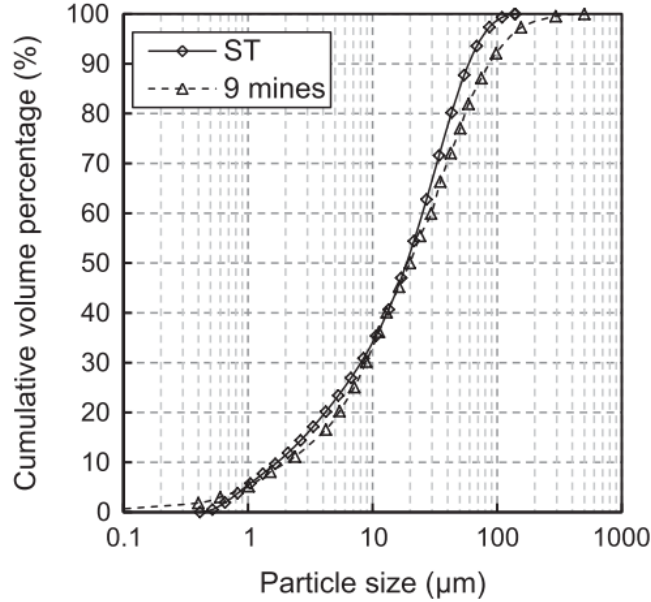


Figure 3.1 Particle size distribution of studied tailings compared with the average of nine Canadian hard-rock mine tailings [23].

3.1.3 Polypropylene microfibers

To analyze the effects of fiber inclusion on the cyclic response of FR-CPB, monofilament polypropylene (PP) microfibers, as shown in Figure 12, were employed. The synthetic fiber produced by Euclid Chemicals, complies with ASTM C1116 and ASTM D7508 and provides excellent resistance to acid and alkali, according to the manufacturer’s website. The main physical and mechanical properties of the adopted fibers are listed in Table 3.3.

Table 3.3 Physical and mechanical characteristics of polypropylene fibers.

Fiber Type	Polypropylene
Length (mm)	6, 13, 19
Average diameter (μm)	18
Specific gravity	0.91
Tensile Strength (MPa)	500
Melting Point (°C)	160
Water Absorption	Negligible



Figure 3.2 Adopted polypropylene fibers - from left to right: 6 mm, 13 mm, and 19 mm.

3.2 Mix recipe and curing method

FR-CPB specimens in this study were created using a water-cement ratio of 7.6 and a cement content of 4.5% (see Equation 3.1 for mass of cement calculation). Table 3.4 and Table 3.5 detail the specimen groups, fiber length and fiber content employed, and the curing times for the cyclic tensile and compressive tests, respectively. The specimens were cast in a two-step process: (1) dry mixing the tailings, cement, and fibers for five minutes to ensure proper fiber distribution, and (2) wet mixing for eight minutes by adding water. After this process, the fresh CPB and FR-CPB paste were poured into two sets of molds: small cylindrical molds (of dimensions 5 cm x 10 cm) used for cyclic compressive tests and large cylindrical molds (of dimensions 10 cm x 20 cm) used for cyclic tensile tests respectively. Samples were cast in one layer and consolidated using an iron tamping rod (15 blows for small molds and 20 blows for large molds) and a rubber mallet (30 taps for both molds) to remove any air bubbles trapped inside the fresh paste. Lastly, the casted specimens were covered with matching lids to prevent moisture exchange with the environment, labeled, and cured at room temperature (approximately 20 °C) in the laboratory room (see Figure 3.3).

$$M_c = \frac{\gamma_{CPB} V_{mold}}{\left[\frac{1}{C_m} + w/c \right]} \quad (3.1)$$

where $\gamma_{CPB} = 20 \frac{kN}{m^3}$ and is the dry density of the selected tailings, V_{mold} is the volume of plastic mold, g is the gravitational constant, C_m is the cement content, and w/c is the water-cement ratio.

Table 3.4. Summary of mix recipe and curing times adopted for cyclic tensile tests.

Group	Mix Recipe	Fiber	Curing Time	Samples
1-A	W/C = 7.6, Cm = 4.5%	Fc = 0.5%	7, 28, 90	6
		Fiber length = 6mm		
1-B	W/C = 7.6, Cm = 4.5%	Fc = 0.5%	7, 28, 90	6
		Fiber length = 13mm		
1-C	W/C = 7.6, Cm = 4.5%	Fc = 0.5%	7, 28, 90	6
		Fiber length = 19mm		
2-A	W/C = 7.6, Cm = 4.5%	Fc = 0.25%	7, 28, 90	6
		Fiber length = 13mm		
2-B	W/C = 7.6, Cm = 4.5%	Fc = 0.75%	7, 28, 90	6
		Fiber length = 13mm		
C	W/C = 7.6, Cm = 4.5%	-	7, 28, 90	6
Total				36

Table 3.5. Summary of mix recipe and curing times adopted for cyclic compressive tests.

Group	Mix Recipe	Fiber	Curing Time	Samples
1-A	W/C = 7.6, Cm = 4.5%	Fc = 0.5%	7, 28, 90	18
		Fiber length = 6mm		
1-B	W/C = 7.6, Cm = 4.5%	Fc = 0.5%	7, 28, 90	18
		Fiber length = 13mm		
1-C	W/C = 7.6, Cm = 4.5%	Fc = 0.5%	7, 28, 90	18
		Fiber length = 19mm		
2-A	W/C = 7.6, Cm = 4.5%	Fc = 0.25%	7, 28, 90	18
		Fiber length = 13mm		
2-B	W/C = 7.6, Cm = 4.5%	Fc = 0.75%	7, 28, 90	18
		Fiber length = 13mm		
C	W/C = 7.6, Cm = 4.5%	-	7, 28, 90	18
Total				108

To study the evolutive cyclic compressive and tensile behaviors and properties of FR-CPB, the prepared specimens were cured for 7, 28, and 90 days respectively. In total, 120 small cylindrical samples (12:108 trial to official tests) were created for cyclic compressive testing and 50 large cylindrical samples (14:36 trial to official tests) for cyclic tensile tests.



Figure 3.3 Cylindrical samples cured in the laboratory.

3.3 Mechanical testing program

Several trial tests were performed to select a suitable loading rate and displacement increment that would ensure clear hysteresis loops to further the understanding of the damage process of FR-CPB under cyclic loading conditions. After this trial period, a loading/unloading rate of 0.033 mm/s and a definite deformation of 15 mm (or 15% strain) were selected. Once the target curing time is reached, each sample is carefully removed from its molds using compressed air and then cut using a table saw to achieve a flat sample surface to avoid stress concentrations during testing. In this study, the MultiPurpose TestWare Software model number 793 (MTS 793.00) was used to perform displacement-controlled cyclic compressive tests. The testing system (seen in Figure 3.4) consists of a remote controller and loading frame that can measure up to 444.8 kN (10 kips). The MTS machine is a comprehensive test design environment and an industry-proven application tool set to conduct a full spectrum of testing from static uniaxial materials testing to highly dynamic multiaxial simulations. Additionally, to ensure reproducibility of the test results, three samples were tested for each curing condition and mix recipe.

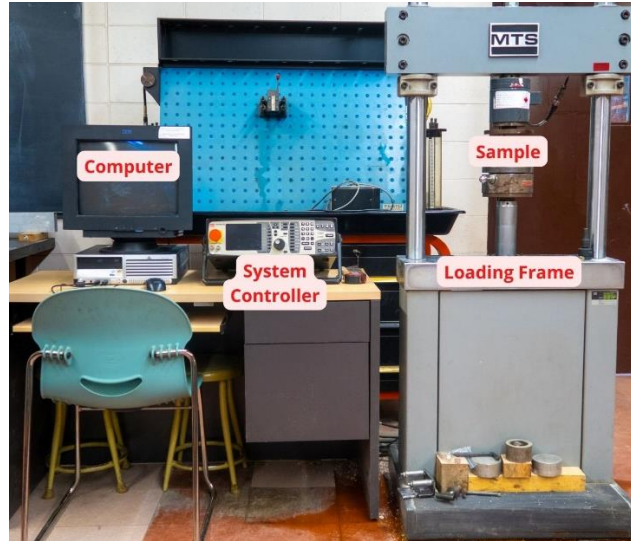


Figure 3.4. Experimental setup of MTS system controller and loading frame.

3.3.1 Cyclic compressive tests

The selected loading rate and displacement increment were programmed into the test system using a custom cyclic sequence that applies compressive loading and records load-displacement data every 0.5 seconds. This custom sequence is illustrated by the schematic in Figure 3.5, where a 0.25% strain increment is applied in the pre-peak zone (0 to 2%) and 1% strain increment in the post-peak region. By applying such a hierarchical loading strategy, a better understanding of the mechanical response of FR-CPB under cyclic compressive loading can be obtained for the pre- and post-peak regions, respectively. Further, cylindrical samples are removed from their molds and trimmed at both ends using a table saw, each sample cut length was recorded for strain calculations, and cyclic tests are carried out thereafter.

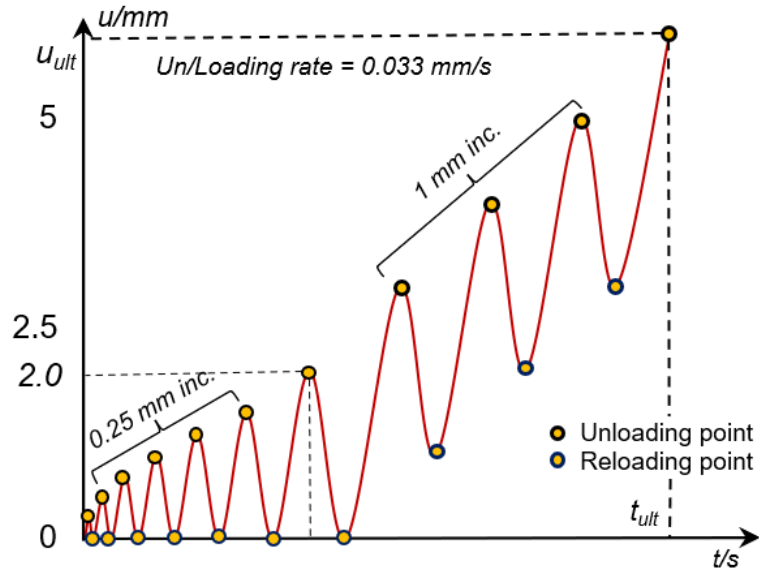


Figure 3.5. Schematic diagram of cyclic compressive loading procedure (adopted in part from [48]).

3.3.2 Cyclic tensile tests

After the target curing time has been achieved, samples are removed from their mold using compressed air and cut into three cylindrical samples (each 5 cm in width) using a table saw to achieve a perpendicular surface to avoid stress concentrations during testing. Figure 3.7 illustrates typical loading configurations for the Brazilian Tensile Testing method. In the experiment, each cylindrical sample is subjected to cyclic compressive loading parallel to the vertical diametrical plane [110] using the custom sequence seen in Figure 3.6 and the test configuration seen in Figure 3.7(c) was utilized. The sequence is similar to the previous hierarchal loading scheme, albeit the increment is applied up to 2.5% (8 hysteresis loops at 0.25% strain).

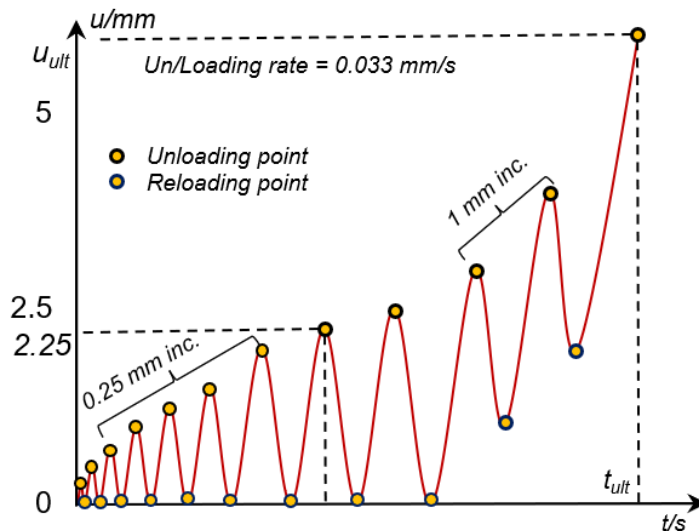


Figure 3.6 Schematic diagram of cyclic tensile loading procedures (adopted in part from [48]).

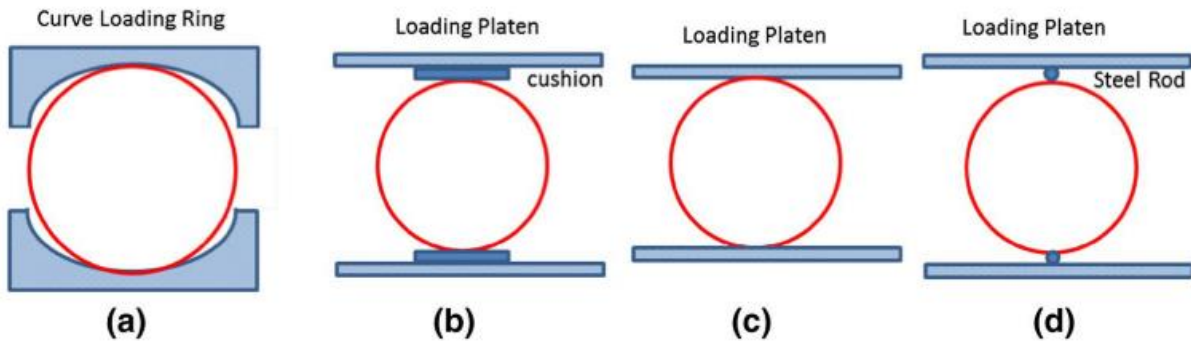


Figure 3.7 Loading configurations of typical Brazilian testing [111].

3.4 Scanning electron microscope (SEM) analysis

In this study, The Scanning Electron Microscope/ Energy Dispersive Spectrometer (SEM/EDXA) facilities at Lakehead University were used to observe the evolutive changes in the cementitious microstructure as FR-CPB ages, and the cement hydration process is fully realized. The equipment used was a Hitachi Su-70 Schottky Field Emission SEM. SEM imagery may provide valuable information relating to the interaction of fiber reinforcement, cementitious matrix, and the interfacial transition zone (ITZ) [8]; defined as the fiber-matrix interfacial transition zone (FM-ITZ). Moreover, SEM may be used to observe the morphology of the fracture surface in CPB as well as the hydration products, which contribute directly to the strength development of CPB [112].

3.5 Determination methods of mechanical properties of FR-CPB

To understand the cyclic tensile response of FR-CPB, the cumulative dissipation energy, secant modulus, degraded stress, and damping index are calculated.

3.5.1 Cumulative dissipation energy

When FRCCs experience plastic deformation, energy is dissipated through mechanisms such as matrix cracking, fiber sliding, and fiber pullout. Previous works have demonstrated the multi-cracking characteristics of FRCCs, which enhance composites' energy dissipation capacity under cyclic tensile loading [16]. The cumulative dissipation energy may be used to describe the transformation of FR-CPB's cementitious matrix from brittle in nature to a more ductile and/or tough one. The dissipated energy in this study is determined by calculating the area of each hysteresis loop by subtracting the area under the unloading curve from the area under the reloading curve. A graphical representation can be seen in Figure 3.7(A) and can be obtained using Equation 3.1.

$$D_e = RL_{area} - UL_{area} \quad (3.2)$$

with

$$\begin{cases} UL_{area} = \left(\frac{\sigma_1 + \sigma_2}{2} \right) \times (\varepsilon_1 - \varepsilon_2) \times 100 \\ RL_{area} = \left(\frac{\sigma_2 + \sigma_1}{2} \right) \times (\varepsilon_2 - \varepsilon_1) \times 100 \end{cases}$$

where, D_e represents the dissipated energy per loop, $\frac{RL}{UL_{area}}$ is the area under the reloading and unloading curve, respectively, $\sigma_{1,2}$ & $\varepsilon_{1,2}$ corresponds to the n^{th} pair of stresses and strains along reloading and unloading curves.

3.5.2 Secant modulus

Cyclic loading induces damage accumulation in the cementitious matrix resulting in significant stress degradation and subsequent reduction in material stiffness [50]. The secant modulus of a cementitious composite may be used to determine the stiffness of the material in the inelastic region of the stress-strain curve. In early load cycles, the loading and unloading paths are almost identical, signaling very little damage to the cementitious composite or reduction in stiffness [48]. As the load cycles increase, stiffness reduction is evident in the distinction between loading/unloading paths which is known as hysteresis. Through the determination of this mechanical property, the evolutionary trends of FR-CPB's stiffness, as well as the effect of cyclic loading conditions, may be understood. This property is determined by calculating the slope of the line connecting the unloading and reloading points, as seen in Figure 3.7(B). The secant modulus was calculated using equation 3.2:

$$S. M_i = \frac{\left(\frac{\sigma_{peak} - \sigma_{min}}{\varepsilon_{\sigma,peak} - \varepsilon_{\sigma,plastic}} \right) \times 100}{1000} \quad (3.3)$$

where, σ_{peak} and σ_{min} are the peak stress and minimum stress for the i^{th} loop, $\varepsilon_{\sigma,peak}$ represents the strain corresponding to the peak stress and $\varepsilon_{\sigma,plastic}$ is the plastic at the end of the unloading phase.

3.5.3 Degraded stress

As previously mentioned, microscale damage accumulation and macroscale stress deterioration cause matrix degradation and subsequent reduction in its' ability to sustain the applied loads.

Understanding the degraded stress of FR-CPB gives insight into the effects of cyclic loading on

the constitutive behavior, and the contributing damage mechanisms may be identified. Specifically, the degraded stress is defined as the reloading stress corresponding to the same total strain before unloading. Although the pre-peak zone loading and unloading paths are similar, stress degradation is evident due to crack propagation and damage accumulation in the fiber-reinforced cementitious matrix. In this study, Figure 3.7(C) depicts the degraded stress for FR-CPB. It is determined by identifying the total strain before unloading with a vertical line that intersects the reloading curve; this value represents the degraded stress.

3.5.4 Damping index

When a system/structure experiences dynamic loadings, the amplitude of oscillation is increased. In other words, that system undergoes excitation. It has been previously found that the damping characteristics of FRCCs are mainly affected by fiber inclusion, fiber-matrix interfaces, moisture, pore spaces, and the presence of micro-cracks [113]. Furthermore, the process of energy dissipation also increases this level of excitation. Determination of the damping capacities of FR-CPB may be an important mechanical property to further highlight the significance of understanding the evolutive properties of FR-CPB under cyclic tensile loading conditions. Moreover, the integrity of mining structures and the lives of mine occupants are paramount in applying CPB as a tailing disposal method. Furthermore, factors such as the presence of micro-cracks, fiber inclusion, fiber-matrix interface, and pore space all contribute to the damping characteristics of FRCC [22]. In this study, the damping index is determined by dividing the cumulative energy dissipated at the i^{th} loop by the corresponding total plastic strain energy at the i^{th} loop. The damping index is expressed as,

$$D_i = \frac{D_{e,cum.}}{\sum S_{e,plastic}} \quad (3.4)$$

where, $D_{e,cum.}$ represents the cumulative energy dissipated and $\sum S_{e,plastic}$ represents the total plastic strain energy. The damping index is then plotted against the cumulative energy dissipation to understand the evolution of the composites dampening capacity under cyclic compressive loadings (as seen in Figure 3.7(D)).

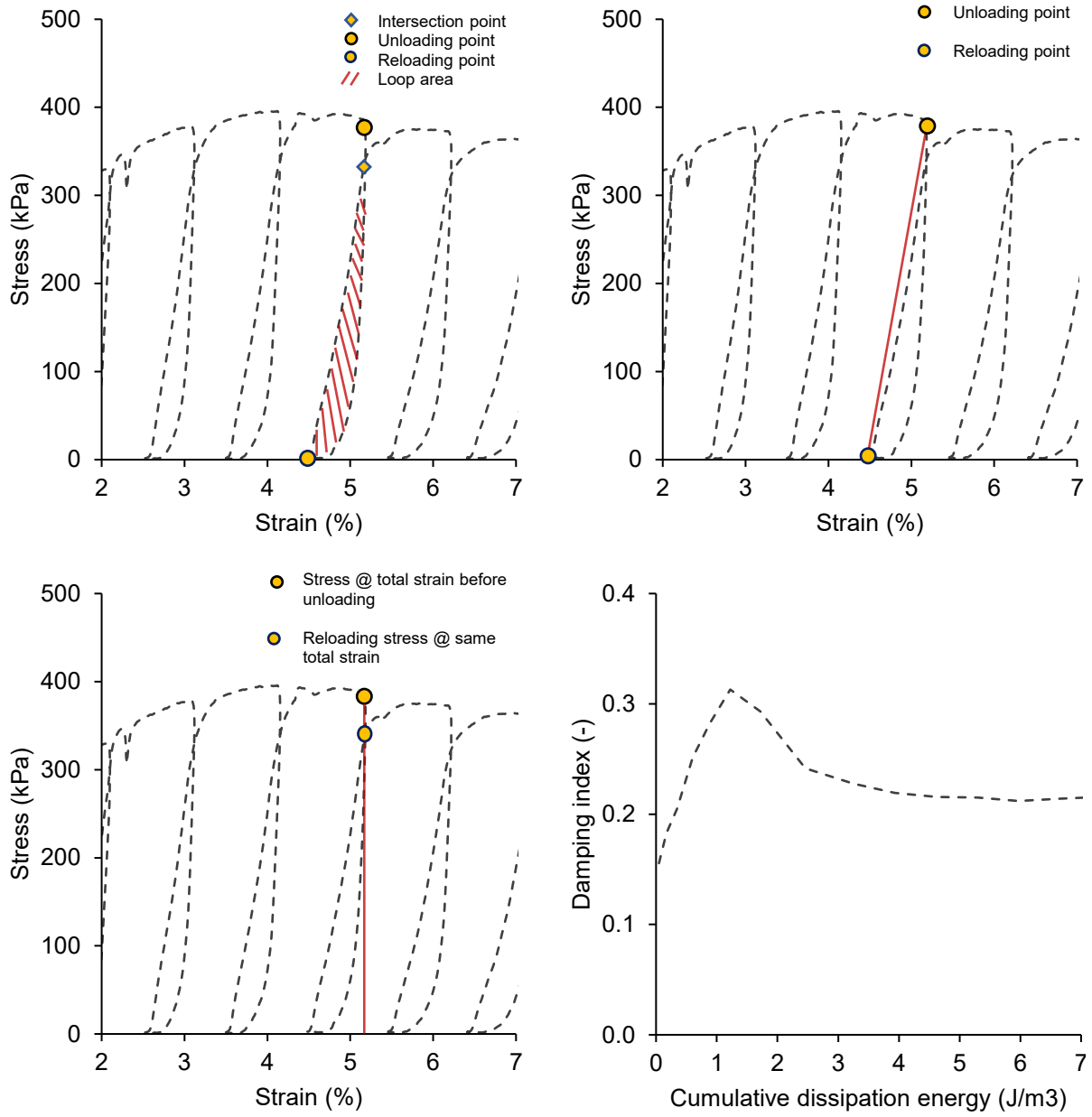


Figure 3.8 Definition of mechanical properties of FR-CPB: (a) hysteretic dissipation energy, (b) secant modulus, (c) degraded stress, and (d) damping index.

4.1 Compressive behavior and properties of FR-CPB under cyclic loadings

The general compressive behavior of FR-CPB is illustrated in Figures 4.1 and Figure 4.2. The mechanical response is dominated by the synergistic effect created by the evolution of the newly formed fiber-matrix network. FR-CPB demonstrates an improved ability to withstand cyclic compressive loadings, and the inclusion of fibers transforms the brittle cementitious matrix into a ductile one. As a result, FR-CPB's mechanical properties are enhanced, and the level of cyclic-induced damage is alleviated. Subsequently, the transformation of macroscale failure patterns is shifted from localization of large macroscale cracks, bulking, and blocking [8] to a higher degree of crack restraint and thus lower crack mouth openings.

4.1.1 Effect of fiber length on the evolutive cyclic compressive behavior of FR-CPB

FR-CPB demonstrates curing time-dependent stress-strain behaviors, including the improvement of (1) pre-peak strain hardening, (2) peak stress (compressive strength), (3) brittleness (strain corresponding to the peak stress shows an obvious decrease with curing time), and (4) enhancement of post-peak residual strength with curing time. In FR-CPB, strength development is attributed to a combined effort from the cementitious matrix and fibers. The applied stress is first resisted by the cementitious matrix (uncracked), and fibers only play a part when their tensile strength is mobilized, i.e., through matrix cracking mechanisms such as fiber pull-out and fiber-matrix debonding [16]. Furthermore, the increase in curing time results in a stronger cementitious matrix that contributes to the improved peak strength and the increasing trend in brittleness (reduction in strain corresponding to the peak stress). Subsequently, the fiber-matrix bond plays a vital role in the strength development of FR-CPB, especially in the early stages of the loading process.

Observing Figure 4.1, fiber length affects the pre-peak behavior and peak stress by influencing the slope of the pre-peak branch, which is inconsistent with findings obtained by the previous studies on conventional FRCC [16,103]. In previous studies, it has been found that the pre-peak behavior is insensitive to the inclusion of synthetic fibers. This is because synthetic fibers are relatively soft compared to the bulk matrix. Therefore, the effectiveness of fiber reinforcement

requires sufficient deformation (i.e., microcrack opening) in the matrix to break up cohesive bonds and mobilize the composites' frictional strength. However, conventional FRCC with a higher cement content (typically 3.3 times higher than that used by CPB materials) leads to a stronger and stiffer cementitious matrix, which causes very limited deformation during the pre-peak stage. Hence, the mechanical response and properties of cementitious matrix dominate the pre-peak behavior of conventional FRCC. However, FR-PCB with a relatively low cement content forms a soft bulk matrix and the mobilized friction sliding between tailings particle plays a more important role at the pre-peak stage. Consequently, a relatively large deformation can be obtained from CPB material during the strain-hardening process and thus activate the pre-peak fiber reinforcement to a greater extent. In the post-peak stage: longer fibers further increase the residual strength. However, when the fiber length is greater than 13mm, the post-peak improvement becomes limited. Two potential reasons to explain this observation are: (1) longer fiber can transfer the stress into the bulk matrix to a greater extent and thus form a larger reinforced regime in the bulk matrix. Consequently, the FR-CPB with longer fibers becomes tougher under cyclic loading. (2) To study the effect of fiber length, the fiber content is fixed for all FR-CPB samples. Thus, increasing the fiber length also leads to the decrease in the number of fibers at a given regime of the bulk matrix, which will inevitably weaken the local reinforcement. Additionally, hysteretic loops are very narrow at the pre-peak stage, while wider hysteretic loops are consistently measured at the post-peak stage at all curing times. The existence of narrow pre-peak hysteretic loops further confirms the effectiveness of fiber reinforcement at the pre-peak stage. Moreover, an increase in the fiber length can further widen both pre- and post-peak hysteretic loops, and thus more external energy can be dissipated. In addition, when the fiber length increases from 6mm to 13mm, the hysteretic behaviors become more pronounced. However, when fiber length is further increased to 19mm, the improvement of hysteretic behavior is limited, which is consistent with findings of the effect of fiber length on the post-peak residual strength of FR-CPB at different curing times [114].

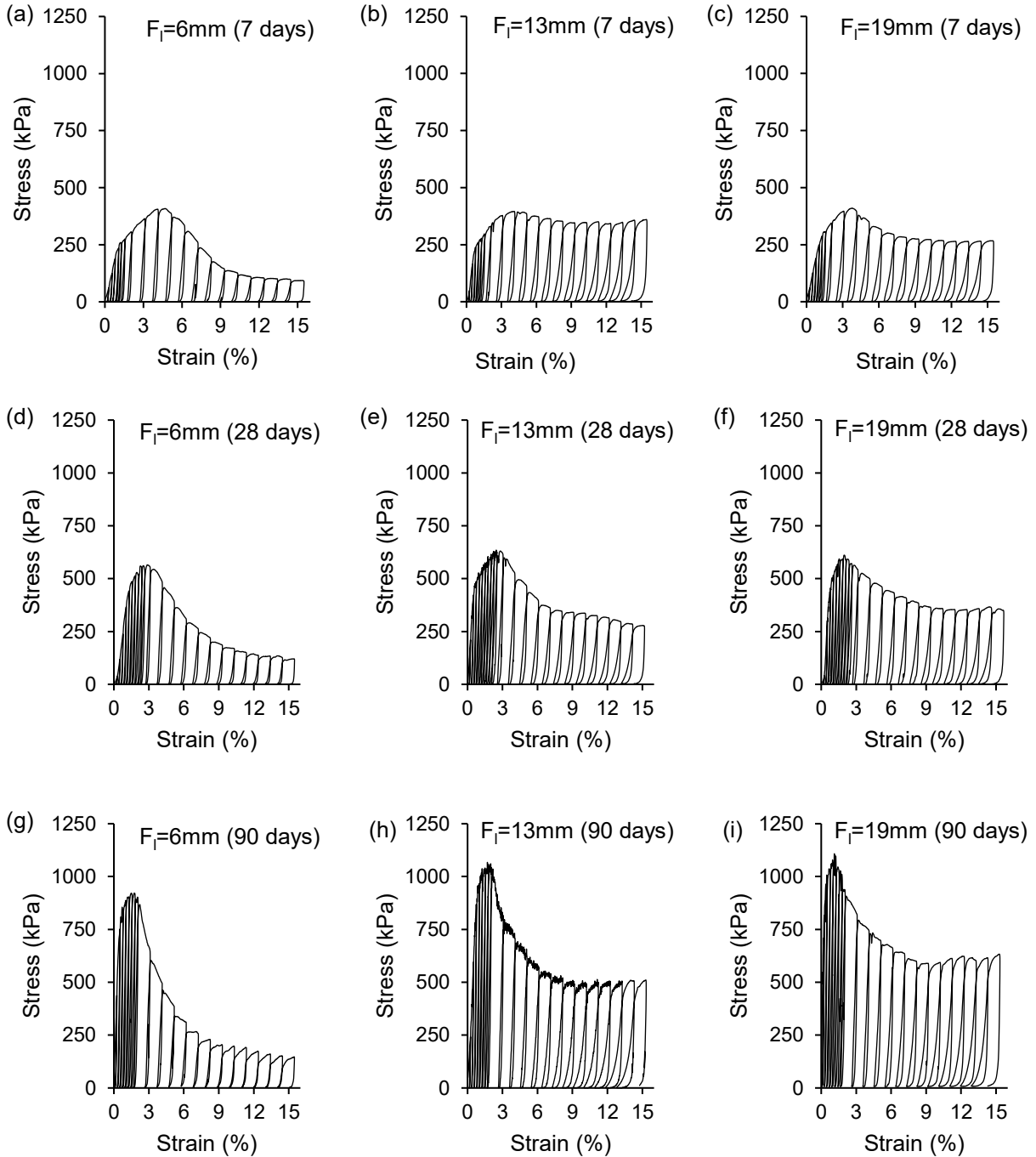


Figure 4.1 Effect of fiber length (6mm, 13mm, and 19mm) on the cyclic compressive stress-strain behavior of FR-CPB with a fixed fiber content of 0.5wt% at 7 days (a, b, and c), 28 days (d, e, and f), and 90 days (g, h, and i).

4.1.2 Effect of fiber content on the evolutive cyclic compressive behavior of FR-CPB

To study the effect of fiber content on the evolutive properties of FR-CPB, a constant fiber length of 13mm was selected, and three variations in fiber content, i.e., 0.25wt%, 0.5wt%, and 0.75wt%. Analyzing the stress-strain curves presented in Figure 4.3 suggests that FR-CPB

demonstrates a high dependency on curing time which is evident in the pre-peak and post-peak branches, respectively. Specifically, pseudo-strain hardening is an evident mechanism in FR-CPB's pre-peak response to cyclic compressive loading, as is strain softening in the post-peak branch. Subsequently, FR-CPB demonstrates a significant improvement in the peak stress and residual strength when fiber content was kept constant for 7, 28, and 90 days (example Figure 19(a,d,g)), respectively. However, when curing time is constant and fiber content is varied, there exists a critical fiber content of 0.5wt%. Beyond this critical value, there is a decreasing trend in the peak strength and shortening in the strain hardening response of FR-CPB. Interestingly, the post-peak branch demonstrates the most improvement when $F_c = 0.75wt\%$. This finding is consistent with the role of fibers in the pre- and post-peak zones correspondingly.

As previously stated, fiber inclusions afford FRCCs multiple cracking characteristics that result in a stronger, more tough cementitious composite with a more uniform cracking process. Recall fiber inclusion introduces new defects or discontinuities in the cementitious matrix through inadequate compactness and may induce matrix crushing leading to local stress concentration and subsequent weakening of the cementitious matrix [103,104]. The limited improvement of FR-CPB with $F_c = 0.75wt\%$ compared to $F_c = 0.5wt\%$ can be explained by the development of the FM-ITZ. Precisely, as shown in Figure 4.2, the inclusion of fibers into CPB matrix unavoidably affects the particles package and thus form a distinct FR-ITZ which are featured with a relatively large porosity. Due to the dependency of mechanical properties on porosity, the weak FR-ITZ represents the weakest regime in the cementitious matrix. Correspondingly, as the fiber content is increased, more FM-ITZs are created, which inevitably results in a reduction of the reinforcing effect. For FR-CPB, this is evident as there is a decreasing trend in peak strength beyond the critical fiber content as these defects increase the rate of crack localization, which also decreases the load at which the first crack appears. In the post-peak branch, the mechanism of strain softening and the passive confinement provided by fibers allow FR-CPB to demonstrate a pronounced softening response leading to a highly ductile failure [99]. Moreover, the high residual stress suggests that the increased fiber content is able to slow post-peak stress deterioration and maintain matrix integrity to a higher degree at the expense of peak strength.

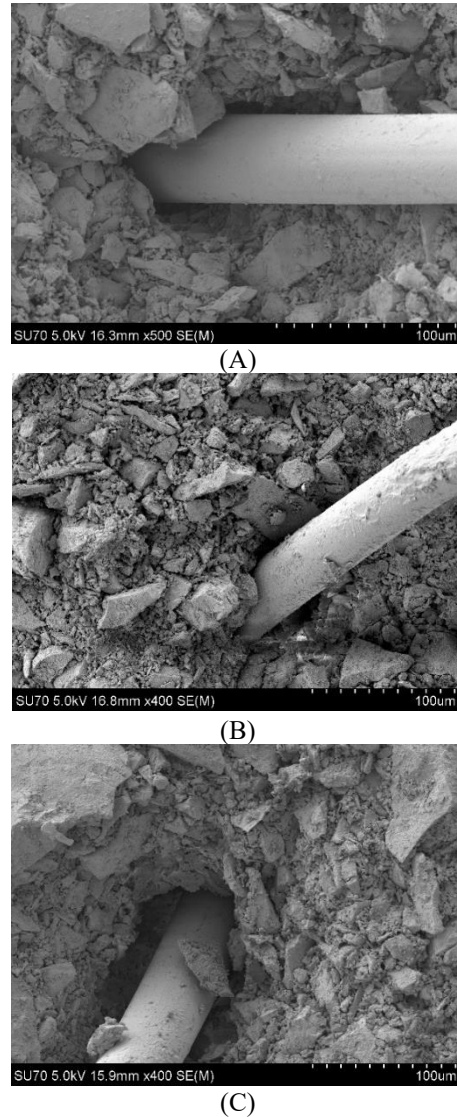


Figure 4.2 Evolution of cementitious microstructure in FR-CPB (A) 3 days, (B) 28 days, (C) 56 days.

Additionally, reinforcement mechanisms such as fiber bridging, fiber sliding, fiber-pullout, and fiber-matrix debonding are responsible for the development of a composite's energy dissipation capacity. By increasing the fiber content, more of these events can take place in the cyclic response of FR-CPB leading to more pronounced hysteresis loops both in pre- and post-peak zones. In the pre-peak zone, FR-CPB shows a rapid growth trend in energy dissipation capacity up to the cycle corresponding to the peak stress and transitions to a steady decrease in the post-peak branch of the stress-strain curve. This rate of decrease in dissipation capacity is sensitive to the fiber content, i.e., a softer material can be achieved even with a fiber content greater than the critical value of $F_c=0.5\text{wt}\%$. Furthermore, the highest degree of softening is noticed for late age FR-CPB (90 days) and $F_c=0.75\text{wt}\%$.

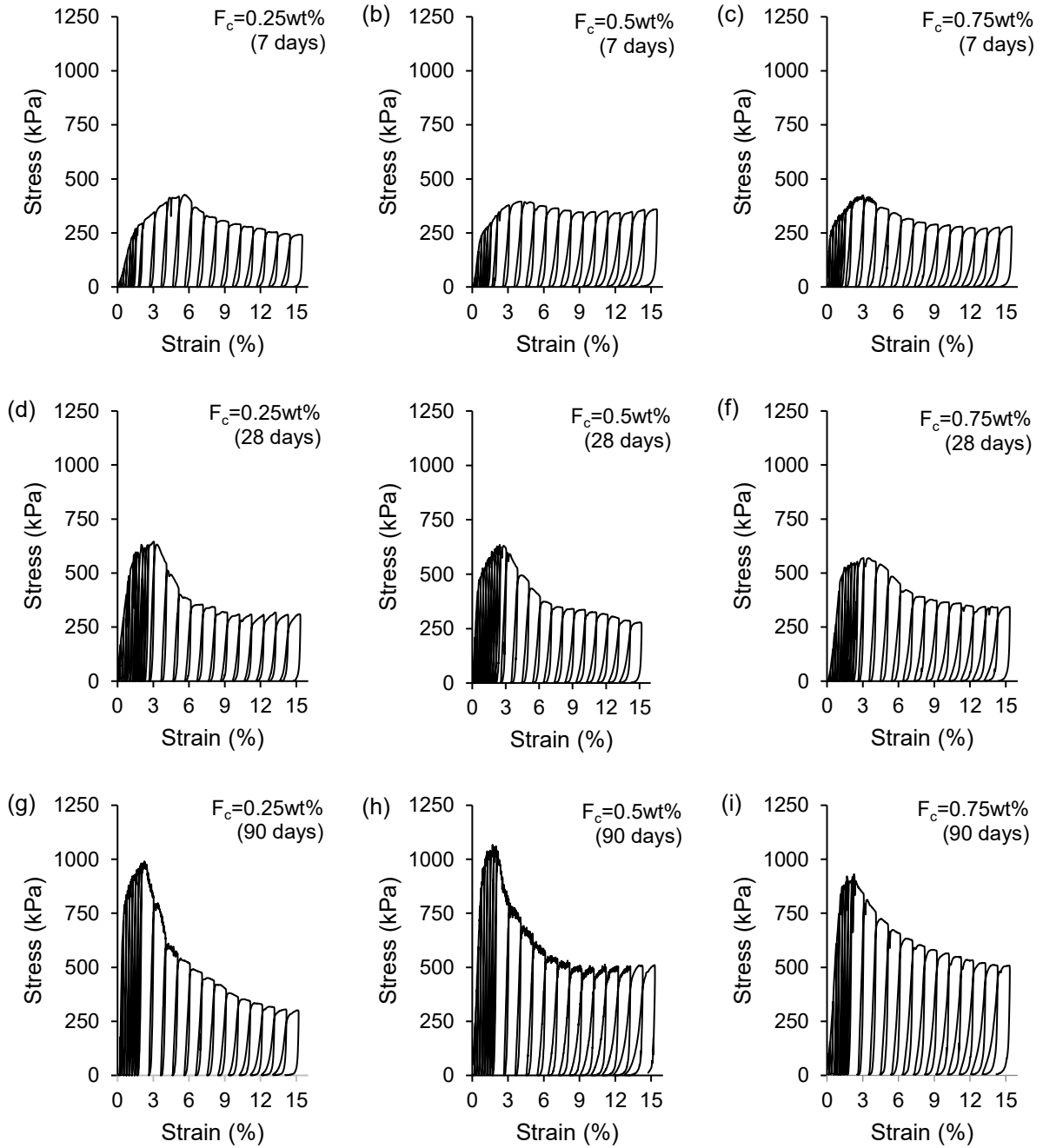


Figure 4.3 Effect of fiber content (0.25wt%, 0.5wt%, and 0.75wt%) on the cyclic compressive stress-strain behavior of FR-CPB with a fixed fiber length of 13mm at 7 days (a, b, and c), 28 days (d, e, and f), and 90 days (g, h, and i).

4.1.3 Effect of fiber inclusion on the hysteretic energy dissipation

FR-CPB shows a high dependency of hysteretic dissipation energy on curing time. FR-CPB at advanced ages, is able to dissipate larger amounts of strain energy and further toughen the materials. The cementitious matrix of early age FR-CPB is unable to fully realize the multi-

cracking characteristic of fiber reinforcement due to the strength development of the microstructure and the fiber-matrix interaction. Specifically, failure of test specimens featured bulging and depressed surfaces accompanied by one or two major cracks. This signifies the absence of the multiple cracking process that can be achieved for specimens cured at later ages. Furthermore, the refined microstructure at later ages causes a stronger interaction between fiber and matrix and thus increases the hysteretic energy dissipation. Consequently, FR-CPB shows a stronger time-dependent evolution of hysteretic energy dissipation.

The pre- and post-peak hysteretic energy dissipation show different evolutionary trends. From Figure 4.4, a slow growth rate can be observed during the pre-peak stage (0 up to 8 cycles or 2% strain). The obtained cumulative energy further confirms the effectiveness of pre-peak reinforcement. At the post-peak stage (beyond 2% strain), a rapid increase in the hysteretic dissipation energy is detected, especially at later ages. Moreover, longer fibers can increase hysteretic energy dissipation as they offer a greater crack bridging capacity by restricting crack opening and/or sliding due to the dowel-action mechanism [87]. However, 19mm and 13mm fibers yield similar hysteretic energy dissipation from early to advanced ages, which clearly indicates the existence of a critical fiber length. In other words, when the fiber length is less than this critical value, an obvious improvement of hysteretic energy dissipation can be obtained through an increase in fiber length. Similarly, an increase in fiber content can improve hysteretic energy dissipation. Moreover, there also exists a critical fiber content ($F_c = 0.5wt\%$). When the fiber content is greater than this critical value, the improvement of hysteretic energy dissipation is relatively limited.

Additionally, a comparison of fiber content and fiber length shows that although the changes in fiber length and fiber content can yield similar evolutionary trends, the improvement extent of hysteretic energy dissipation is different. It can be observed that the hysteretic energy dissipation is more sensitive to the changes in the fiber length. Specifically, damage mechanisms such as fiber pullout and fiber-matrix debonding can be inhibited since longer fibers can offer a greater degree of anchorage. Furthermore, longer fibers can permit a wider crack mouth opening and subsequently allow more energy to be dissipated.

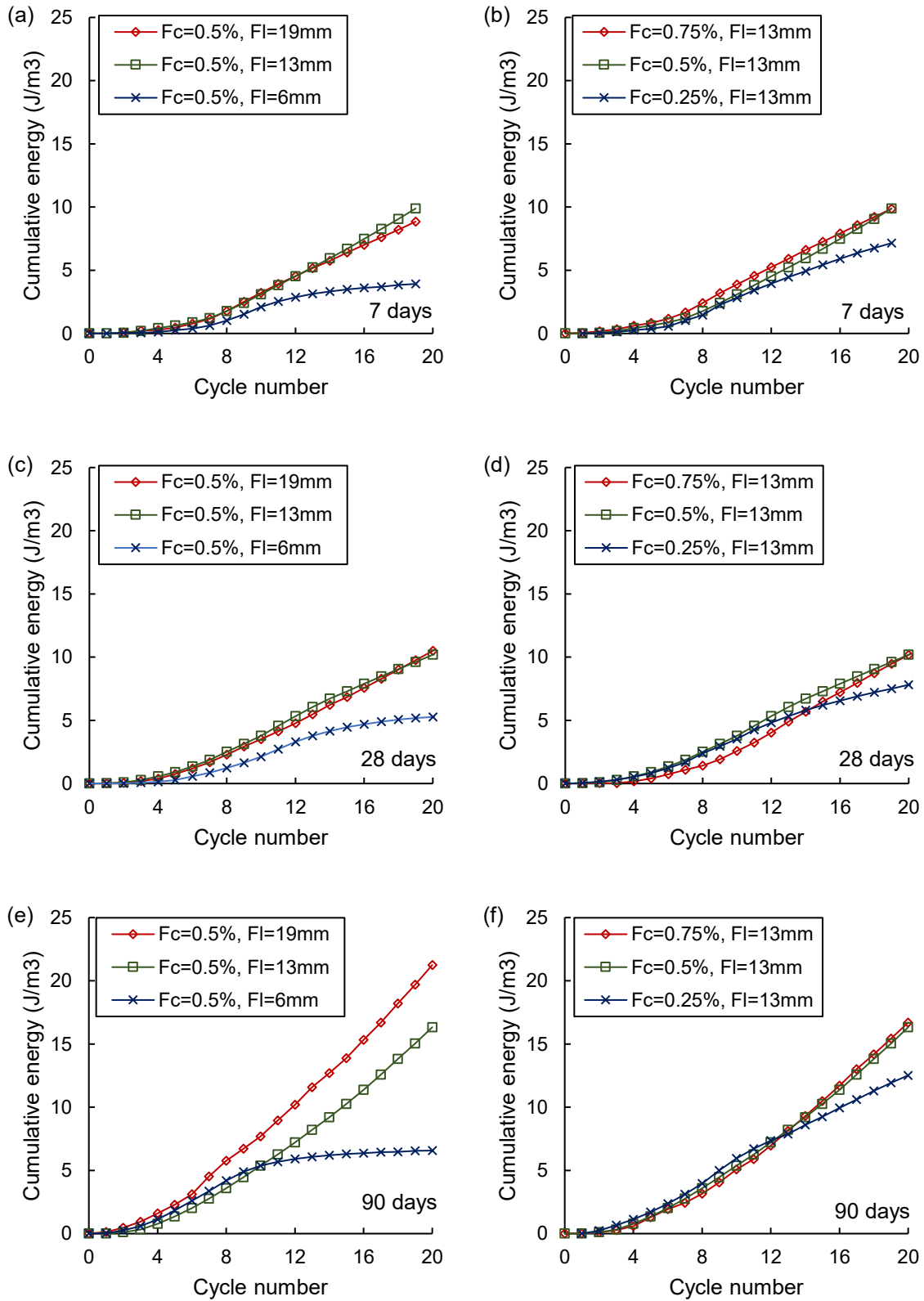


Figure 4.4 Effect of fiber inclusion on the hysteretic dissipation energy of FR-CPB at 7 days (a and b), 28 days (c and d), and 90 days (e and f).

4.1.4 Effect of fiber inclusion on the secant modulus

The relationship between the secant modulus and cumulative energy of FR-CPB explains the damage accumulation under cyclic loading. As more energy is dissipated, the composite becomes less stiff due to cyclic-induced damage to the fiber-reinforced cementitious matrix. Observing Figure 4.5, the secant modulus demonstrates positive evolutive trends under cyclic compressive loading. As FR-CPB ages across the selected curing times, the peak secant modulus is significantly improved. The fiber-reinforced cementitious matrix becomes stronger, leading to significant improvement in its' ability to withstand the applied loads. Specifically, the PP fibers and the cementitious matrix is better able to perform as a network and resist frictional forces during the crack opening and closing processes. Furthermore, FR-CPB at advanced ages is significantly stiffer and cumulatively dissipates more energy due to the strengthened fiber bridging effect. Additionally, analyzing the data for secant modulus of FR-CPB under cyclic compressive loading, it is again confirmed that a fiber length of 13 mm and fiber content of 0.5wt% provides the most effective reinforcement effects. Interestingly, longer fibers improved the secant modulus for 28-day FR-CPB; the opposite is observed for 7-day FR-CPB. In the pre-peak zone, the effectiveness of fiber reinforcement is verified once again as the multiple cracking leads to an increase in secant modulus until the localization of the first crack, where a transition from linear to non-linear behavior on the stress-strain curve is observed. In the post-peak zone, the strain softening behavior is represented as a steady decrease in the secant modulus of FR-CPB as damage is accumulated in the cementitious matrix. Moreover, after the peak stress, the stiffness of the composite decreases significantly with increasing load cycles as a result of crack propagation and subsequent damage accumulation in the matrix. Increasing the fiber length from 6 mm to 13 mm results in a stiffer cementitious matrix and slows the rate of degradation in matrix integrity. However, there exists a critical fiber length of 13 mm as there are no obvious difference in improvement between 13 and 19 mm, respectively. Similarly, a critical fiber content of 0.5wt% is observed. When the effects of both fiber length and fiber content are observed, the secant modulus is more sensitive to the fiber length changes. As stated previously, longer fibers offer a higher degree of anchorage in the cementitious matrix which requires a higher level of strain to cause fiber-matrix debonding or fiber rupture. Consequently, higher damage accumulation in the cementitious matrix is expected for specimens with longer fibers.

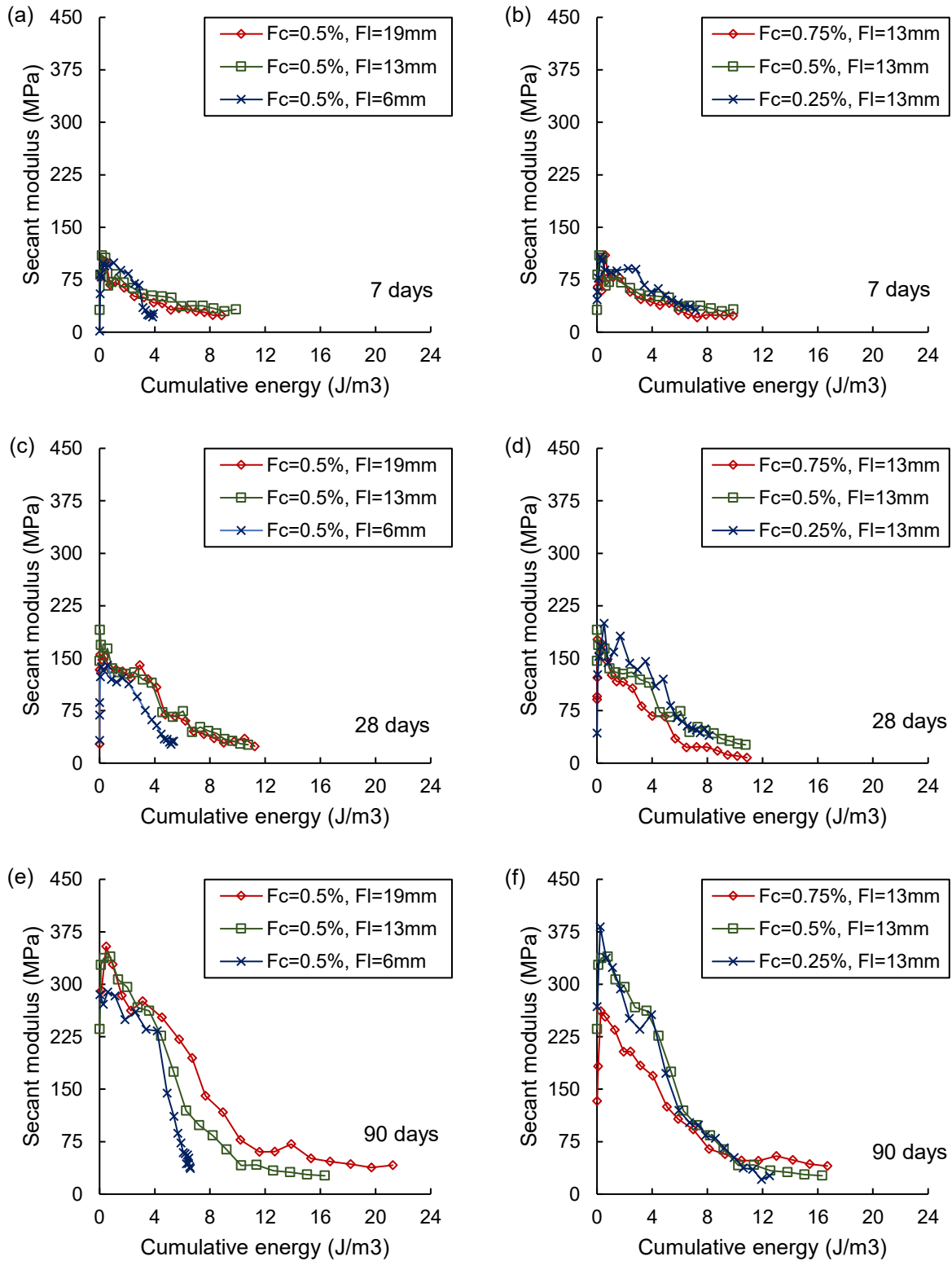


Figure 4.5 Effect of fiber inclusion on the secant modulus of FR-CPB at 7 days (a and b), 28 days (c and d), and 90 days (e and f).

4.1.5 Effect of fiber inclusion on the degraded stress

Observing Figure 4.6, the degraded stress of FR-CPB demonstrates a high dependency on curing time. FR-CPB at late ages has the highest load carrying capacity due to the improvement of the cementitious matrix and fiber-matrix interaction as curing time increases. When FR-CPB is subjected to cyclic compressive loading, the composite suffers local damage, which degrades the load carrying capacity especially as loading cycles increase. For example, if we study the stress-strain diagrams in Figure 18, curing time increases the load at the first crack for FR-CPB.

Furthermore, this degradation begins in the pre-peak zone and becomes most obvious when the stress-strain diagram transitions to a non-linear curve; this signifies the cyclic-induced material degradation. Due to this damage accumulation in the cementitious matrix, the composite is unable to match the level of stress from the previous load cycle, which is where the fibers play an important role. Furthermore, no obvious improvements were obtained from employing 6 mm fibers, especially at 28 days, and no obvious difference in FR-CPB with a fiber length greater than 13 mm (critical fiber length). In the pre-peak zone, material degradation begins at the first crack load and becomes more extreme during the pseudo-strain hardening phase and around the peak load. Findings that validate the effectiveness of fiber reinforcement in the pre-peak zone. Furthermore, this increase in degradation happens due to the increased demand for energy to be dissipated through damage mechanisms such as matrix cracking, fiber debonding, fiber pullout, and fiber rupture. In the post-peak zone, FR-CPB demonstrates significant improvement in the rate of stress degradation. Furthermore, for late age FR-CPB, increasing the fiber length significantly enhances the post-cracking strength and results in a more ductile post-peak response to cyclic compressive loadings. This is further evident in Figure 4.7, where increasing the fiber length improves matrix integrity in the post-peak zone. Likewise, an increase in fiber content also shows similar enhancements with restricting crack propagation and limiting the number of major crack localizations. Moreover, there exists a critical fiber length and fiber content of 13 mm and 0.5wt%, respectively. Although there are positive evolutionary trends when both fiber length and fiber content are increased, the degraded stress of FR-CPB is more sensitive to changes in fiber length. Both peak strength and residual stress are higher when fiber content is kept constant at 0.5wt%, and fiber length is set to 13 mm and 19 mm, respectively. However, the same cannot be said for a fiber content greater than 0.5wt%.

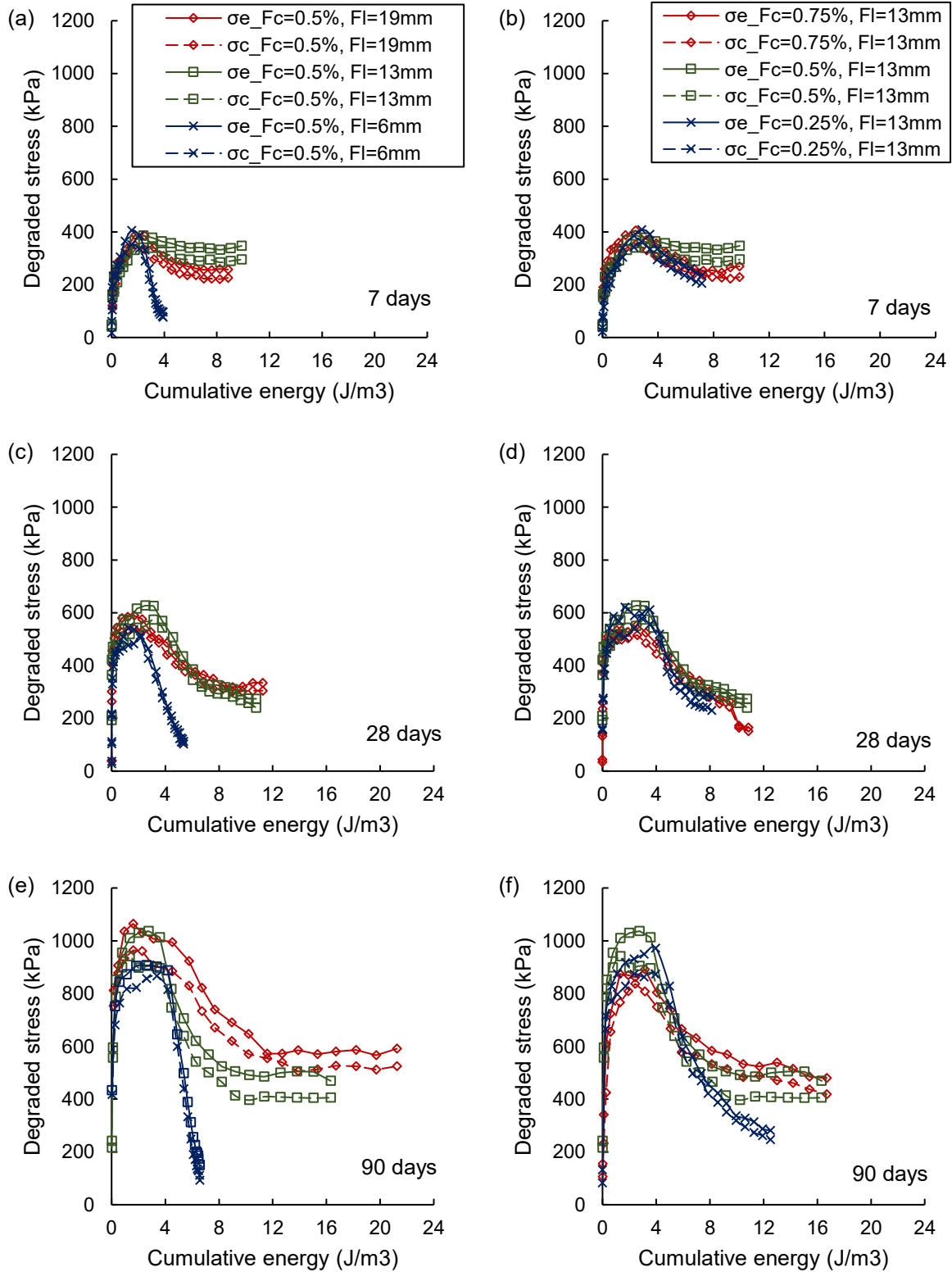


Figure 4.6 Effect of fiber inclusion on the degraded stress of FR-CPB at 7 days (a and b), 28 days (c and d), and 90 days (e and f).



Figure 4.7 Effect of fiber length (a-6mm, b-13mm, and c-19mm) and fiber content (d-0.25wt%, e-0.5wt%, and f 0.75wt%) on the post-peak failure patterns of 90-day FR-CPB.

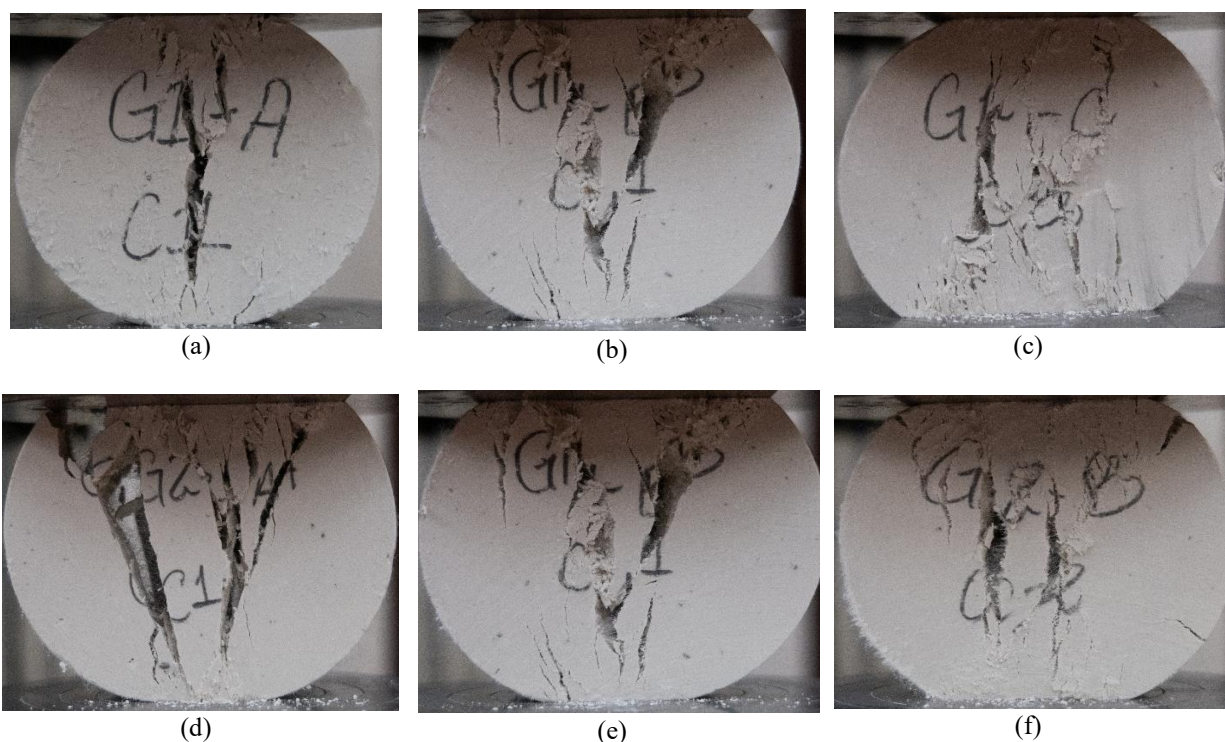


Figure 4.8 Effect of fiber length (a-6mm, b-13mm, and c-19mm) and fiber content (d-0.25wt%, e-0.5wt%, and f-0.75wt%) on the post-peak failure patterns of 90-day FR-CPB.

4.1.6 Effect of fiber inclusion on the damping index

FR-CPB's damping characteristics show a high dependency on curing time. This is evident from the damping index plots shown in Figure 4.8. In early age FR-CPB, the ability of the composite to dampen the effects of cyclic loading is heavily dependent on the combined effect of cementitious matrix and fiber inclusion. Specifically, increasing the fiber length significantly improved the damping index of 7-day and 28-day FR-CPB. Contrastingly, the influence of increasing the fiber content is not as evident across the selected curing times. A stronger, more tough cementitious matrix is able to effectively absorb more deformation energy and reduce stress concentrations in the cementitious matrix, which improves the damping of FR-CPB. In addition, the presence of fibers introduces different damage mechanisms such as fiber rupture and fiber pullout that cause uniform cracking and aid in crack propagation, which further enhances the damping characteristics of FR-CPB. It should also be noted that since the FM-ITZ is the weakest regime in the bulk matrix of FR-CPB, a high contribution of a composite's damping capacity is generated here. More specifically, the relative friction generated when fibers

are displaced and the crack propagation in the FM-ITZ significantly contributes to the composite's damping.

In the pre-peak zone, the fiber-reinforced microstructure experiences significant micro-cracking as energy is dissipated, especially in the pseudo-strain hardening phase. In early age FR-CPB, the peak damping index is achieved at lower cumulative energy, and the slope of the pre-peak branch is very small. At later curing times, a significant increase is noticed in the slope of the pre-peak branch as well as the cumulative energy dissipated corresponding to the peak damping index. In the post-peak region, an increase in fiber length enhances the residual damping of FR-CPB, especially at early ages. As curing time increases, the area under the damping index curves increases, and there is a significant improvement in the cumulative energy dissipated by FR-CPB. From early to late ages, FR-CPB shows no major improvements when fiber content is varied.

When we observe the effects of fiber inclusion, improvement to the damping characteristics of FR-CPB is more sensitive to fiber length changes. The pre-peak response, peak damping index, and post-cracking damping index are improved when fiber length is varied compared to fiber content, especially at early age FR-CPB. Moreover, increasing fiber length allows FR-CPB to dissipate a higher cumulative energy while maintaining a relatively high damping index in the post-peak region.

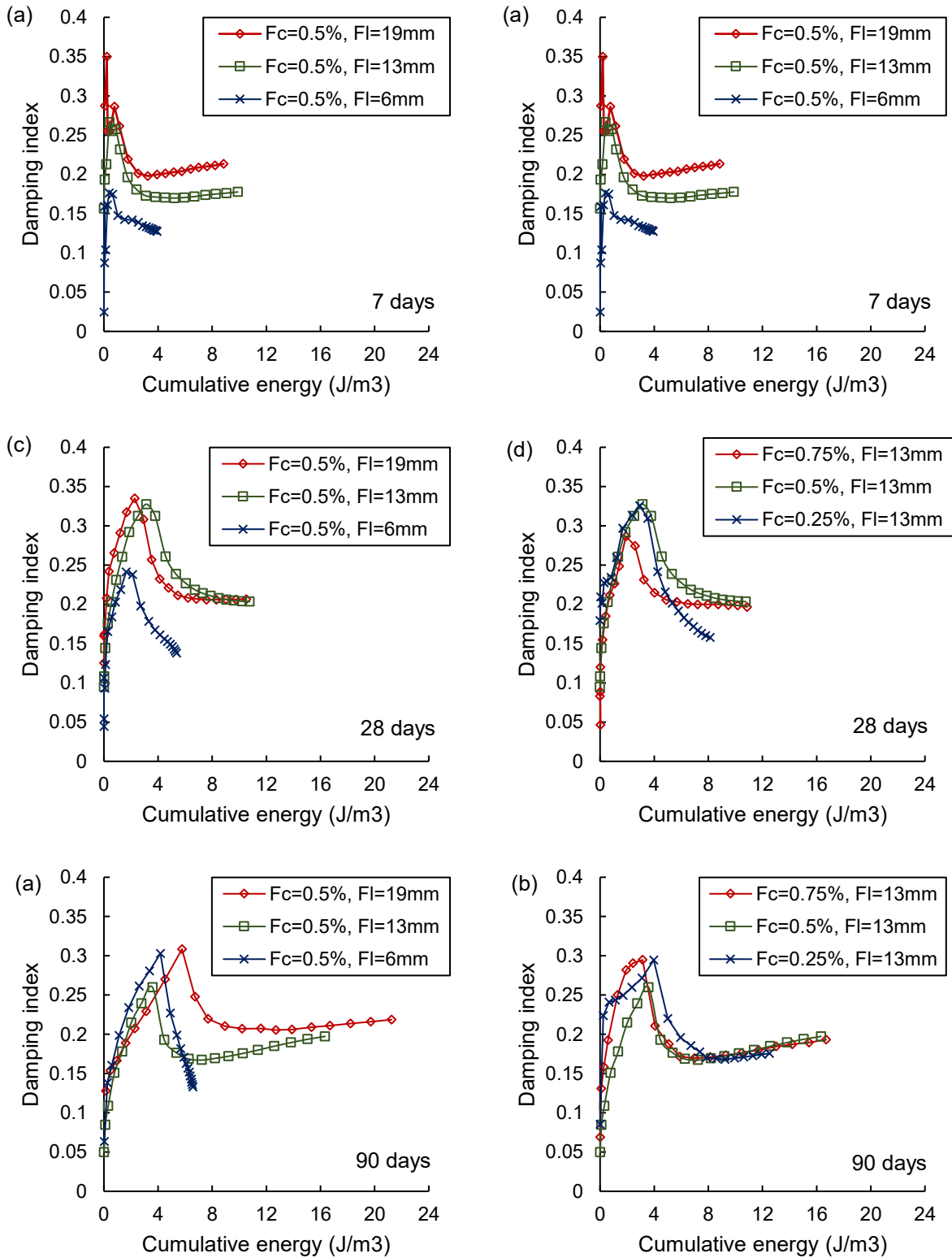


Figure 4.9 Effect of fiber inclusion on the damping index of FR-CPB at 7 days (a and b), 28 days (c and d), and 90 days (e and f).

4.2 Tensile behavior and properties of FR-CPB under cyclic loadings

The tensile behavior of FR-CPB under cyclic loadings is illustrated in Figure 4.9 and Figure 4.10. From observation, the damage process of FR-CPB demonstrates clear multiple cracking characteristics through the phenomenon of pseudo-strain hardening, emphasizing the benefits of fiber inclusion on both pre- and post-peak branches. Moreover, the rate of crack localization is slowed as FR-CPB is able to maintain matrix integrity as fiber parameters are changed.

Furthermore, the mechanical properties of FR-CPB are significantly improved due to the crack bridging capabilities of the included fibers.

4.2.1 Effect of fiber length on the evolutive cyclic tensile behavior of FR-CPB

Observing Figure 4.9, FR-CPB's stress-strain behavior demonstrates a high dependency on curing time. As FR-CPB ages, there exists a positive evolutionary trend in pre-peak strain hardening, brittleness as the strain corresponding to the first crack stress is reduced as the curing time increases and significant improvement of the post-peak residual strength. Furthermore, the cyclic tensile response of FR-CPB features a pronounced softening effect when 6 mm fibers are employed and diminishes when the fiber length is increased to 13 mm and 19 mm, respectively. This pronounced softening effect is followed by the pseudo-strain hardening phenomenon where fiber reinforcement restricts initial tension cracks hereby promoting the multiple cracking characteristics in FR-CPB as observed in FRCCs [115]. Moreover, the hydration process is more realized in later age FR-CPB which contributes to a stronger fiber-matrix interaction and increases bond strength [116]. Recall that cementitious materials possess relatively weak tensile strength, and therefore, as FR-CPB ages, longer fibers are required to bridge microcracks through mobilization of their tensile capacities [16]. Noteworthy, there exist a critical fiber length of 13 mm as there are no significant improvements when 19 mm fibers are employed.

The cyclic tensile response of FR-CPB from early to late ages suggests that fiber reinforcement plays a key role in bridging micro-cracks leading to a stronger and stiffer cementitious matrix in the pre-peak zone. This is contrary to previous findings that the role of fiber reinforcement is limited in the pre-peak zone and more significant in the post-peak branch of FRCCs [16]. FR-CPB specimens cured for 7 days with 6 mm fibers had a strain at first cracking of 1.47% with a first crack strength of 50 kPa, while for 90-day specimens with the same fiber parameters, the

strain and first crack strength were 1.11% and 129 kPa respectively: a reduction of 24.5% in first crack strain and a 158% increase in first crack strength. Evidently, this reduction in the strain at first cracking is a result of the increased brittleness of FR-CPB. This confirms that the cementitious matrix contributes significantly to the strength development of FR-CPB. Furthermore, when 6 mm fibers are employed, the specimens cured for 28 and 90 days, respectively, are unable to maintain matrix integrity for the duration of the cyclic tensile test (15 mm deformation limit), failing at 9% and 7% strain, respectively. As fiber length is increased, the specimens maintain matrix integrity, and the strain hardening behavior is more pronounced; thus, FR-CPB demonstrates a higher peak tensile strength. The same observation is present in the post-peak branch, where a longer fiber length increases the residual strength of FR-CPB. For specimens with 13-mm fiber and a 7-day curing time, the residual strength was 99.8 kPa compared to 191.8 kPa for FR-CPB cured for 90 days with the same fiber length. Recall, fiber inclusion introduces a dowelling effect (or dowel action) which restricts particle sliding and transfers the stress into the bulk matrix leading to a larger reinforcement regime [63]. Since fiber content is kept constant, increasing the fiber length reduces the number of fibers at any given point in the bulk matrix, which reduces the local reinforcing effect. Therefore, FR-CPB demonstrates the most consistent enhancement to pre-peak, peak tensile stress, and post-peak residual strength when a fiber length of 13 mm is employed.

The tensile hysteretic behavior of FR-CPB is highlighted by narrow loops in the pre-peak stage and wider loops in the post-peak stages. Specifically, the narrow hysteresis loops in the pre-peak stage confirm the effectiveness of fiber reinforcement in the pre-peak branch, while wider post-peak hysteresis loops suggest the increased energy dissipation capacity of FR-CPB. Furthermore, increasing the fiber length widens both pre-peak and post-peak hysteresis loops resulting in a more ductile response of FR-CPB. Although hysteresis loops become more pronounced when fiber length is increased from 6 mm to 13 mm, there are no obvious improvements when a fiber length of 19 mm is employed.

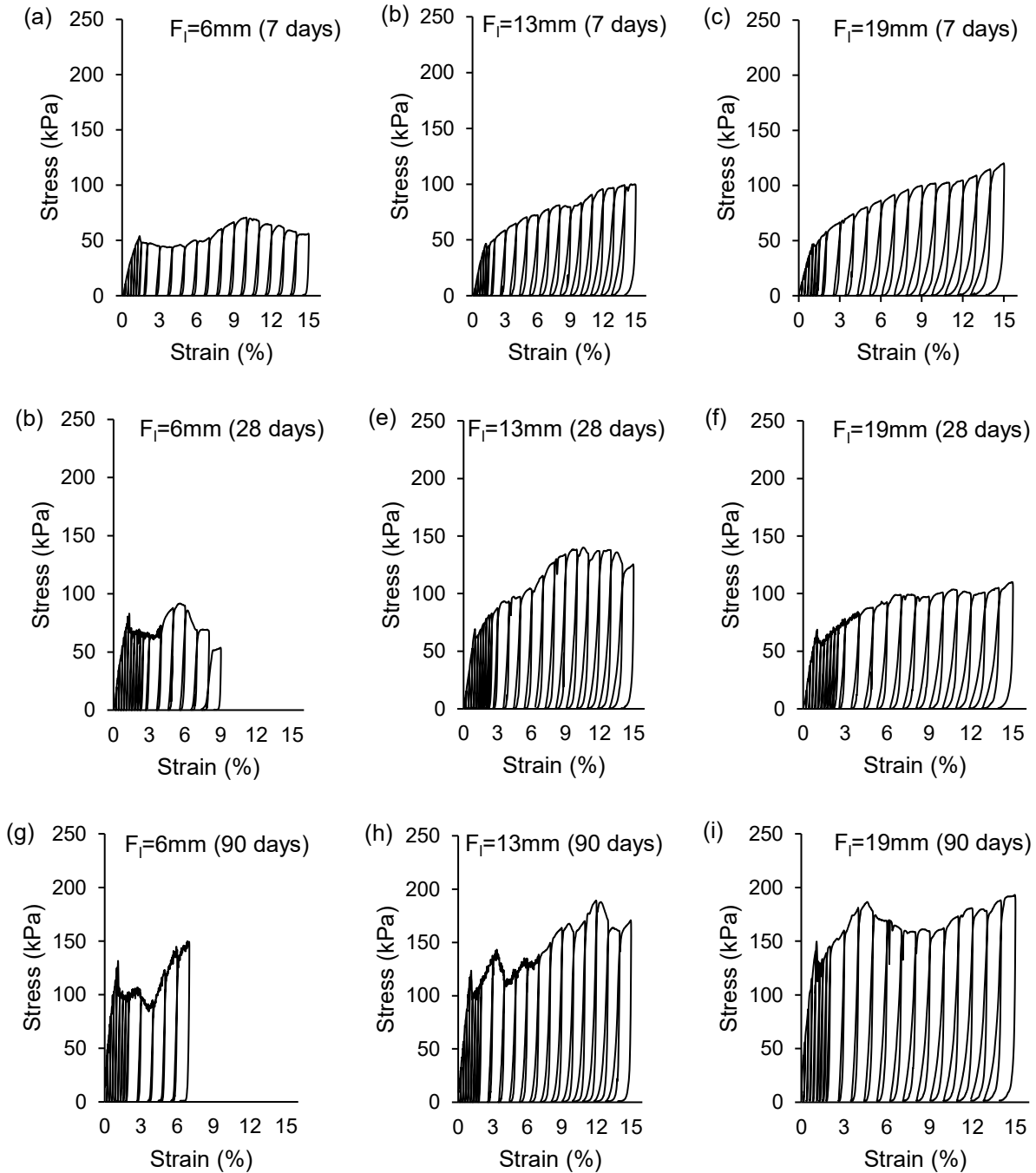


Figure 4.10 Effect of fiber length (6mm, 13mm, and 19mm) on the cyclic tensile stress-strain behavior of FR-CPB with a fixed fiber content of 0.5wt% at 7 days (a, b, and c), 28 days (d, e, and f), and 90 days (g, h, and i).

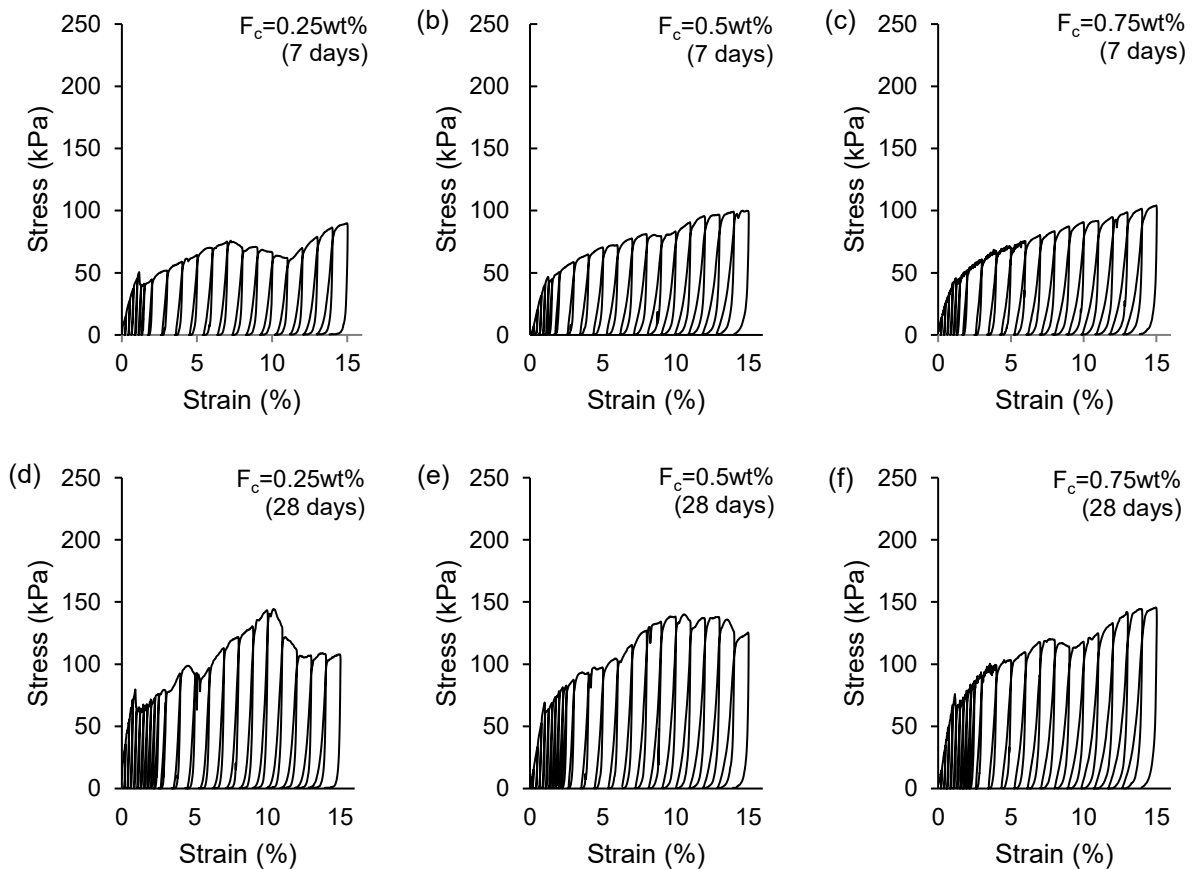
4.2.2 Effect of fiber content on the evolutive cyclic tensile behavior of FR-CPB

To study the effect of fiber content on the evolutive cyclic tensile response of FR-CPB, a fixed fiber length of 13 mm and three fiber contents were selected, namely 0.25wt%, 0.5wt%, and 0.75wt%. Observing Figure 4.10, FR-CPB shows positive evolutionary trends in stress-strain

behavior when curing time is increased. As curing time increases and fiber content is kept constant, there is a strengthened fiber-matrix interaction as pseudo-strain hardening behavior becomes more pronounced. As a result, significant improvement is observed in first crack strength, peak tensile stress, and residual strength. When curing time is kept constant, and fiber content is varied, FR-CPB demonstrates similar improvements in peak tensile stress and residual strength; however, the first crack strength is reduced. Recall, fiber reinforcement introduces discontinuities in the cementitious matrix leading to stress concentrations and weakening of the cementitious matrix [103,104]. Therefore, when fiber content is increased, there are more fibers in any one area of the bulk matrix leading to a larger number of discontinuities and weakening of the local reinforcement. Subsequently, a critical fiber content of 0.5wt% is observed for FR-CPB. Remarkably, for 28- and 90-day specimens, a fiber content of 0.75wt% cancels the softening effect in the post-peak branch, and the residual stress surpasses the initial peak tensile stress. As previously stated, fiber reinforcement plays a role in the pre-peak response of FR-CPB by affording the composite with a multiple-cracking characteristic through pseudo-strain hardening behavior. Analyzing Figure 8, the slope of the branch before the first crack strength is impacted by the increase in curing time, while increasing the fiber content does not have this effect. Therefore, in the early stages of cyclic tensile response, the cementitious matrix supports the load until first cracking occurs after which fibers play a role [37]. This is further supported by the first cracking strength of FR-CPB specimens cured for 7, 28, and 90 days with 0.25wt% fiber content, namely: 49.4 kPa, 79.7 kPa, and 129.5 kPa, respectively. Furthermore, the same evolutionary trends are observed where an increase in curing time and fiber content contributes to a higher peak tensile strength of FR-CPB. For specimens with 0.25wt% fibers and cured for 7, 28, and 90 days the peak tensile strengths were 74.7 kPa, 143.7 kPa, and 161 kPa, respectively. In the post-peak zone, fiber content plays a significant role in slowing post-peak stress deterioration and maintaining matrix integrity. Specifically, a specimen cured for 90 days with 0.25wt% has a residual strength of 88.4 kPa compared to its counterpart with 0.5wt% having a residual strength of 170 kPa. Furthermore, increasing the fiber content to 0.75wt% improves the residual strength of 90-day FR-CPB to 205.5 kPa. Although significant improvements can be made to the residual strength of 90-day FR-CPB with a higher fiber content, an increase beyond the critical fiber content (0.5wt%) creates numerous FM-ITZs which inevitably weakens the reinforcing effect leading to a reduction in peak strength and the first cracking strength. This

finding is more noticeable for 7- and 28-day FR-CPB and further confirms the critical fiber content of 0.5wt%.

Fiber inclusion, especially its volume content, plays a significant role in a composites' energy dissipation capacity. Different damage mechanisms, including fiber-matrix debonding and fiber-pullout, allows FR-CPB to form a more uniform multi-cracking process and dampen the enhanced oscillation caused by the external loading [22]. Furthermore, increasing the fiber content enables FR-CPB to deform more and maintain structural integrity beyond failure, which can be explained by the wider hysteresis loops observed in Figure 8. However, increasing the fiber content beyond the critical value ($F_c = 0.5\text{wt}\%$) increases the energy dissipation capacity at an expense of first crack strength and peak tensile strength especially for early age FR-CPB.



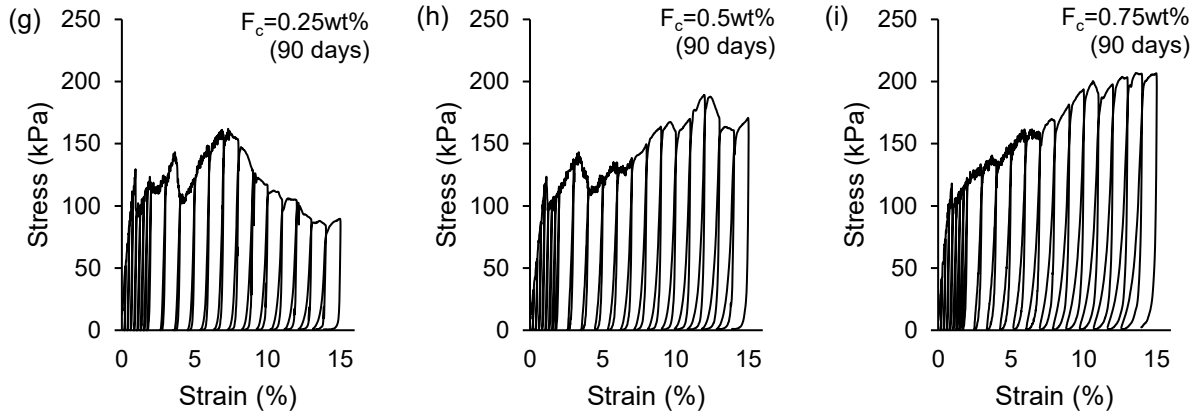
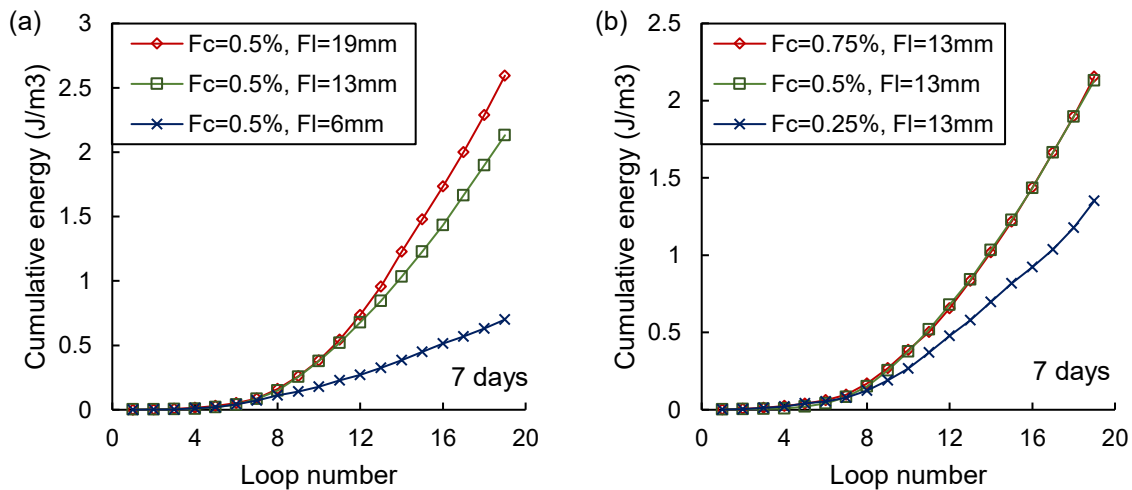


Figure 4.11 Effect of fiber content (0.25wt%, 0.5wt%, and 0.75wt%) on the cyclic tensile stress-strain behavior of FR-CPB with a fixed fiber length of 13mm at 7 days (a, b, and c), 28 days (d, e, and f), and 90 days (g, h, and i).

4.2.3 Effect of fiber inclusion on the hysteretic energy dissipation

FR-CPB shows a high dependency on curing time w.r.t energy dissipation capacity. Recall, plastic deformation due to external loading requires FRCCs to dissipate energy through mechanisms such as matrix cracking, fiber sliding, and/or fiber-pullout. The more prominent these events are, the more energy can be absorbed and allow the composite to become tougher [48]. Furthermore, the fiber reinforcing effect on the cementitious matrix is greater as the matrix becomes more refined through full realization of the cement hydration processes since the fiber-matrix network plays a major role in strength development [21]. Cyclic test results show that fiber inclusion enhances the energy dissipation capacity of FR-CPB for all curing times in this study. Specifically, when fiber length is varied and fiber content remains constant, 7-day FR-CPB reinforced with 19 mm fibers dissipates 2.5 J/m^3 of energy (see Figure 4.11). On the other hand, the same amount of energy can be dissipated when fiber length is set constant to 13 mm and the fiber content is 0.75wt%; this trend remains true for subsequent curing periods. However, as FR-CPB becomes more brittle and the multiple cracking behaviors are fully realized, emphasis is placed on fiber length to bridge cracks more efficiently. For 90-day FR-CPB specimens reinforced with 19 mm fibers + 0.5wt%, the energy dissipated is 3.88 J/m^3 , while the same amount of energy is dissipated when FR-CPB is reinforced with 13 mm fibers + 0.5wt%. Moreover, FR-CPB demonstrates the most consistent enhancement in energy dissipation capacity when reinforced with a fiber length of 13 mm and fiber content of 0.5wt%.

From Figure 27, the obtained cumulative energy dissipated in the early stages of cyclic tests further confirms the effectiveness of pre-peak fiber reinforcement. There is a clear transitional point where the growth rate of energy dissipation switches from slow to rapid, especially for late-aged FR-CPB. Furthermore, due to the inherent weak tensile strength of soft cementitious materials such as CPB, longer fibers can increase the hysteretic energy dissipation by bridging cracks and restricting particle sliding to a higher degree [87]. Moreover, when fiber length is increased from 6 mm to 13 mm, the improvements to the cumulative energy dissipation are obvious; however, when fiber length is increased beyond 13 mm, the enhancement is limited hereby confirming 13 mm as the critical fiber length. Similarly, increasing the fiber content from 0.25wt% to 0.5wt% shows clear improvements to the hysteretic energy dissipation of FR-CPB, while increasing the fiber content to 0.75wt% shows limited improvements to hysteretic energy dissipation. While both fiber parameters can provide enhancements to FR-CPB's hysteretic energy dissipation capacity, it is more sensitive to changes in fiber length than changes in fiber content. Further, when longer fibers are employed, mechanisms such as fiber-matrix debonding and fiber pull-out allow FR-CPB to dissipate more energy as cracks are permitted due to the dowelling effect.



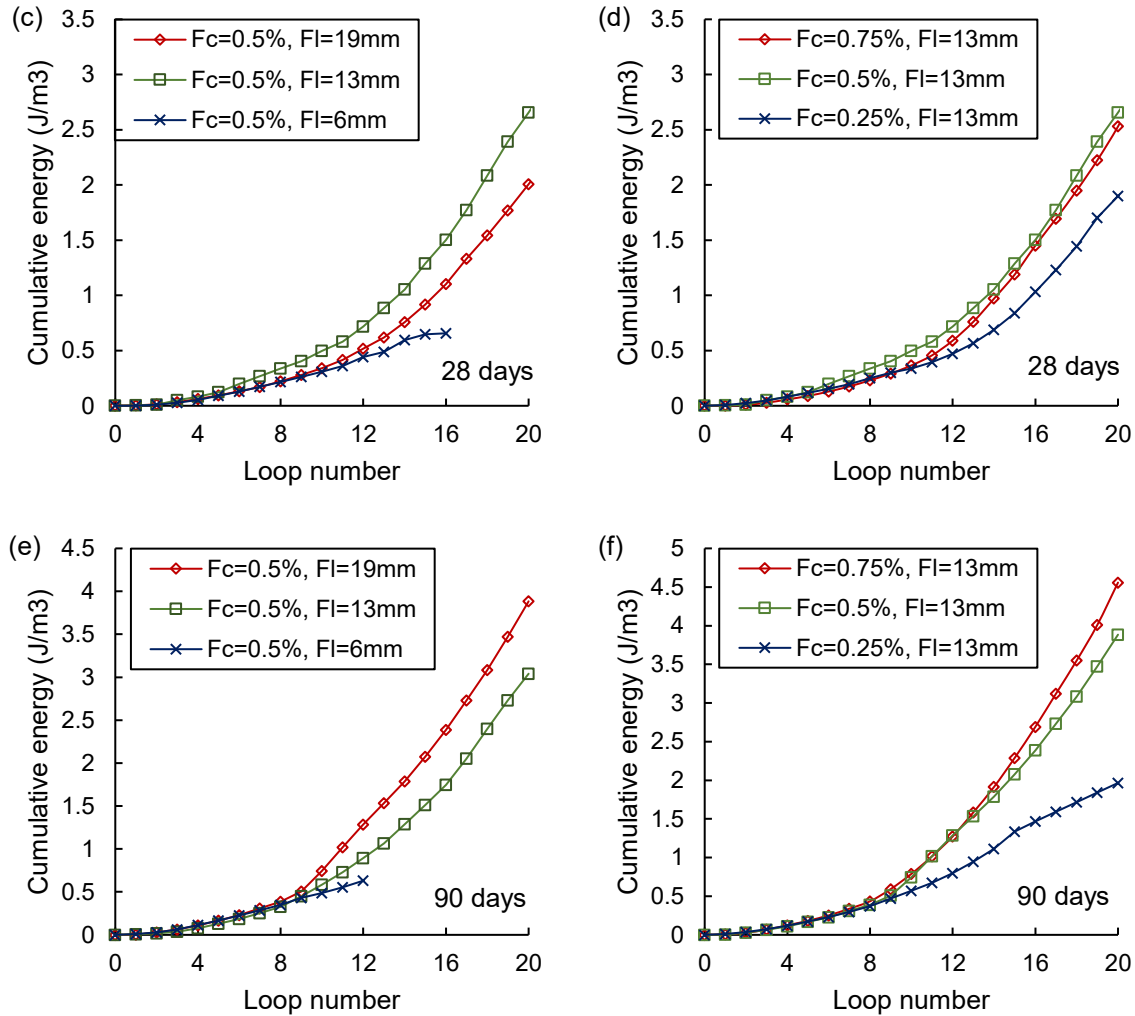


Figure 4.12 Effect of fiber inclusion on the hysteretic dissipation energy of FR-CPB at 7 days (a and b), 28 days (c and d), and 90 days (e and f).

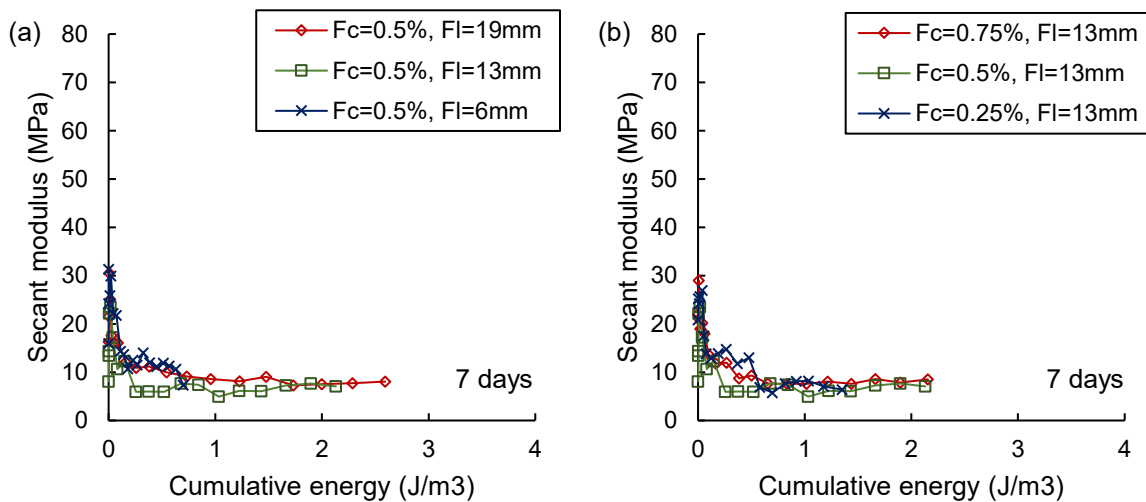
4.2.4 Effect of fiber inclusion on the secant modulus

The secant modulus of FR-CPB shows a high dependency on curing time under cyclic tensile loading. Late-age FR-CPB cured for 90 days showed the highest secant modulus of 75.5 MPa, a 139% increase compared to the 31.3 MPa observed for 7-day specimens. As curing time increases, the fiber-matrix network becomes stiffer, stronger, and more durable and can withstand the applied loads more efficiently. As previously stated, the pre-cracked strength of FR-CPB is solely dependent on the cementitious matrix and the full realization of the cement hydration process. Furthermore, the multi-cracking process is fully realized, and FR-CPB can dissipate more energy as deformation continues, especially when fiber length is increased.

Interestingly, analysis of the results presented in Figure 4.12, again confirms that a fiber length of 13 mm and fiber content of 0.5wt% provided the most consistent fiber reinforcing effect.

In the pre-peak zone, the cementitious matrix offers the initial stiffness until fiber reinforcement bridges micro-cracks and the material undergoes strain hardening. This is illustrated as the progressive increase in secant modulus until the peak value has been reached, after which the localization of macro-cracks causes the secant modulus to suffer a sudden drop. Material stiffness that's loss cannot be regained; however, fiber reinforcement helps to aid in the rate of degradation by bridging cracks and directing this stress back into the bulk matrix. This is evident especially in the post-peak zone, as increasing the fiber length allows FR-CPB to dissipate more energy while increasing the residual secant modulus. Similarly, increasing the fiber content enables FR-CPB to maintain a higher degree of stiffness; however, there exists a critical fiber length of 13 mm and critical fiber content of 0.5wt% as any increase beyond these parameters offers limited enhancements.

Comparing the effects of fiber length and fiber content, the secant modulus of FR-CPB is more sensitive to the changes in fiber length. The longer fibers offer a higher resistance to fiber-matrix debonding and fiber pull-out due to their dowel action mechanism. Subsequently, a higher strain rate and/or crack opening velocity is required to debond fibers and ultimately loosen the microstructure leading to pronounced micro-crack development and damage accumulation in the cementitious matrix [16].



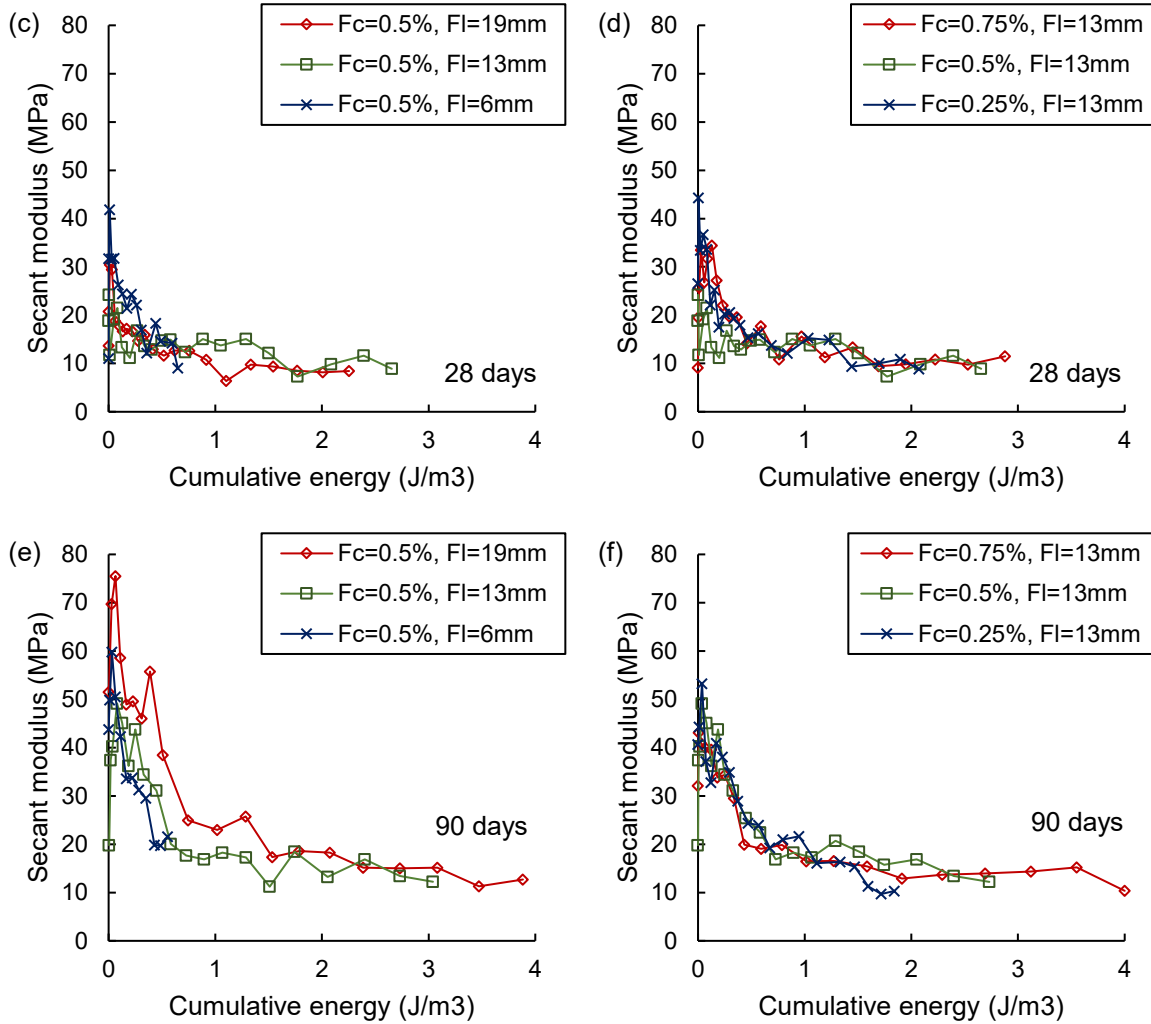


Figure 4.13 Effect of fiber inclusion on the secant modulus of FR-CPB at 7 days (a and b), 28 days (c and d), and 90 days (e and f).

4.2.5 Effect of fiber inclusion on the degraded stress

The degraded stress of FR-CPB demonstrates a high dependency on curing time. Specifically, the full realization of the hydration process and the subsequent multiple cracking afforded by the strengthened fiber-bridging effect enables late-age FR-CPB to demonstrate the highest load carrying capacity. As previously established, the first cracking strength is increased with curing time, leading to an increased demand for energy to be dissipated. Subsequently, a longer fiber length is better able to restrict the wider crack openings and provide a larger reinforcing effect to the bulk matrix. For FR-CPB cured for 90 days, the peak stress when 19 mm fibers are employed is 179.7 kPa (0.5wt%) and 194.9 kPa when fiber content is 0.75wt% (13 mm fiber length); an increase of 66.5% and 106.9% respectively compared to their 7-day counterparts. Although the

higher peak stress was obtained by raising fiber content, the increased fiber content resulted in a higher rate of stress degradation as is observed with the increase in fiber length. This can be explained by previous findings that explain the exceedance of critical fiber content leads to a decrease in the peak strength of cemented tailings backfill reinforced with fiber reinforcement [117].

Furthermore, a longer fiber length can restrict crack propagation and abate the localization of macro-cracks to a higher degree, which is illustrated further in Figure 4.13, where the post-peak failure patterns of FR-CPB are shown. It is observed that by increasing the fiber length and fiber content in FR-CPB, the localization of macro-cracks is reduced, and FR-CPB can maintain matrix integrity for the duration of the cyclic test. Furthermore, this confirms previous findings that both tensile and shear cracks exist when cementitious composites are subjected to complex loading [55]. There is further evidence of this observed in the degraded stress curves presented in Figure 29, where the stress drop after first cracking is more pronounced when 6 mm fibers are employed. As the fiber length and content are increased, the post-peak branches are strengthened through the pseudo-strain hardening phenomena and, in some cases, create a secondary peak where the residual strength is the highest stress experienced by the fiber-matrix network. Upon further observation, the increase in fiber length and fiber content manifest adverse effects in the degradation of load carrying capacity of FR-CPB. Specifically, a longer fiber length leads to a higher degree of degradation as more energy is dissipated and subsequently more cyclic-induced damage is accumulated in the cementitious matrix; the same is observed for increased fiber content. As a result, a critical fiber length of 13 mm and critical fiber content of 0.5wt% produces the most consistent enhancement in tempering the stress degradation rate of FR-CPB.

Although increasing both fiber length and fiber content enhances the degraded stress of FR-CPB and contributes to positive evolutionary trends, there exists a higher degree of sensitivity to changes in fiber length. Moreover, a critical fiber length of 13 mm and a critical fiber content of 0.5wt% is observed where FR-CPB experiences the most beneficial reinforcing effects.

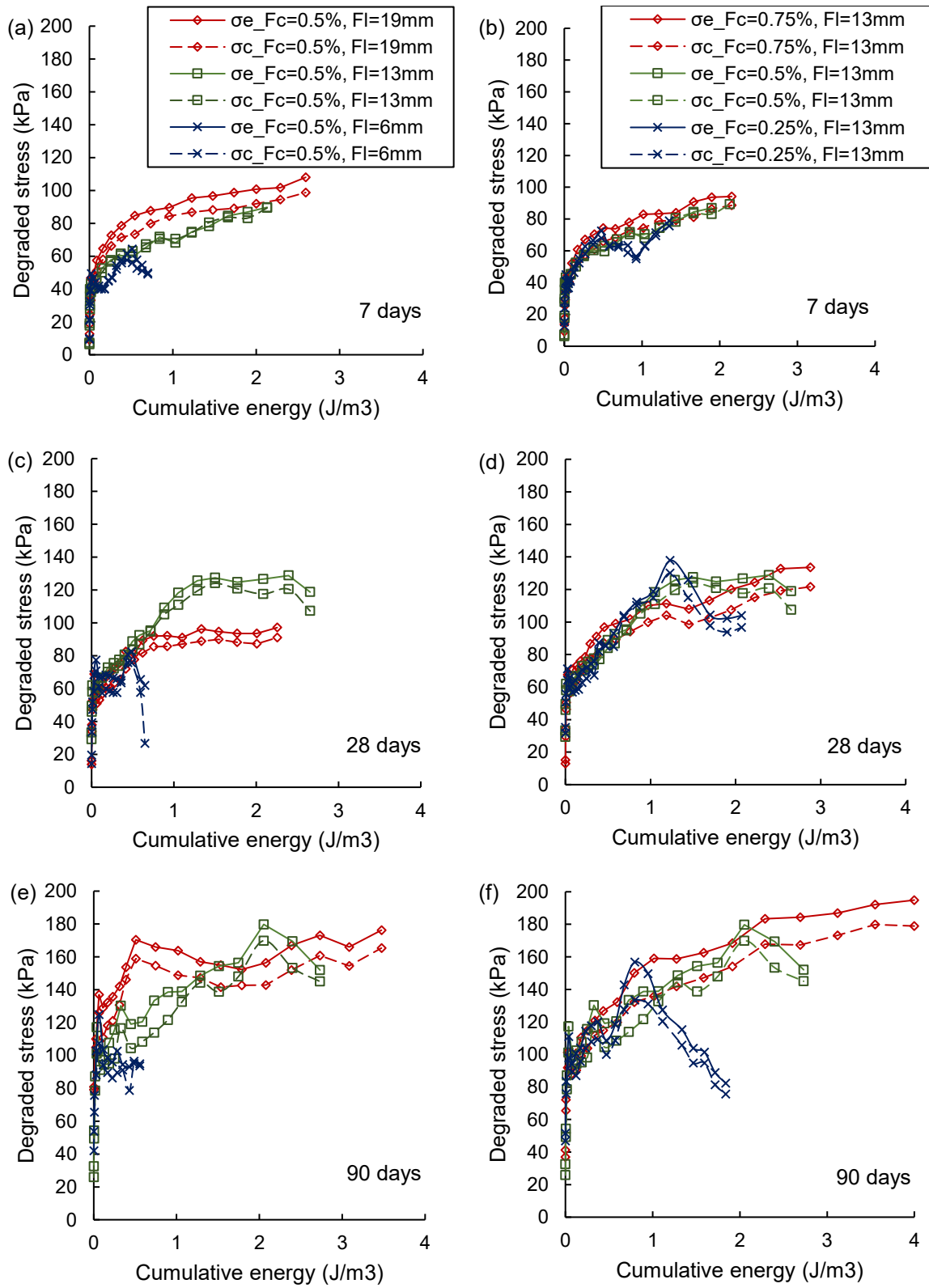


Figure 4.14 Effect of fiber inclusion on the degraded stress of FR-CPB at 7 days (a and b), 28 days (c and d), and 90 days (e and f).

4.2.6 Effect of fiber inclusion on the damping index

Observing Figure 4.14 FR-CPB's damping index demonstrates high dependence on curing time, especially from the 7 to 28-day range. Recall, the damping properties of FRCCs depend largely on the inherent matrix discontinuities such as micro-cracks and pore space, fibers, moisture, and the FM-ITZs. Therefore, as FR-CPB ages and the hydration process is further realized, the damping index increases. As a result, the fiber-matrix network can dissipate more energy through the multi-cracking processes and subsequently reduce stress concentration, hereby improving damping. Moreover, when fiber parameters of 13 mm fiber length + 0.5wt% fiber content were employed, the damping index obtained for 7, 28, and 90-day FR-CPB were 0.067 J/m^3 , 0.119 J/m^3 , and 0.123 J/m^3 respectively. Additionally, employing a fiber length and fiber content beyond the critical value of 13 mm and 0.5wt% respectively reduces the damping characteristics of FR-CPB.

As FR-CPB ages, the slope of the pre-peak branch of the damping index curve changes to almost vertical. Specifically, the fiber-reinforced matrix experiences cyclic damage accumulation, especially during the pseudo-strain hardening phase, where fibers bridge micro-cracks and abates crack propagation. In other words, energy is dissipated through microplastic strain energy through fiber-matrix debonding, fiber breakage, and frictional resistance at FM-ITZ [22]. In the post-peak zone, increasing the fiber length enhances the residual damping of early age FR-CPB. For late-aged FR-CPB (> 28 days), increasing the fiber length extends the post-peak branch, and more energy can be dissipated; however, there is little deviation in improvement between 13 mm and 19 mm fibers. Consequently, FR-CPB's damping characteristics are most consistent when 13 mm fibers + 0.5wt% are employed.

Comparing the effects of both fiber length and fiber content, the damping index is more sensitive to changes in fiber length. The peak damping index is directly correlated to the length of fiber employed, while the post-peak branch favors fiber content. By increasing fiber length, the fiber-matrix network can absorb more deformation energy through toughening of the matrix, which reduces the stress concentration and improves the damping characteristics of FR-CPB.

Moreover, increasing fiber parameters beyond the critical values weaken the reinforcing effect, and subsequently, the damping capacity of FR-CPB is lessened.

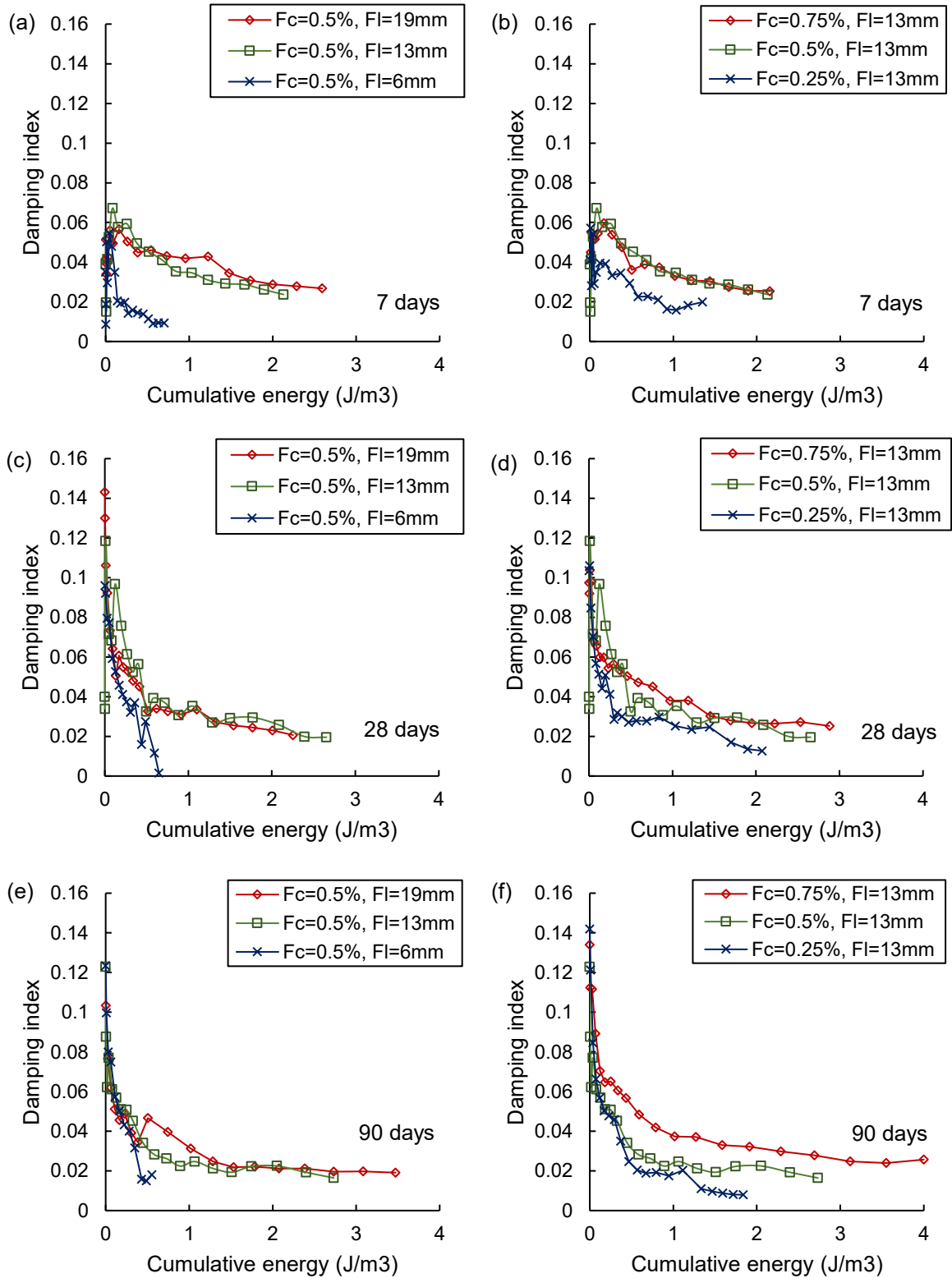


Figure 4.15 Effect of fiber inclusion on the damping index of FR-CPB at 7 days (a and b), 28 days (c and d), and 90 days (e and f).

Chapter 5 Conclusions and recommendations

5.1 Conclusions

Cemented paste backfill (CPB) technology is increasingly used in the mining industry due to the technical, economic, and environmental benefits it carries. Conventional storage methods such as tailings ponds are bypassed as tailings are transferred as paste into underground voids (called stopes) to provide support to the surrounding rock mass. Additionally, the engineering application of CPB depicts the dominant forces that the structure will be subjected to, and a thorough understanding of the different types of loadings will improve the safe design and implementation of CPB technology. Furthermore, the complexity of in-situ loadings caused by seismicity and mine operations highlights the need for CPB structures to possess adequate strength and mechanical performance. However, CPB is considered a soft cementitious material that possesses low strength parameters, and a large part of the operational cost is tied to the cement binder. Subsequently, fiber reinforcement is seen as a promising technique to enhance the mechanical properties of cementitious composites and alleviate the capital-intensive nature of employing paste tailings as a suitable tailing disposal method as it requires large quantities of cement to be used. Therefore, furthering the understanding of the fiber reinforcement technique is vital in ensuring the safe and cost-effective application of CPB as a mine backfilling method. To further understand the cyclic compressive and tensile responses of FR-CPB and the evolution of its' mechanical properties, a comprehensive testing program was developed and executed in this Thesis research. This body of work presented the evolutive cyclic compressive, and tensile behaviors and properties of polypropylene fiber reinforced backfill composite (FR-CPB), from which the following conclusions may be drawn:

1. There exist a critical fiber length of 13 mm and a critical fiber content of 0.5wt% which validate previous findings for FR-CPB. When these fiber parameters are employed, FR-CPB demonstrates the most consistent improvement in strength parameters in both pre- and post-peak regions. As a result, there is an inherent level of synergy in the fiber-matrix network, which allows FR-CPB to maintain matrix integrity and subsequently alleviate cyclic-induced damage accumulation to a higher degree. Furthermore, the aging of FR-CPB leads to a strengthened fiber bridging effect which enhances the deformation capacity

of FR-CPB. In doing so, FR-CPB is stiffer and becomes tougher through the multiple cracking processes highlighted by the phenomenon of pseudo-strain hardening. It should be noted that employing fiber parameters beyond the critical values introduces numerous FM-ITZs, which adversely affect the local reinforcing effect. Employing a fiber length beyond 13 mm demonstrates limited overall improvement but using a fiber content beyond 0.5wt% shows an improvement in the FR-CPB's softening capacities in the post-peak zone. As a result, fiber parameters may be selected depending on the requirements and nature of the engineering application, as different combinations may offer specific design solutions.

2. The general cyclic compressive behavior of FR-CPB shows clear curing time-dependent behaviors. As the cementitious matrix ages, the composite develops an improved strength and load carrying capacity through the full realization of the cement hydration process, which results in less voids and initial defects. FR-CPB demonstrates significant improvement in stiffness and becomes tough through its increased energy dissipation capacity. Furthermore, a strengthened fiber-matrix interaction is observed as changing both the fiber length and fiber content shows a positive evolutive trend in the peak strength and residual strength of FR-CPB. However, the cementitious matrix experiences cyclic-induced damage caused by mechanisms such as matrix crushing and frictional resistance between the sides of cracks which is evident from the depressed surfaces at the macroscale. Additionally, the rate of stress degradation is significantly diminished as fiber inclusion significantly increases the damping characteristics of FR-CPB. Consequently, a critical fiber length and fiber content of 13 mm and 0.5wt%, respectively, will provide the most consistent enhancement to the cyclic compressive response of FR-CPB.
3. The cyclic tensile response of FR-CPB is similar to the evolutive trends under cyclic compression. This suggests that the cementitious matrix plays a far more significant role in the strength development of FR-CPB. As the matrix ages, the influence of fibers on first crack strength is non-existent; however, the multiple cracking characteristics and fiber bridging forces are of great importance beyond this point. Since CPB possess a weak tensile capacity, matrix integrity is a function of fiber length as they offer a greater doweling action leading to a stronger reinforcement regime. Therefore, when fiber length

is too short, or fiber content is less than optimal, tensile cracks dominate the failure of FR-CPB under cyclic tensile loading. This failure pattern is a result of fiber pullout, fiber rupture, and fiber-matrix debonding due to damage accumulation in the cementitious matrix caused by crack opening and closing. However, when the critical fiber parameters are employed, FR-CPB demonstrates an improved cyclic response and significant enhancement are observed in cumulative energy dissipation, stiffness, rate of stress degradation, and damping index. Though FR-CPB's mechanical response is more sensitive to changes in fiber length, increasing both fiber length and fiber content demonstrated positive evolutive trends in all mechanical properties suggesting a strengthened fiber-bridging effect.

4. Although FR-CPB possesses unique characteristics such as low cement content and no coarse aggregate, which contributes to its' weak tensile capacity, the phenomenon of pseudo-strain hardening proves that FR-CPB can deform to a greater extent before the peak strength confirming the effectiveness of fiber reinforcement in the pre-peak zone. This is most evident under compressive loading, where the peak strength is achieved at a higher strain (%) for early age FR-CPB, and as FR-CPB ages, the tensile capacity of fibers is activated much sooner, i.e., peak strength at lower strain (%). Interestingly, the first cracking strength and peak tensile capacity are also functions of fiber length, where this phenomenon is present in FR-CPB under cyclic tensile loading. Furthermore, FR-CPB demonstrates a marked improvement in its' post-cracking capacity confirming previous findings of a positive reinforcing effect in the post-peak zone. In the branch of the cracking process, both a longer fiber length and higher fiber content enhance the residual strength of FR-CPB by restricting crack growth and delaying macrocrack localization. However, too few fibers cannot adequately restrict crack growth, and too many fibers create numerous FM-ITZ leading to preferential regimes of crack propagation. Subsequently, employing a fiber length and/or content beyond the critical value can increase the residual strength of FR-CPB to a higher degree, however, at the expense of peak tensile stress.

This thesis research has clearly demonstrated the positive evolutionary trends in the cyclic response and mechanical performance of FR-CPB. Furthermore, this body of work aims to aid

and advance the safe design and implementation of cemented paste technology as a viable disposal method for mine tailings waste.

5.2 Recommendations for future work

Based on the experimental study and the above conclusions of this Thesis research, there are a few recommendations for future work. Firstly, it has been previously established that the consolidation of CPB is strongly affected by several multiphysics processes, including thermal (T), hydraulic (H), mechanical (M), and chemical (C) (THMC). These processes and their interactions within the CPB mass govern the strength development and subsequent evolution of the mechanical properties of CPB. For example, there may be volume change due to the chemical process of binder hydration, where there is a strong coupling between the rate of hydration and the heat generated, leading to changes in the mechanical properties and evolution of FR-CPB's strength. Therefore, it is imperative to conduct m.

Second, it has been found that the loading rate has a vital effect on the UCS behavior of CPB. Specifically, increased loading rates can have a strengthening effect on the UCS behavior of CPB samples. One reason is that an increase in loading rate reduces the time needed for material response, and as a result, the strain is more localized. Consequently, energy is rapidly accumulated until its eventual release, which is simultaneous in nature akin to a rockburst. For these reasons, it is recommended that further works be completed to study the effects of different strain rates on the cyclic response of FR-CPB and the evolution of the mechanical properties. Furthermore, the size of laboratory samples compared to the in-situ structures are of great disparity. Thus, it is also recommended that various composite sizes are considered to replicate the results presented herein this body of work.

Lastly, the particle size distribution of tailings consists of particles at the micro level. In conjunction with synthetic fibers, hydraulic binder, and water, the particles of the cementitious matrix of FR-CPB exist in a multi-scale dimension. Furthermore, the fiber-matrix network of FR-CPB contains initial voids and microcracks as it is heterogeneous in nature. Subsequently, different scale fibers may abate crack propagation at different scale levels leading to a more uniform and controlled cracking process in FR-CPB. More specifically, nanoscale fibers may be

used to bridge nanoscale cracks, microscale fibers to bridge microcracks, and macroscale fibers for macrocracks. By applying such a hierarchal reinforcement technique, a certain level of synergy and cohesion may be established in the fiber-matrix network leading to a more refined microstructure.

Through these recommendations, further understanding may be gained regarding the cyclic mechanical response of FR-CPB. In doing so, further advancement of two noble engineering technologies, such as cemented paste backfill and fiber reinforcement, may be achieved.

Chapter 6 **References**

- [1] Alainachi IH. Shaking Table Testing of Cyclic Behaviour of Fine-Grained Soils Undergoing Cementation : Cemented Paste Backfill 2020.
- [2] 10 Key Facts on Canada’s Minerals Sector n.d. <https://www.nrcan.gc.ca/maps-tools-and-publications/publications/minerals-mining-publications/10-key-facts-on-canadas-minerals-sector/18423> (accessed September 12, 2022).
- [3] Qi C, Fourie A. Cemented paste backfill for mineral tailings management: Review and future perspectives. *Miner Eng* 2019;144. <https://doi.org/10.1016/j.mineng.2019.106025>.
- [4] Edraki M, Baumgartl T, Manlapig E, Bradshaw D, Franks DM, Moran CJ. Designing mine tailings for better environmental, social and economic outcomes: A review of alternative approaches. *J Clean Prod* 2014;84:411–20. <https://doi.org/10.1016/j.jclepro.2014.04.079>.
- [5] Yilmaz E, Fall M. Paste tailings management. 2017. <https://doi.org/10.1007/978-3-319-39682-8>.
- [6] Bauchau OA, Craig JI. Constitutive behavior of materials 2009:53–99. https://doi.org/10.1007/978-90-481-2516-6_2.
- [7] Jafari M, Shahsavari M, Grabinsky M. Experimental Study of the Behavior of Cemented Paste Backfill under High Isotropic Compression. *J Geotech Geoenvironmental Eng* 2020;146:1–5. [https://doi.org/10.1061/\(asce\)gt.1943-5606.0002383](https://doi.org/10.1061/(asce)gt.1943-5606.0002383).
- [8] Chen X, Shi X, Zhou J, Chen Q, Li E, Du X. Compressive behavior and microstructural properties of tailings polypropylene fibre-reinforced cemented paste backfill. *Constr Build*

- Mater 2018;190:211–21. <https://doi.org/10.1016/j.conbuildmat.2018.09.092>.
- [9] Yi XW, Ma GW, Fourie A. Compressive behaviour of fibre-reinforced cemented paste backfill. *Geotext Geomembranes* 2015;43:207–15. <https://doi.org/10.1016/j.geotextmem.2015.03.003>.
- [10] Libos ILS, Cui L. Mechanical properties and behavior of early-age fiber-reinforced cemented paste backfill. *Int Conf Civil, Struct Transp Eng* 2020:193-1-193–6. <https://doi.org/10.11159/iccste20.193>.
- [11] Festugato L, Fourie A, Consoli NC. Cyclic shear response of fibre-reinforced cemented paste backfill. *Geotech Lett* 2013;3:5–12. <https://doi.org/10.1680/geolett.12.00042>.
- [12] Yang L, Xu W, Yilmaz E, Wang Q, Qiu J. A combined experimental and numerical study on the triaxial and dynamic compression behavior of cemented tailings backfill. *Eng Struct* 2020;219:110957. <https://doi.org/10.1016/j.engstruct.2020.110957>.
- [13] Skrzypkowski K. 3D Numerical Modelling of the Application of Cemented Paste Backfill on Displacements Around Strip Excavations. *Energies* 2021;14. <https://doi.org/10.3390/en14227750>.
- [14] Suazo G, Fourie A, Doherty J. Cyclic Shear Response of Cemented Paste Backfill. *J Geotech Geoenvironmental Eng* 2017;143:04016082. [https://doi.org/10.1061/\(asce\)gt.1943-5606.0001581](https://doi.org/10.1061/(asce)gt.1943-5606.0001581).
- [15] Zhang C, Cao M. Fiber synergy in multi-scale fiber-reinforced cementitious composites. *J Reinf Plast Compos* 2014;33:862–74. <https://doi.org/10.1177/0731684413514785>.
- [16] McLean J, Cui L. Multiscale Geomechanical Behavior of Fiber-Reinforced Cementitious

- Composites Under Cyclic Loading Conditions—A Review. *Front Mater* 2021;8:1–13.
<https://doi.org/10.3389/fmats.2021.759126>.
- [17] Jun P, Mechtcherine V. Behaviour of strain-hardening cement-based composites (SHCC) under monotonic and cyclic tensile loading: Part 1 - Experimental investigations. *Cem Concr Compos* 2010;32:801–9. <https://doi.org/10.1016/j.cemconcomp.2010.07.019>.
- [18] Yun HD, Yang IS, Kim SW, Jeon E, Choi CS, Fukuyama H. Mechanical properties of high-performance hybrid-fibre-reinforced cementitious composites (HPHFRCCs). *Mag Concr Res* 2007;59:257–71. <https://doi.org/10.1680/mac.2007.59.4.257>.
- [19] Xu L, Li B, Chi Y, Li C, Huang B, Shi Y. Stress-strain relation of steel-polypropylene-blended fiber-reinforced concrete under uniaxial cyclic compression. *Adv Mater Sci Eng* 2018;2018. <https://doi.org/10.1155/2018/9174943>.
- [20] Cao S, Yilmaz E, Song W. Fiber type effect on strength, toughness and microstructure of early age cemented tailings backfill. *Constr Build Mater* 2019;223:44–54.
<https://doi.org/10.1016/j.conbuildmat.2019.06.221>.
- [21] Chen X, Shi X, Zhang S, Chen H, Zhou J, Yu Z, et al. Fiber-reinforced cemented paste backfill: The effect of fiber on strength properties and estimation of strength using nonlinear models. *Materials (Basel)* 2020;13:1–21. <https://doi.org/10.3390/ma13030718>.
- [22] Long WJ, Li HD, Mei L, Li W, Xing F, Khayat KH. Damping characteristics of PVA fiber-reinforced cementitious composite containing high-volume fly ash under frequency-temperature coupling effects. *Cem Concr Compos* 2021;118:103911.
<https://doi.org/10.1016/j.cemconcomp.2020.103911>.

- [23] Fall M, Belem T, Samb S, Benzaazoua M. Experimental characterization of the stress-strain behaviour of cemented paste backfill in compression. *J Mater Sci* 2007;42:3914–22. <https://doi.org/10.1007/s10853-006-0403-2>.
- [24] Libos ILS, Cui L, Liu X. Effect of curing temperature on time-dependent shear behavior and properties of polypropylene fiber-reinforced cemented paste backfill. *Constr Build Mater* 2021;311:125302. <https://doi.org/10.1016/j.conbuildmat.2021.125302>.
- [25] Jafari M, Shahsavari M, Grabinsky M. Drained Triaxial Compressive Shear Response of Cemented Paste Backfill (CPB). *Rock Mech Rock Eng* 2021;54:3309–25. <https://doi.org/10.1007/s00603-021-02464-5>.
- [26] Lin J-X, Song Y, Xie Z-H, Guo Y-C, Yuan B, Zeng J-J, et al. Static and dynamic mechanical behavior of engineered cementitious composites with PP and PVA fibers. *J Build Eng* 2020;29:101097. <https://doi.org/10.1016/j.jobbe.2019.101097>.
- [27] Wu D, Liu Y cheng, Zheng Z xue, Wang S. Impact Energy Absorption Behavior of Cemented Coal Gangue-Fly Ash Backfill. *Geotech Geol Eng* 2016;34:471–80. <https://doi.org/10.1007/s10706-015-9958-5>.
- [28] Xu W bin, Liu B, Wu W lü. Strength and deformation behaviors of cemented tailings backfill under triaxial compression. *J Cent South Univ* 2020;27:3531–43. <https://doi.org/10.1007/s11771-020-4568-7>.
- [29] Liu N, Cui L, Wang Y. Analytical Assessment of Internal Stress in Cemented Paste Backfill. *Adv Mater Sci Eng* 2020;2020:1–13. <https://doi.org/10.1155/2020/6666548>.
- [30] Xu W, Li Q, Zhang Y. Influence of temperature on compressive strength, microstructure

- properties and failure pattern of fiber-reinforced cemented tailings backfill. *Constr Build Mater* 2019;222:776–85. <https://doi.org/10.1016/j.conbuildmat.2019.06.203>.
- [31] Wang Z-C, Duan D-Y, Wang S-H, Mo Y, Yin Y-G. Mechanical Behavior of the Novel Gradient Concrete Tower of a Cable-Stayed Bridge. *Front Mater* 2021;8. <https://doi.org/10.3389/fmats.2021.676440>.
- [32] Li B, Chi Y, Xu L, Shi Y, Li C. Experimental investigation on the flexural behavior of steel-polypropylene hybrid fiber reinforced concrete. *Constr Build Mater* 2018;191:80–94. <https://doi.org/10.1016/j.conbuildmat.2018.09.202>.
- [33] Dönmez D, Dönmez AA, Gençoğlu M. Mechanical response of textile reinforced cementitious composite tubes under monotonic and cyclic loadings. *Constr Build Mater* 2020;251. <https://doi.org/10.1016/j.conbuildmat.2020.118963>.
- [34] Huang Z, Cao S, Yilmaz E. Investigation on the flexural strength, failure pattern and microstructural characteristics of combined fibers reinforced cemented tailings backfill. *Constr Build Mater* 2021;300:124005. <https://doi.org/10.1016/j.conbuildmat.2021.124005>.
- [35] Cao S, Yilmaz E, Yin Z, Xue G, Song W, Sun L. CT scanning of internal crack mechanism and strength behavior of cement-fiber-tailings matrix composites. *Cem Concr Compos* 2021;116:103865. <https://doi.org/10.1016/j.cemconcomp.2020.103865>.
- [36] Xue G, Yilmaz E, Feng G, Cao S, Sun L. Reinforcement effect of polypropylene fiber on dynamic properties of cemented tailings backfill under SHPB impact loading. *Constr Build Mater* 2021;279:122417. <https://doi.org/10.1016/j.conbuildmat.2021.122417>.
- [37] Xue G, Yilmaz E, Song W, Cao S. Mechanical, flexural and microstructural properties of

- cement-tailings matrix composites: Effects of fiber type and dosage. *Compos Part B Eng* 2019;172:131–42. <https://doi.org/10.1016/j.compositesb.2019.05.039>.
- [38] Cao S, Zheng D, Yilmaz E, Yin Z, Xue G, Yang F. Strength development and microstructure characteristics of artificial concrete pillar considering fiber type and content effects. *Constr Build Mater* 2020;256:119408. <https://doi.org/10.1016/j.conbuildmat.2020.119408>.
- [39] Boulekbache B, Hamrat M, Chemrouk M, Amziane S. Flexural behaviour of steel fibre-reinforced concrete under cyclic loading. *Constr Build Mater* 2016;126:253–62. <https://doi.org/10.1016/j.conbuildmat.2016.09.035>.
- [40] Hu J hong, Sun M qing, Li J, Wang Y jun. Mechanical performances and evolution of stiffness of thin-walled strain hardening cement-based composites pipes during cyclic loading. *Constr Build Mater* 2018;184:400–7. <https://doi.org/10.1016/j.conbuildmat.2018.07.001>.
- [41] Zhou Y, Zhong Q, Xing F, Sui L, Huang Z, Guo M. Influence of cyclic loading on the tensile fracture characteristics of ultra-high performance engineered cementitious composites. *Constr Build Mater* 2020;240:117937. <https://doi.org/10.1016/j.conbuildmat.2019.117937>.
- [42] Guo M, Zhong Q, Zhou Y, Hu B, Huang Z, Yue Y. Influence of flexural loading and chloride exposure on the fatigue behavior of high-performance lightweight engineered cementitious composites. *Constr Build Mater* 2020;249:118512. <https://doi.org/10.1016/j.conbuildmat.2020.118512>.
- [43] Wang P, Zhao M, Du X, Liu J. Dynamic Response of Bridge Pier under Combined

- Earthquake and Wave–Current Action. *J Bridg Eng* 2019;24:04019095.
[https://doi.org/10.1061/\(asce\)be.1943-5592.0001471](https://doi.org/10.1061/(asce)be.1943-5592.0001471).
- [44] Qiu J, Luo L, Li X, Li D, Chen Y, Luo Y. Numerical investigation on the tensile fracturing behavior of rock-shotcrete interface based on discrete element method. *Int J Min Sci Technol* 2020;30:293–301. <https://doi.org/10.1016/j.ijmst.2020.03.007>.
- [45] Bernard ES. Age-dependent changes in post-crack performance of fibre reinforced shotcrete linings. *Tunn Undergr Sp Technol* 2015;49:241–8.
<https://doi.org/10.1016/j.tust.2015.05.006>.
- [46] Sjölander A, Hellgren R, Malm R, Ansell A. Verification of failure mechanisms and design philosophy for a bolt-anchored and fibre-reinforced shotcrete lining. *Eng Fail Anal* 2020;116:104741. <https://doi.org/10.1016/j.engfailanal.2020.104741>.
- [47] Liu X, Wu T, Liu Y. Stress-strain relationship for plain and fibre-reinforced lightweight aggregate concrete. *Constr Build Mater* 2019;225:256–72.
<https://doi.org/10.1016/j.conbuildmat.2019.07.135>.
- [48] Li B, Chi Y, Xu L, Li C, Shi Y. Cyclic tensile behavior of SFRC: Experimental research and analytical model. *Constr Build Mater* 2018;190:1236–50.
<https://doi.org/10.1016/j.conbuildmat.2018.09.140>.
- [49] Pakravan HR, Ozbakkaloglu T. Synthetic fibers for cementitious composites: A critical and in-depth review of recent advances. *Constr Build Mater* 2019;207:491–518.
<https://doi.org/10.1016/j.conbuildmat.2019.02.078>.
- [50] Khlef FL, Barbosa AR, Ideker JH. Tension and Cyclic Behavior of High-Performance

- Fiber-Reinforced Cementitious Composites. *J Mater Civ Eng* 2019;31:1–15.
[https://doi.org/10.1061/\(ASCE\)MT.1943-5533.0002844](https://doi.org/10.1061/(ASCE)MT.1943-5533.0002844).
- [51] Caverzan A, Cadoni E, di Prisco M. Tensile behaviour of high performance fibre-reinforced cementitious composites at high strain rates. *Int J Impact Eng* 2012;45:28–38.
<https://doi.org/10.1016/j.ijimpeng.2012.01.006>.
- [52] Chung JH, Son DH, Kim SY, Bae B Il, Choi CS. Hysteretic behavior of reinforced concrete coupling beams according to volume fraction of steel fiber. *Sustain* 2021;13:1–17. <https://doi.org/10.3390/su13010182>.
- [53] Aggelis DG, Soulioti D V., Sapouridis N, Barkoula NM, Paipetis AS, Matikas TE. Acoustic emission characterization of the fracture process in fibre reinforced concrete. *Constr Build Mater* 2011;25:4126–31. <https://doi.org/10.1016/j.conbuildmat.2011.04.049>.
- [54] Aggelis DG. Classification of cracking mode in concrete by acoustic emission parameters. *Mech Res Commun* 2011;38:153–7. <https://doi.org/10.1016/j.mechrescom.2011.03.007>.
- [55] Yuyama S, Li Z wang, Ito Y, Arazoe M. Quantitative analysis of fracture process in RC column foundation by moment tensor analysis of acoustic emission. *Constr Build Mater* 1999;13:87–97. [https://doi.org/10.1016/S0950-0618\(99\)00011-2](https://doi.org/10.1016/S0950-0618(99)00011-2).
- [56] Soulioti D, Barkoula NM, Paipetis A, Matikas TE, Shiotani T, Aggelis DG. Acoustic emission behavior of steel fibre reinforced concrete under bending. *Constr Build Mater* 2009;23:3532–6. <https://doi.org/10.1016/j.conbuildmat.2009.06.042>.
- [57] Mechtcherine V, Millon O, Butler M, Thoma K. Mechanical behaviour of strain hardening cement-based composites under impact loading. *Cem Concr Compos* 2011;33:1–11.

- <https://doi.org/10.1016/j.cemconcomp.2010.09.018>.
- [58] Müller S, Mechtcherine V. Fatigue behaviour of strain-hardening cement-based composites (SHCC). *Cem Concr Res* 2017;92:75–83.
<https://doi.org/10.1016/j.cemconres.2016.11.003>.
- [59] Yu KQ, Yu JT, Dai JG, Lu ZD, Shah SP. Development of ultra-high performance engineered cementitious composites using polyethylene (PE) fibers. *Constr Build Mater* 2018;158:217–27. <https://doi.org/10.1016/j.conbuildmat.2017.10.040>.
- [60] Xu L, Li B, Ding X, Chi Y, Li C, Huang B, et al. Experimental Investigation on Damage Behavior of Polypropylene Fiber Reinforced Concrete under Compression. *Int J Concr Struct Mater* 2018;12. <https://doi.org/10.1186/s40069-018-0302-3>.
- [61] Carnovale D, Vecchio FJ. Effect of fiber material and loading history on shear behavior of fiber-reinforced concrete. *ACI Struct J* 2014;111:1235–44.
<https://doi.org/10.14359/51686809>.
- [62] Hung CC, Su YF, Yu KH. Modeling the shear hysteretic response for high performance fiber reinforced cementitious composites. *Constr Build Mater* 2013;41:37–48.
<https://doi.org/10.1016/j.conbuildmat.2012.12.010>.
- [63] Thomas T, Claus B. Non-Linear Finite Element Analysis of Shear Critical Reinforced Concrete Beams. *Delft Univ Technol* 2009.
- [64] Pekoz HA, Pincheira JA. Strength and Stiffness Degrading Single Degree of Freedom Systems. *Conference* 2004.
- [65] Toé Casagrande MD, Coop MR, Consoli NC. Behavior of a Fiber-Reinforced Bentonite at

- Large Shear Displacements. *J Geotech Geoenvironmental Eng* 2006;132:1505–8.
[https://doi.org/10.1061/\(asce\)1090-0241\(2006\)132:11\(1505\)](https://doi.org/10.1061/(asce)1090-0241(2006)132:11(1505)).
- [66] Cui L, Fall M. Modeling of pressure on retaining structures for underground fill mass. *Tunn Undergr Sp Technol* 2017;69:94–107. <https://doi.org/10.1016/j.tust.2017.06.010>.
- [67] Cui L, Fall M. Numerical Simulation of Consolidation Behavior of Large Hydrating Fill Mass. *Int J Concr Struct Mater* 2020;14:23. <https://doi.org/10.1186/s40069-020-0398-0>.
- [68] Chakilam S, Cui L. Effect of polypropylene fiber content and fiber length on the saturated hydraulic conductivity of hydrating cemented paste backfill. *Constr Build Mater* 2020;262:120854. <https://doi.org/10.1016/j.conbuildmat.2020.120854>.
- [69] Scrivener KL, Crumbie AK, Laugesen P. The interfacial transition zone (ITZ) between cement paste and aggregate in concrete. *Interface Sci* 2004;12:411–21.
<https://doi.org/10.1023/B:INTS.0000042339.92990.4c>.
- [70] Prokopski G, Halbiniak J. Interfacial transition zone in cementitious materials. *Cem Concr Res* 2000;30:579–83. [https://doi.org/10.1016/S0008-8846\(00\)00210-6](https://doi.org/10.1016/S0008-8846(00)00210-6).
- [71] Chasioti SG, Vecchio FJ. Shear behavior and crack control characteristics of hybrid steel fiber-reinforced concrete panels. *ACI Struct J* 2017;114:209–20.
<https://doi.org/10.14359/51689164>.
- [72] Pupurs A. *Micro-Crack Initiation and Propagation in Fiber Reinforced Composites*. 2012.
- [73] Dinh NH, Park SH, Choi KK. Effect of dispersed micro-fibers on tensile behavior of uncoated carbon textile-reinforced cementitious mortar after high-temperature exposure. *Cem Concr Compos* 2021;118:103949.

<https://doi.org/10.1016/j.cemconcomp.2021.103949>.

- [74] Li Q-H, Yin X, Huang B-T, Luo A-M, Lyu Y, Sun C-J, et al. Shear Interfacial Fracture of Strain-Hardening Fiber-Reinforced Cementitious Composites and Concrete: A Novel Approach. *Eng Fract Mech* 2021;253:107849.
<https://doi.org/10.1016/j.engfracmech.2021.107849>.
- [75] Huang BT, Weng KF, Zhu JX, Xiang Y, Dai JG, Li VC. Engineered/strain-hardening cementitious composites (ECC/SHCC) with an ultra-high compressive strength over 210 MPa. *Compos Commun* 2021;26:100775. <https://doi.org/10.1016/j.coco.2021.100775>.
- [76] Pereira EB, Fischer G, Barros JAO. Image-based Detection and Analysis of Crack Propagation in Cementitious Composites. *Proc Int RILEM Conf Adv Constr Mater Through Sci Eng* 2011:1–8.
- [77] Otsuka K, Date H. Otsuka2000.Pdf. *Eng Fract Mech* 2000;65:1–13.
- [78] Jankowski LJ et al. Formation of the Fracture 1990;36.
- [79] Brooks Z. Fracture Process Zone : Microstructure and Nanomechanics inMicrostructure and nanomechanics in quasi-brittle materials 2013.
- [80] Park K, Paulino GH, Roesler J. Cohesive fracture model for functionally graded fiber reinforced concrete. *Cem Concr Res* 2010;40:956–65.
<https://doi.org/10.1016/j.cemconres.2010.02.004>.
- [81] Erarslan N. Microstructural investigation of subcritical crack propagation and Fracture Process Zone (FPZ) by the reduction of rock fracture toughness under cyclic loading. *Eng Geol* 2016;208:181–90. <https://doi.org/10.1016/j.enggeo.2016.04.035>.

- [82] Li ZX, Li CH, Yan JB. Seismic behaviour of hybrid-fibre reinforced concrete shear keys in immersed tunnels. *Tunn Undergr Sp Technol* 2019;88:16–28.
<https://doi.org/10.1016/j.tust.2019.02.022>.
- [83] Choun YS, Park J. Evaluation of seismic shear capacity of prestressed concrete containment vessels with fiber reinforcement. *Nucl Eng Technol* 2015;47:756–65.
<https://doi.org/10.1016/j.net.2015.06.006>.
- [84] Ying M, Jin-Xin G. Seismic failure modes and deformation capacity of reinforced concrete columns under cyclic loads. *Period Polytech Civ Eng* 2018;62:80–91.
<https://doi.org/10.3311/PPci.9893>.
- [85] Nataraja MC, Dhang N, Gupta AP. Stress–strain curves for steel-fiber reinforced concrete under compression. *Cem Concr Compos* 1999;21:383–90. [https://doi.org/10.1016/S0958-9465\(99\)00021-9](https://doi.org/10.1016/S0958-9465(99)00021-9).
- [86] Krahl PA, Gidrão G de MS, Carrazedo R. Cyclic behavior of UHPFRC under compression. *Cem Concr Compos* 2019;104:103363.
<https://doi.org/10.1016/j.cemconcomp.2019.103363>.
- [87] Li B, Xu L, Chi Y, Huang B, Li C. Experimental investigation on the stress-strain behavior of steel fiber reinforced concrete subjected to uniaxial cyclic compression. *Constr Build Mater* 2017;140:109–18. <https://doi.org/10.1016/j.conbuildmat.2017.02.094>.
- [88] Deng M, Zhang Y. Cyclic loading tests of RC columns strengthened with high ductile fiber reinforced concrete jacket. *Constr Build Mater* 2017;153:986–95.
<https://doi.org/10.1016/j.conbuildmat.2017.07.175>.

- [89] Yu K, Ding Y, Liu J, Bai Y. Energy dissipation characteristics of all-grade polyethylene fiber-reinforced engineered cementitious composites (PE-ECC). *Cem Concr Compos* 2020;106:103459. <https://doi.org/10.1016/j.cemconcomp.2019.103459>.
- [90] Abbas YM, Iqbal Khan M. Fiber–Matrix Interactions in Fiber-Reinforced Concrete: A Review. *Arab J Sci Eng* 2016;41:1183–98. <https://doi.org/10.1007/s13369-016-2099-1>.
- [91] Mohonee VK, Goh KL. Effects of fibre–fibre interaction on stress uptake in discontinuous fibre reinforced composites. *Compos Part B Eng* 2016;86:221–8. <https://doi.org/10.1016/j.compositesb.2015.10.015>.
- [92] Libos ILS, Cui L. Time- and temperature-dependence of compressive and tensile behaviors of polypropylene fiber-reinforced cemented paste backfill. *Front Struct Civ Eng* 2021;15:1025–37. <https://doi.org/10.1007/s11709-021-0741-9>.
- [93] Alkan H, Cinar Y, Pusch G. Rock salt dilatancy boundary from combined acoustic emission and triaxial compression tests. *Int J Rock Mech Min Sci* 2007;44:108–19. <https://doi.org/10.1016/j.ijrmms.2006.05.003>.
- [94] Amini Y, Hamidi A, Asghari E. Shear strength–dilation characteristics of cemented sand–gravel mixtures. *Int J Geotech Eng* 2014;8:406–13. <https://doi.org/10.1179/1939787913Y.0000000026>.
- [95] Wang S, Xu L, Yin C, Chen Z, Chi Y. Experimental investigation on the damage behavior of ultra-high performance concrete subjected to cyclic compression. *Compos Struct* 2021;267:113855. <https://doi.org/10.1016/j.compstruct.2021.113855>.
- [96] Jiang MJ, Yan HB, Zhu HH, Utili S. Modeling shear behavior and strain localization in

- cemented sands by two-dimensional distinct element method analyses. *Comput Geotech* 2011;38:14–29. <https://doi.org/10.1016/j.compgeo.2010.09.001>.
- [97] Cui L, Fall M. An evolutive elasto-plastic model for cemented paste backfill. *Comput Geotech* 2016;71:19–29. <https://doi.org/10.1016/j.compgeo.2015.08.013>.
- [98] Ramesh K, Seshu DR, Prabhakar M. Constitutive behaviour of confined fibre reinforced concrete under axial compression. *Cem Concr Compos* 2003;25:343–50. [https://doi.org/10.1016/S0958-9465\(02\)00051-3](https://doi.org/10.1016/S0958-9465(02)00051-3).
- [99] Zhou J, Pan J, Leung CKY. Mechanical Behavior of Fiber-Reinforced Engineered Cementitious Composites in Uniaxial Compression. *J Mater Civ Eng* 2015;27:04014111. [https://doi.org/10.1061/\(asce\)mt.1943-5533.0001034](https://doi.org/10.1061/(asce)mt.1943-5533.0001034).
- [100] Siva CR, Pankaj A. Flexural behavior of reinforced concrete beams with high performance fiber reinforced cementitious composites. *J Cent South Univ* 2019;26:2609–22. <https://doi.org/10.1007/s11771-019-4198-0>.
- [101] Tahenni T, Chemrouk M, Lecompte T. Effect of steel fibers on the shear behavior of high strength concrete beams. *Constr Build Mater* 2016;105:14–28. <https://doi.org/10.1016/j.conbuildmat.2015.12.010>.
- [102] Banthia N, Gupta R. Hybrid fiber reinforced concrete (HyFRC): Fiber synergy in high strength matrices. *Mater Struct Constr* 2004;37:707–16. <https://doi.org/10.1617/14095>.
- [103] Boulekbache B, Hamrat M, Chemrouk M, Amziane S. Flowability of fibre-reinforced concrete and its effect on the mechanical properties of the material. *Constr Build Mater* 2010;24:1664–71. <https://doi.org/10.1016/j.conbuildmat.2010.02.025>.

- [104] Boulekbache B, Hamrat M, Chemrouk M, Amziane S. Influence of yield stress and compressive strength on direct shear behaviour of steel fibre-reinforced concrete. *Constr Build Mater* 2012;27:6–14. <https://doi.org/10.1016/j.conbuildmat.2011.07.015>.
- [105] Trainor KJ, Foust BW, Landis EN. Measurement of Energy Dissipation Mechanisms in Fracture of Fiber-Reinforced Ultrahigh-Strength Cement-Based Composites. *J Eng Mech* 2013;139:771–9. [https://doi.org/10.1061/\(asce\)em.1943-7889.0000545](https://doi.org/10.1061/(asce)em.1943-7889.0000545).
- [106] Mínguez J, Gutiérrez L, González DC, Vicente MA. Plain and Fiber-Reinforced Concrete Subjected to Cyclic Compressive Loading: Study of the Mechanical Response and Correlations with Microstructure Using CT Scanning. *Appl Sci* 2019;9:3030. <https://doi.org/10.3390/app9153030>.
- [107] Huang BT, Li QH, Xu SL, Liu W, Wang HT. Fatigue deformation behavior and fiber failure mechanism of ultra-high toughness cementitious composites in compression. *Mater Des* 2018;157:457–68. <https://doi.org/10.1016/j.matdes.2018.08.002>.
- [108] Mínguez J, Gutiérrez L, González DC, Vicente MA. Plain and fiber-reinforced concrete subjected to cyclic compressive loading: Study of the mechanical response and correlations with microstructure using CT scanning. *Appl Sci* 2019;9. <https://doi.org/10.3390/app9153030>.
- [109] Nasir O, Fall M. Shear behaviour of cemented pastefill-rock interfaces. *Eng Geol* 2008;101:146–53. <https://doi.org/10.1016/j.enggeo.2008.04.010>.
- [110] Kennedy TW. Practical method of conducting the indirect tensile test 1972:53.
- [111] Li H, Lai B, Liu H. Determination of Tensile Elastic Parameters from Brazilian Tensile

- Test: Theory and Experiments. *Rock Mech Rock Eng* 2019;52:2551–68.
<https://doi.org/10.1007/s00603-019-1738-8>.
- [112] Xiu Z, Wang S, Ji Y, Wang F, Ren F, Nguyen VT. Loading rate effect on the uniaxial compressive strength (UCS) behavior of cemented paste backfill (CPB). *Constr Build Mater* 2021;271:121526. <https://doi.org/10.1016/j.conbuildmat.2020.121526>.
- [113] Noushini A, Samali B, Vessalas K. Effect of polyvinyl alcohol (PVA) fibre on dynamic and material properties of fibre reinforced concrete. *Constr Build Mater* 2013;49:374–83.
<https://doi.org/10.1016/j.conbuildmat.2013.08.035>.
- [114] Xue G, Yilmaz E, Song W, Cao S. Fiber length effect on strength properties of polypropylene fiber reinforced cemented tailings backfill specimens with different sizes. *Constr Build Mater* 2020;241:118113. <https://doi.org/10.1016/j.conbuildmat.2020.118113>.
- [115] Bandelt MJ, Frank TE, Lepech MD, Billington SL. Bond behavior and interface modeling of reinforced high-performance fiber-reinforced cementitious composites. *Cem Concr Compos* 2017;83:188–201. <https://doi.org/10.1016/j.cemconcomp.2017.07.017>.
- [116] Figueiredo TCSP, Curosu I, Gonzáles GLG, Hering M, Silva F de A, Curbach M, et al. Mechanical behavior of strain-hardening cement-based composites (SHCC) subjected to torsional loading and to combined torsional and axial loading. *Mater Des* 2021;198:109371. <https://doi.org/10.1016/j.matdes.2020.109371>.
- [117] Xue G, Yilmaz E, Song W, Yilmaz E. Influence of fiber reinforcement on mechanical behavior and microstructural properties of cemented tailings backfill. *Constr Build Mater* 2019;213:275–85. <https://doi.org/10.1016/j.conbuildmat.2019.04.080>.